

TUNING PHOTOPHYSICAL PROPERTIES IN *CLOSO*-DECABORANE CLUSTER
DERIVATIVES

by

Mustapha B. Abdulmojeed

A Thesis Submitted in Partial Fulfillment
of the Requirements for the Degree of
Master of Science in Chemistry

Middle Tennessee State University

2020

Thesis Committee:

Dr. Andrienne C. Friedli, Major Advisor

Dr. Piotr Kaszynski, Committee Member

Dr. Kevin Bicker, Committee Member

Dr. Justin Miller, Committee Member

Tuning Photophysical Properties in *Closo*-Decaborane Cluster Derivatives

by

Mustapha B. Abdulmojeed

Approved:

Dr. Andrienne C. Friedli, Committee Chair



Dr. Piotr Kaszynski, Committee Member

Dr. Kevin L. Bicker, Committee Member

Dr. Justin M. Miller, Committee Member

Dr. Paul G. Van Patten, Chair, Department of Chemistry

Dr. David L. Butler, Dean, College of Graduate Studies

ACKNOWLEDGEMENTS

All thanks belong to God who has made it possible to complete this piece of work. Thanks to my wife for her love, care and understanding, taking care of our kids while I was away. Special thanks to my advisor, Dr. Andrienne Friedli for her support, guide and patiently delivered instructions through-out the course of this project. Dziękuję to my co-advisor, Dr. Piotr Kaszynski whose constant push and motivation from across the Atlantic Ocean kept me going, no amount of words could express my gratitude to both of you. Sincere appreciation also goes to Dr. Szymon Kapuscinski who is not just an excellent senior colleague but a great personality whose help in this work cannot be measured. I also want to thank MTSU chemistry department for the funding opportunity. I extend my gratitude to all faculty members in the department for creating a conducive and welcoming environment to learn and train as a chemist. I am also indebted to my research committee who painstakingly reviewed my thesis and the graduate coordinator, Dr. Charles Chusuei for maintaining constant communication and ensuring that I stayed on track. Thanks to the National Science Foundation (NSF-DMR 1161250) for providing funding for this project. Finally, I would like to acknowledge all my amazing colleagues at MTSU chemistry department, for creating such an atmosphere that promotes personal and intellectual growth.

ABSTRACT

Closo-decaborane ($[closo-B_{10}H_{10}]^{2-}$) is a three-dimensional, electron rich, sigma aromatic system with orbital symmetry that allows for efficient electronic interaction with π -substituents at the apical positions. This thesis project deals with the design, synthesis, and characterization of a class of compounds with tunable photophysical properties. The prototypical system is the pyridinium $[closo-B_{10}H_9-NC_5H_5]^-$ anion (**1a**), which exhibits an intense band in the visible region that results from intramolecular electron transfer from the HOMO, predominantly localized on the cage, to the LUMO, localized on the pyridine. The level of the HOMO is controlled by substituents at the antipodal B1 boron atom (series **1**), while the energy of the LUMO is changed by variation of the azine at the B10 positions (series **7**). The control of the HOMO-LUMO gap leads to the control of the absorption energy.

Two synthetic methods were developed for installation of nucleophiles (CN, N₃, OAc, halogen, and SCN, pyridine, morpholine; series **1**) at the B1 and azines (pyridine, pyridazine, pyrimidine, pyrazine; series **7**) at the B10 positions, relying on selective activation of the apical B-H bond towards nucleophilic substitution via oxidation with $PhI(OAc)_2$. Trends in substituent effects on spectroscopic properties (NMR and UV) were analyzed and compared to other $[closo-B_{10}H_{10}]^{2-}$ derivatives. The HOMO-LUMO gap as measured by the λ_{max} varied from 329.5 to 368.5 nm in series **1** (0.398 eV range) and from 339.5 to 409 nm (0.621 eV range) in series **7**, indicating that the system is more sensitive to perturbations of the LUMO energy.

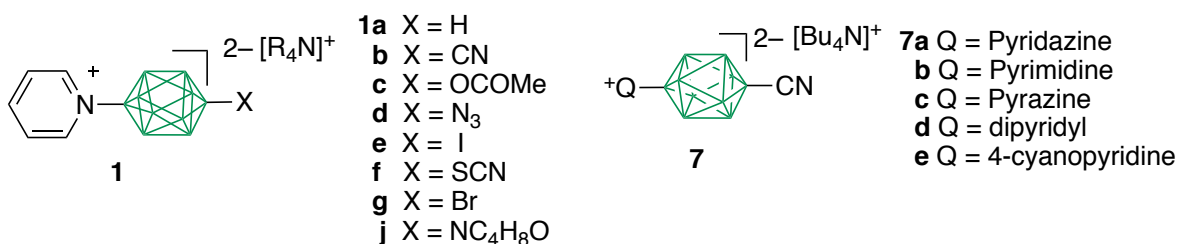


TABLE OF CONTENTS

1.0 CHAPTER I: INTRODUCTION	1
1.1 Structure of Boron Clusters	3
1.1.1 Bonding in Boron Clusters	4
1.1.2 Wade's rule and sigma-aromaticity	6
1.2 Boron cluster applications	7
1.2.1 Boron clusters as sources of Boron in BNCT	7
1.2.2 Boron clusters in polymeric materials.	8
1.2.3 Boron clusters in liquid crystals	9
1.2.4 Boron clusters in Non-Linear optical materials (NLO)	9
1.2.5 Boron clusters in luminescent materials	10
1.2.6 Metallocarboranes	13
1.3 Boron clusters and π -aromatic systems	14
1.4 <i>Closo</i> -decaborane cluster	15
1.5 Functionalizing <i>closo</i> -decaborane cluster	16
1.6 Research Questions	17
1.7 Research Objectives	19
1.8 Thesis statement	19
2.0 CHAPTER II: Tuning absorption energies via modifying the HOMO energies in [<i>closo</i> -B ₁₀ H ₈ -1-(NC ₅ H ₅)-10-X]	20
2.1 Introduction	20
2.2 Results and discussions	21
2.2.1 Synthesis	21
2.2.2 Crystal and molecular structure	26
2.2.3 Photophysical properties	31
2.2 Conclusion	37
2.3 Computational details	38
2.4 Experimental	39

3.0 CHAPER III: Tuning absorption energies via modifying the LUMO energies in [<i>closo</i> - B ₁₀ H ₈ -1-CN-10-(Q ⁺)]	53
3.1 Introduction	53
3.2 Results and discussions	55
3.2.1 Synthesis	55
3.2.2 Crystal and molecular structures	57
3.2.3 Photophysical properties	59
3.2.4 IR spectroscopy	64
3.3 Conclusion	65
3.4 Experimental	66
References	71
Appendices	76
Appendix I: NMR spectra of series 1	77
Appendix II: NMR spectra of series 7, 8 and compound 10	107
Appendix III: Copyright permissions.	122

LIST OF FIGURES

Figure 1.1: Jablonski diagram illustrating various photophysical process	2
Figure 1.2: Skeletal representation of common <i>closo</i> -boranes.	3
Figure 1.3: Structures of $[B_6H_6]^{2-}$, B_5H_9 and B_4H_{10}	5
Figure 1.4: Molecular orbital diagram and a schematic diagram of a B-H-B bond.	5
Figure 1.5: Illustration of bis-betaine II derivative.	10
Figure 1.6: Carborane-appended 1,3,5-triphenylbenzene (TB).	11
Figure 1.7: Structure of <i>o</i> -carborane and π -conjugated trifunctional <i>o</i> -carborane.	12
Figure 1.8: Structures of <i>closo</i> - and <i>nido</i> -diphosphine carborane complexes	14
Figure 1.9: HOMO contours of $[closo-B_{10}H_{10}]^{2-}$ anion.	15
Figure 1.10: Substitution of $[closo-B_{10}H_{10}]^{2-}$ anion.	16
Figure 1.11: Frontier molecular orbitals of <i>closo</i> - $B_{10}H_9$ -1-pyridinium	18
Figure 2.1: Structures of Series 1 and 2	21
Figure 2.2: Two synthetic approach to preparation of series 1 .	22
Figure 2.3: Atomic displacement ellipsoid representation of series 1	29
Figure 2.4: Packing diagram for 1b [Et ₄ N] and 1g [Et ₄ N].	31
Figure 2.5: Electronic spectra of series 1	32
Figure 2.6: UV and fluorescence spectra of 1b .	33
Figure 2.7: Frontier molecular orbitals of 1b	33
Figure 2.8: Correlation of DFT calculated energy of series 1 .	35
Figure 2.9: Correlation of experimental energy of series 1	35
Figure 2.10: Correlation of HOMO and LUMO energies of series 1	36
Figure 3.1: TD-DFT calculations showing effect of substituents on pyridine.	53
Figure 3.2: Structures of Series 7 and 8	54
Figure 3.3: Atomic displacement ellipsoid representation of 7a , 7c and 8b	58
Figure 3.4: Packing diagram for 7a and 7c	59
Figure 3.5: Electronic spectra of series 7	60
Figure 3.6: UV and fluorescence spectra of 7d .	63
Figure 3.7: Correlation of HOMO and LUMO energies vs exp. energies	65

LIST OF TABLES

Table 2.1: Selected interatomic distances and angles for series 1	28
Table 2.2: Selected experimental and calculated transition energies for series 1	34
Table 3.1: Selected Interatomic distances and angles for series 7	58
Table 3.2: Selected experimental and calculated transition energies for series 7	61
Table 3.3: IR CN stretching of series 7a-7e	64

LIST OF SCHEMES

Scheme 1.1: Functional group transformation of <i>closo</i> -decaborane.	17
Scheme 2.1: Synthesis of intermediates 4 .	23
Scheme 2.2: Preparation of 1d and 1e using Method A.	24
Scheme 2.3: Preparation of 1b , 1c , 1f and 1g from 6 using Method B.	25
Scheme 2.4: Preparation of 1j and attempted deprotonation to 1i .	26
Scheme 3.1: Synthesis of 1b from 6 .	55
Scheme 3.2: Three step approach to synthesis of 7 through intermediates 8 .	55
Scheme 3.3: Synthesis of series 7 and 10 side product from 6 .	56

CHAPTER I

1.0 Introduction

The search for new materials with tunable photophysical properties is of great importance to the design of light emitting diodes, semiconductor lasers, biological and environmental probes, chemical sensors among others.¹⁻³ Photophysics involves several processes that molecules undergo when they interact with light without any change in their chemical structure. When a molecule is exposed to light, a light-absorbing region (chromophore) becomes excited to a higher electronic energy level and subsequently undergoes non-radiative (vibrational) relaxation or radiative relaxation by emitting light of lower frequency (fluorescence). Some electrons flip to a triplet spin state before the molecule finally relaxes to the ground state via a non-radiative or a radiative (phosphorescence) process (Figure 1.1). Since the discovery of single molecule fluorescence by Moerner,¹ there has been an exponential increase in the number of known fluorescent materials due to their several applications.

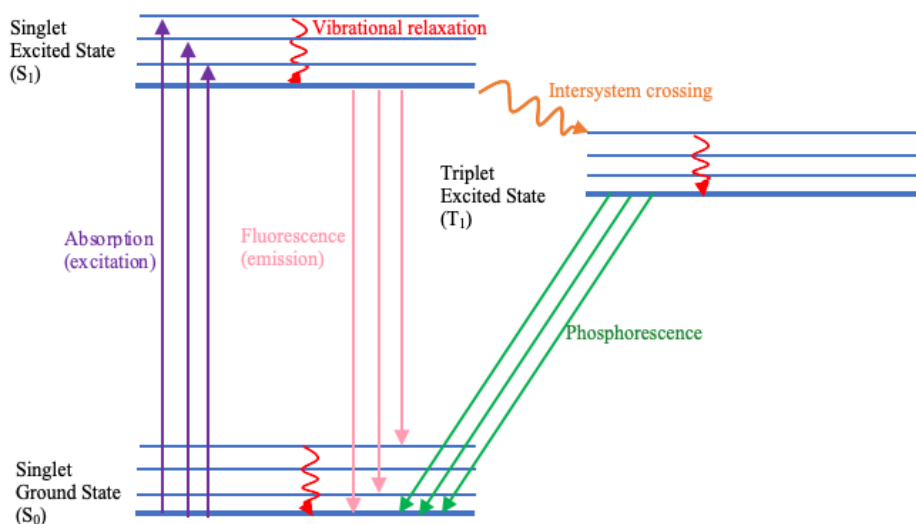


Figure 1.1. A Jablonski diagram illustrating various photophysical processes.

Photoactive materials vary greatly in structure, ranging from inorganic metal oxides (*e.g.* ruby ($\text{Al}_2\text{O}_3: \text{Cr}^{3+}$), to organic molecules (*e.g.* anthracene) to quantum dots (*e.g.* CdS). Recently, the realm of materials in this field has been expanded with the discovery of luminescence in polyhedral boron clusters.⁴

Polyhedral boron clusters are an extensive family of compounds characterized by three-center two-electron bonds resulting in three-dimensional, highly polarizable, electron delocalized σ -bonds between 6 and 12 boron atoms, and including up to two carbon atoms (**A–H**, Figure 1.2). The unique electronic properties of boron clusters, combined with their rigid geometry, high thermal, chemical and electrochemical stability, make them interesting components for new materials.

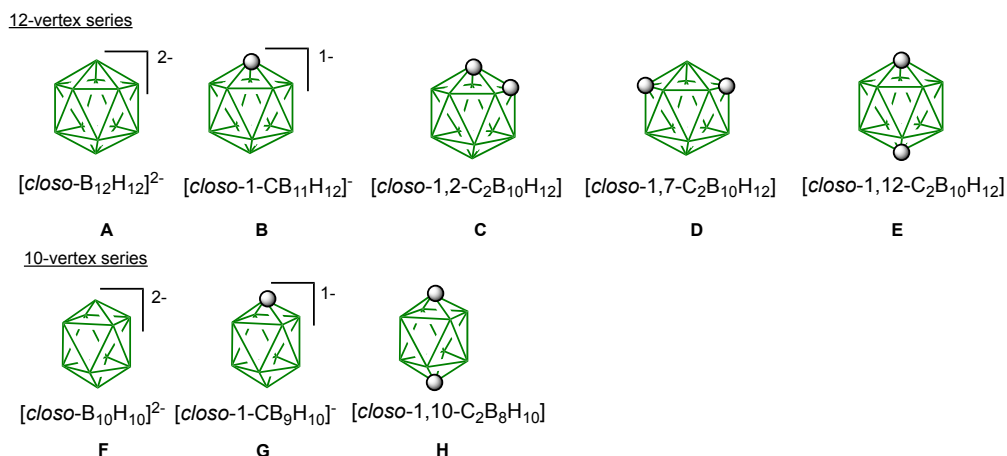


Figure 1.2. Skeletal representations of common *closo*-boranes. In structures **A–H** each green vertex corresponds to a B-H fragment and the CH groups are marked by filled circles.

In the following sections, we describe the chemistry of boron clusters, highlight recent studies on their applications, especially photophysical properties, and show the uniqueness of the *closo*-decaborane cluster (**F**) as a structural element.

1.1 Structure of Boron Clusters

Alfred Stock showed in a series of studies conducted between 1912 and 1936 that boron forms a range of hydrides of different nuclearities. Since then, different classes of boron hydride clusters have been recognized. In the *closo*-cluster, the atoms form a closed, deltahedral cage with the general formula $[B_nH_n]^{2-}$ (e.g. **A** and **F** in Figure 1.2, $[closo-B_6H_6]^{2-}$ Figure 1.3a). The *nido*-cluster is an open cage cluster derived from a closed deltahedron with one vertex unoccupied and the general chemical formulae B_nH_{n+4} or $[B_nH_{n+4}]^{-}$ (e.g. $[nido-B_5H_9]$, Figure 1.3a). Removal of two vertices from a closed deltahedron leads to an *arachno*-cluster with general formulae B_nH_{n+6} or $[B_nH_{n+5}]^{-}$ (e.g.

[*arachno*-B₄H₁₀], Figure 1.3a).⁵⁻⁷ Replacement of a {BH} unit with one or two {CH} units leads to the corresponding carborane (Figure 1.2, **B – E**, 12 vertex, **G and H**, 10 vertex)

1.1.1 Bonding in Boron clusters

A valence bond method called Styx rules was used Lipscomb to describe the bonding in boron clusters.⁵ He thought of normal covalent bonds as two center two electron bonds (2c-2e) since two atoms supply two orbitals, which interact to form one bonding and one antibonding orbital. If two electrons fill the bonding orbital, a covalent bond is formed. Because a 2c-2e bond does not account for the experimentally determined B-H-B bonds in B₂H₆, a three center two electron bond (3c-2e) was proposed to explain such bonding. Here, three atoms supply three orbitals, which interact to form one bonding orbital, a non-bonding and an anti-bonding orbital, two electrons may fill the bonding orbital to form a three-center bond (Figure 1.4).

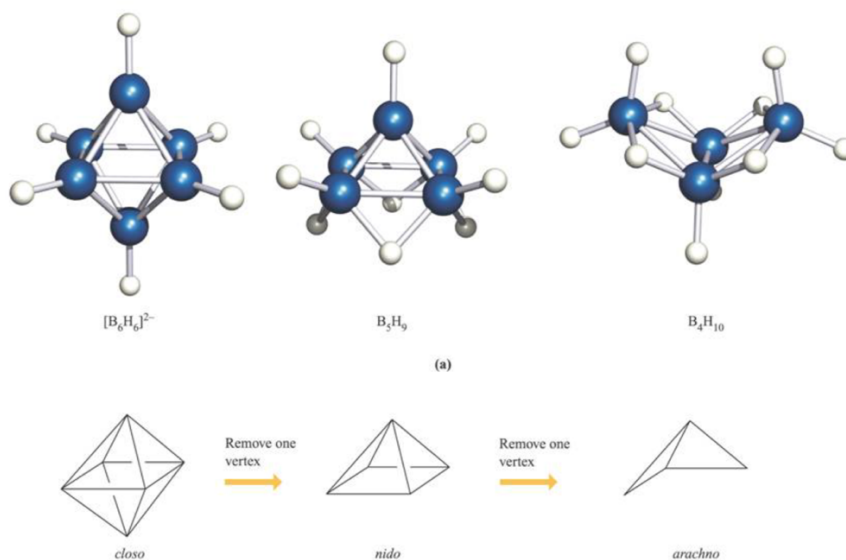


Figure 1.3. (a) structures of $[\text{closo-B}_6\text{H}_6]^{2-}$, $\text{nido-B}_5\text{H}_9$ and $\text{arachno-B}_4\text{H}_{10}$, blue and white spheres = B and H, respectively; (b) schematic representation of the derivation of *nido* ($n = 5$) and *arachno* ($n = 4$) clusters from a *closo* cluster ($n = 6$). Source: Inorganic chemistry by Housecroft and Sharp, Third Edition.

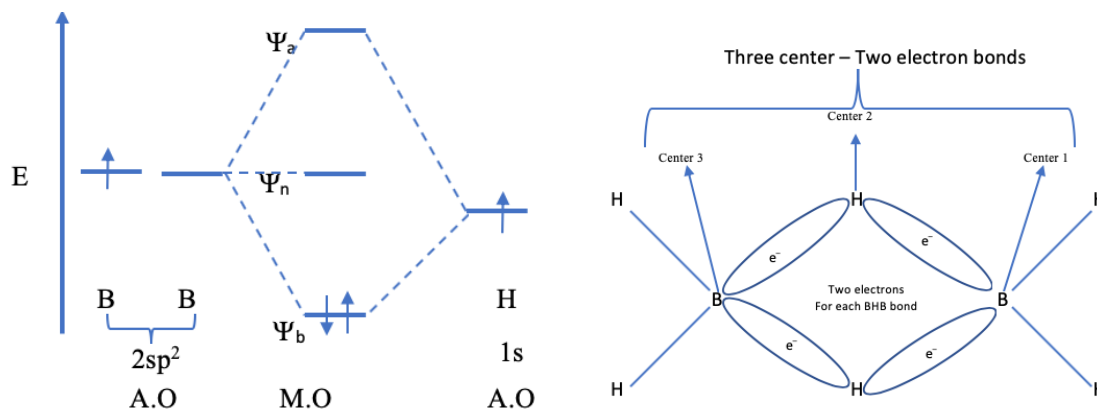


Figure 1.4. Molecular orbital diagram (left) and a schematic representation (right) of a B-H-B bond.

This treatment was extended to more complex deltahedral boron clusters. Each cluster is given a unique four-digit number known as the Styx number where s = number of hydrogen bridges, (B–H–B) t = number of boron-boron three center bonds (B–B–B), y = number of boron–boron single bonds, (B–B) and x = number of extra H atoms on B–H; *i.e.* BH₂. For example [B₆H₆]²⁻ has a Styx number of 0430. This means it has zero B–H–B bond, four B–B–B bonds, three B–B bonds and zero extra B–H bonds.⁵

1.1.2 Wade's rule and sigma-aromaticity

Lipscomb's 3c-2e concept was able to explain bonding in B₂H₆ and limited number of clusters. However, experimental evidence suggests that bonding in boron clusters cannot be described using localized bonding models, rather a delocalized approach is more accurate.

Thus Wade, Williams, and Mingos developed an empirical set of rules known as Wade's rule, which is summarized thus: for a cluster with n vertices, the *closo* form requires $(n + 1)$ pairs of electrons which occupy $(n + 1)$ MOs, the *nido*-form requires $(n + 2)$ pairs of electrons which occupy $(n + 2)$ MOs and the *arachno*-form requires $(n + 3)$ electrons which occupy $(n + 3)$ MOs. For example, in [*closo*-B₆H₆]²⁻ there are six {BH}-units with no extra H atoms, each unit provides two valence electrons (boron has three valence electrons, one electron is used to form a bond with a hydrogen atom), there are two electrons from the 2- charge, and thus the total number of cage-bonding electrons available = $(6 \times 2) + 2 = 14$ electron = 7 pairs. Therefore [*closo*-B₆H₆]²⁻ has seven pairs of electrons to bond six {BH}-units. This implies that there are $(n + 1)$ pairs of electrons for n vertices which means [B₆H₆]²⁻ is a *closo*-cluster.

This concept was used to explain the relative stabilities of deltahedral boranes. For instance, the dicesium salt of [*closo*-B₁₂H₁₂]²⁻ survives temperatures above 810 °C without decomposition. Theoretical studies linked this stability to the highly delocalized bonding in the boron framework, with 13 pairs of electrons occupying 13 bonding MOs on the polyhedral surface. This was labeled by Lipscomb as super-aromaticity or a 3-dimensional analog of π -aromaticity in benzene also known as σ -aromaticity. Aihara and King confirmed the idea of σ -aromaticity in deltahedral boranes and other related clusters such as the carboranes.^{8,9}

1.2 Boron cluster applications

Polyhedral boron hydrides and related compounds have several unique properties that suit different applications. They have been used in the synthesis of boron delivery agents in Boron Neutron Capture Therapy (BNCT), thermally stable polymers, liquid crystals, non-linear optical materials, and luminescent materials. While the focus here is on their application as photoactive materials, a brief review of their use across diverse fields is mentioned below.¹⁰

1.2.1 Boron Clusters as sources of Boron in BNCT

The ¹⁰B isotope is present in about 20 % of naturally occurring boron atoms. This isotope can absorb neutrons from slow neutron sources and produce α particles, which can selectively kill tumor cells, as was reported by Locher in 1935.¹⁰ However, the lack of suitable boron compounds (non-toxic and soluble in biological systems) prevented the development of this technique. The discovery of polyhedral borane anions [B_nH_n]²⁻ and their carborane analogs, which are non-toxic and high in boron content, led to the resurgence of BNCT. Hatanaka¹¹ reported the treatment of human brain tumors with BNCT

with some success over several years using the mercapto-substituted derivative [*closo*-B₁₂H₁₁-1-SH]²⁻. Since then, BNCT has been used clinically for decades to treat tumors such as primary and metastatic melanomas and high-grade brain tumors.

Boron clusters such as the sodium salt of sulfhydryl boron hydride Na₂[*closo*-B₁₂H₁₁-1-SH] (BSH), neutral isomeric carboranes *ortho*-, *meta*-, and *para*-C₂B₁₀H₁₁ (**C**, **D** and **E**, Figure 1.2), and negatively charged [*closo*-B₁₂H₁₂]²⁻ (**A**, Figure 1.2) have been incorporated into nucleoside lipids, carbohydrates, and peptides as boron delivery agents.¹¹

1.2.2 Boron Clusters as Polymeric Materials

Boron clusters are excellent precursors for synthesis of architecturally novel macromolecules and polymers whose unique properties could be tailored to specific applications. Chujo and Kokado reported the synthesis of polymers with *o*-carborane (**C**, Figure 1.2) and *p*-phenylene – ethylene sequences. The unique ability of *o*-carborane to cause aggregation-induced emission *i.e.* AIE (non-emissive molecules are caused to emit by forming aggregates) was exploited in the design of polymers which exhibit color in the solid-state. Polymers with such properties are important for the fabrication of organic light emitting diodes (OLED) in thin films or by vapor deposition.¹²

1.2.3 Boron clusters as liquid crystals

Liquid crystals are materials that exhibit fluid properties at room temperature but have partially ordered structure and birefringence. They are often applied in electro-optical displays. Boron clusters are very attractive rigid cores for constructing molecular rods that show distinctive liquid crystalline behavior. This can be attributed to their thermal stability, delocalized bonding, ease of derivatization and three-dimensional cage structure.¹³

Recently Kaszynski *et al* synthesized a series of 4-alkoxypyridine derivatives of bis-zwitterionic *closo*-decaborate cluster $[B_{10}H_{10}]^{2-}$ (**F**, Figure 1.2) that exhibited multiple liquid crystalline and soft crystalline phases.¹⁴

1.2.4 Boron clusters as Non-Linear Optical materials (NLO)

NLO materials possess the ability to convert an applied electromagnetic field to a new one with altered properties such as frequency and pulse. These materials have applications in data storage, retrieval, communications, and optical switching. Molecular hyperpolarizability (β), which describes the energy dependence of dipole moment, is an important measure of an NLO system.¹⁵ Conjugated organic molecules with donor-acceptor (push-pull) systems often have large values of β . Recently, experimental and theoretical studies have shown that electron withdrawing borane or carborane clusters can result in increases in β values. *para*-Carboranes (**E**, Figure 1.2) are exceptionally NLO-active, In 2002 Yamamoto *et al*¹⁶ synthesized a series of novel carborane-ferrocene conjugated dyads and investigated their NLO properties. Among the three isomeric forms

of *closo*-C₂B₁₀H₁₂ (**C**, **D** and **E**, Figure 1.2), the *para* isomer exhibited the highest β values. Furthermore, Kaszynski *et al* demonstrated that bis-betaine derivative **II** of [*closo*-B₁₀H₁₀]²⁻ (Figure 1.5) having a π -type onium fragment antipodal to a σ -type onium fragment exhibit moderate hyperpolarizability β comparable to those of conventional NLO materials of relatively similar size.

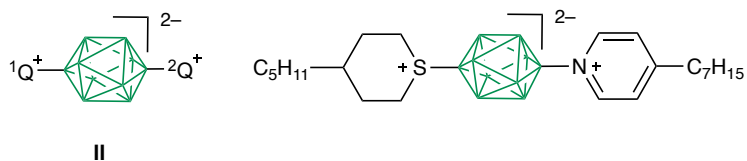


Figure 1.5. Illustration of bis-betaine **II** derivative of [*closo*-B₁₀H₁₀]²⁻ and structure of a typical example.

1.2.5 Boron clusters as luminescent materials

Most studies of luminescence in boron clusters have centered on exploiting the electron withdrawing ability of the clusters and their interactions with π -conjugated substituents. Coupling of the electron deficient *closo-o*-carborane to several fluorophore units is an effective strategy to design molecules with intriguing emission properties. In 2011, a series of carborane-appended 1,3,5-triphenylbenzene (TB) and 1,3,5-tris(biphenyl-4-yl) benzene (TBB) systems containing *ortho*-, *meta*-, and *para*-carborane cluster (Figure 1.6) directly attached to the conjugated cores were synthesized employing Suzuki, Heck, and trimerization reactions. The incorporation of the cluster was linked with a red-shift in the UV absorption and enhanced emission intensities of up to 154%. The *ortho*- isomer has the greatest red shift while the *meta*- isomer has the largest increase in emission intensity.¹⁷

These authors have also previously synthesized a series of star-shaped C_3 -symmetric p -conjugated compounds containing three to six o -carborane clusters. The presence of o -carborane clusters was found to prevent π - π stacking interactions and enhance rigidity in the molecules resulting in 22 – 70 % increase in fluorescence intensity.¹⁸

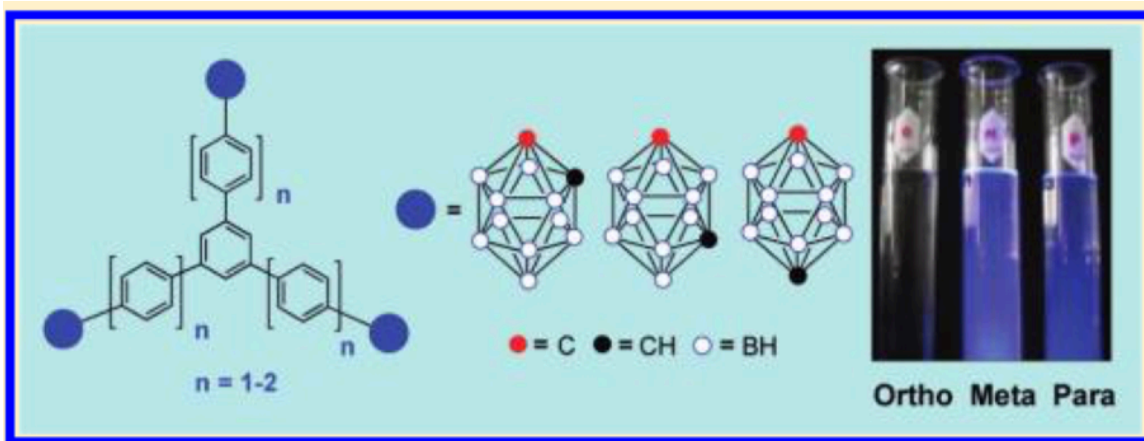


Figure 1.6. Carborane-appended 1,3,5-triphenylbenzene (TB) ($n = 1$) and 1,3,5-tris(biphenyl-4-yl) benzene (TBB) ($n = 2$). Adapted with permission from Dash *et al.* *Inorg. Chem.* **2011**, *50* (12), 5485–5493. Copyright (2011) American Chemical Society.

Aggregation induced-emission (AIE) properties of o -carborane containing luminescent materials was exploited by Chujo *et al* to design water sensitive poly (γ -glutamic acid) (PGA) hydrogels. They synthesized a diglycidyl compound containing o -carborane (C) and cross-linked with PGA hydrogels, they showed that the AIE-dye exhibited reversible fluorescence switching between the swollen and dried states of the hydrogels.¹⁹

Neutral and anionic di-and tetra-carboranyl derivatives of aryl ethers were synthesized by Nunez *et al.*²⁰ Both the *nido* and *closo*-carborane derivatives exhibit a blue

emission with ultraviolet excitation at room temperature in different solvents. They showed that the maximum wavelength of emission depends on the substituent bonded to the second carbon of the cluster, solvent polarity and the organic unit bearing the carborane clusters (benzene or pyridine).

Substituent variation on diphenyl-*o*-carboranes resulted in multicolor tuning of AIE. Different electron-donating and electron withdrawing arylacetylenes were coupled with bis-(4-bromophenyl)-*o*-carborane using palladium coupling reactions bis-*p*-substituted diphenyl-*o*-carboranes. The emission color of the compounds covers much of the visible region from $\lambda_{\max} = 452$ nm (strongly electron withdrawing substituents) to $\lambda_{\max} = 662$ nm (strongly electron donating groups).²¹

O-carborane derivatives containing π -electron systems at the C1, B9 and B12 positions (Figure 1.7) showed dual-emission (normal emission and AIE). The emission intensities were precisely controlled by the degree of aggregate formation in THF and H₂O solutions, resulting in multi-colored emission from blue to orange in the solid state.²²

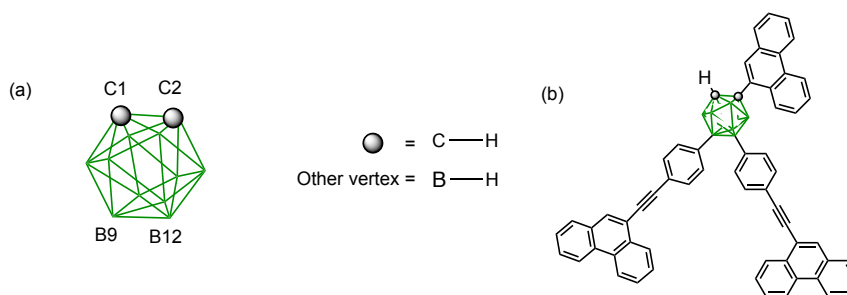


Figure 1.7. a) structure of *o*-carborane showing C1, B9 and B12 positions; b) a π -conjugated trifunctional *o*-carborane.

A paradigm shift in the design of emissive solids and films for opto-electronic devices (flexible displays) and film type chemo-sensors is the discovery of AIE properties in *o*-carborane, recently²³ a series of anthracene substituted *o*-carborane dyads with different substituents (Ph, Me and TMS) attached to the C2 of the cluster allows restricted molecular rotation at the C–C bond, precluding non-radiative decay and enhancing crystalline state emission efficiencies. In particular the Me- and TMS-substituted compound showed excellent quantum efficiencies in the crystalline state. Aside from carboranes, which are arguably the most studied clusters from among boron containing polyhedral clusters, metallocarboranes and binary boranes (contains only boron and hydrogen) have also gained significant attention.

1.2.6 Metallocarboranes

Some boron cluster derivatives containing transition metals and carbon have been reported to show fluorescence and phosphorescence. For example, gold complexes of diphosphine *closo*-carborane anions (Figure 1.8a)²⁴ were not fluorescent, but *nido*-derivatives were. When a phenyl group was attached to the two phosphorus atoms, a metal to ligand charge transfer emission was observed in both. Jelliss reported low temperature (77 K) phosphorescence²⁴ in Re-containing *closo* *o*-carboranes [[3,3-(CO)₂-3-NO-*closo*-3,1,2-ReC₂B₉H₁₁] (Figure 1.8c) and [NEt₄][3,3,3-(CO)₃-8-I-*closo*-3,1,2-ReC₂B₉H₁₀] (Figure 7d).

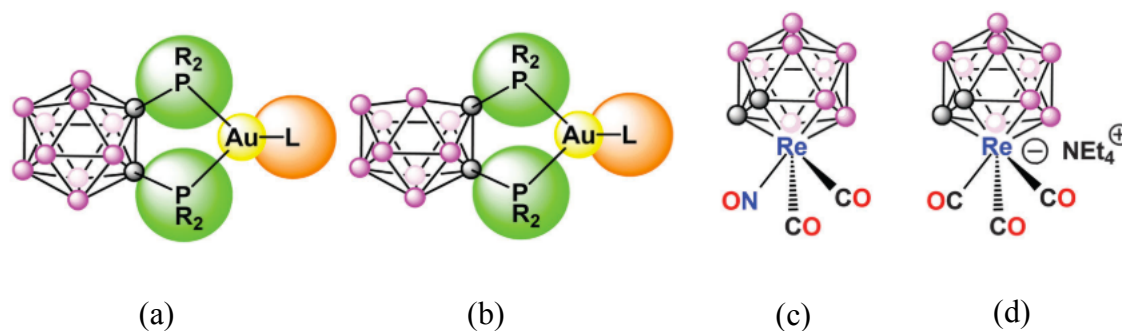


Figure 1.8. Structures of (a) *closo*- and (b) *nido*- diphosphine carborane gold complexes. (c) and (d) are structures of [3,3-(CO)₂-3-NO-*closo*-3,1,2-ReC₂B₉H₁₁] and [NEt₄][3,3,3-(CO)₃-8-I-*closo*-3,1,2-ReC₂B₉H₁₁] source: Mukherjee & Thilagar *Chem. Commun.* **2016**, 52 (6), 1070–1093. Copyright permission.

1.3 Boron clusters and π -aromatic systems.

The photophysical properties of boron clusters is closely related to their interaction with π -aromatic systems. In contrast to carboranes, which are generally used as acceptors in donor-acceptor systems, boron clusters containing only boron and hydrogen, are electron rich and can serve as electron donors. Volkov and co-workers²⁵ studied the structural effects on the absorption and luminescent properties of *nido*-decaborane derivatives (B₁₀H₁₂L₂). They observed that the B–L bond is exceptionally stabilized if L is a π -aromatic moiety such as pyridine, also their absorption spectra exhibit a charge transfer band (CTB) which is attributed to the electronic interaction between the delocalized π orbital of the cluster (HOMO) and the π^* antibonding orbital (LUMO) of the ligand. The CTB was observed to correlate linearly with the Hammett σ_p -constants of substituents attached to the pyridine. Interestingly, they noted that electron-withdrawing groups attached to the pyridine cause a bathochromic shift of the CTB, while electron-donating groups produces a hypsochromic shift.

1.4 *closo*-Decaborane [*closo*-B₁₀H₁₀]²⁻ (F)

Previous studies²⁶ have shown that 10 vertex *closo*-borane clusters such as [*closo*-B₁₀H₁₀]²⁻ and its carborane analog exhibit stronger interactions with π -aromatic substituents attached to the apical positions. This is due to greater amplitude of the π -symmetric HOMO at these positions and its energy, as shown for the [*closo*-B₁₀H₁₀]²⁻ anion (F, Figure 1.9).

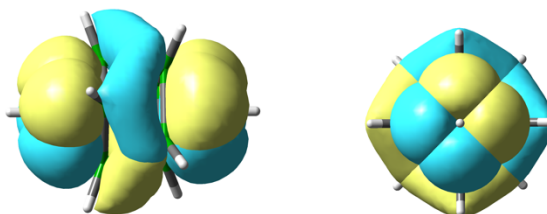


Figure 1.9. Two views of the HOMO contours of the [*closo*-B₁₀H₁₀]²⁻ anion (F). $E_{\text{HOMO}} = -5.16$ eV. CAM-B3LYP/6-31++G(2d,p)//M062x/6-31G(2d,p) in MeCN.

The absence of carbon atoms in this cluster results in higher negative charge of the cluster, leading to higher HOMO energies and stronger electron donating properties. Leveraging on its strong interaction with π substituents and double negative charge, the properties of the derivatives can be controlled, such as ionic strength, solubility in aqueous media, and electronic density around the cage.

Three types of derivatives of this cluster can be conceptualized; (I) the dianion: substitution with two neutral R groups (II) the monoanion: substitution with one onium fragment Q⁺ and an R group (III) neutral bis-zwitterion: double substitution with onium fragments (Figure 1.10).¹³

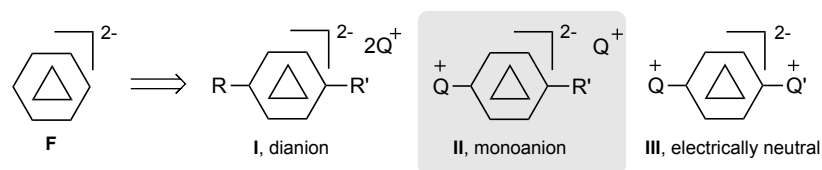
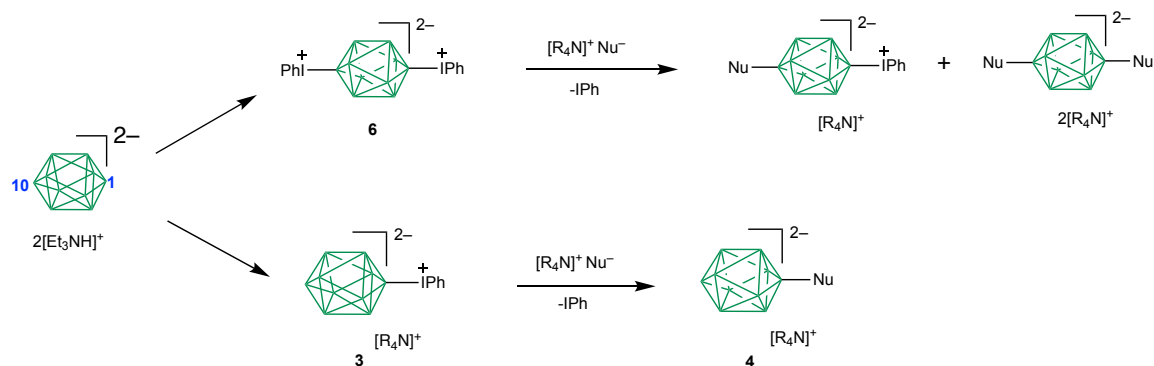


Figure 1.10. Substitution of the $[closo-B_{10}H_{10}]^{2-}$ anion (**F**) with groups R and onium fragments leading to 3 types of products. Q^+ represents an onium fragments, such pyridinium and ammonium.

1.5 Functionalizing the *closo*-decaborane cluster $[closo-B_{10}H_{10}]^{2-}$

Introduction of different groups to the apical positions (*i.e.* position 1 and 10) of a *closo*-decaborane cluster requires a good leaving group that can serve as a synthetic transformation tool through which other groups can be attached to the cluster.²⁷ Recently Kaszynski and Ringstrand²⁸ demonstrated the use of aryl iodonium zwitterions (ArI^+) to synthesize a broad spectrum of *closo*-borate derivatives. In this method, *closo*-decaborate is treated with $PhI(OAc)_2$ under acidic conditions to produce the bis **6** or mono **3** derivatives according to the reaction scheme below. (Scheme 1.1)



Scheme 1.1. Functional group transformation at the apical positions of *closo*-decaborane via an aryliodonium zwitterion.

1.6 Research Questions

The established strong interaction of *closo*-decaborane with aromatic substituents and preliminary theoretical calculations of [*closo*-B₁₀H₉-1-NC₅H₅], shows that the maximum wavelength of absorption in the molecule corresponds to a π - π^* transition between the HOMO localized on the cluster and the LUMO localized on pyridinium. Therefore, the following research questions arises:

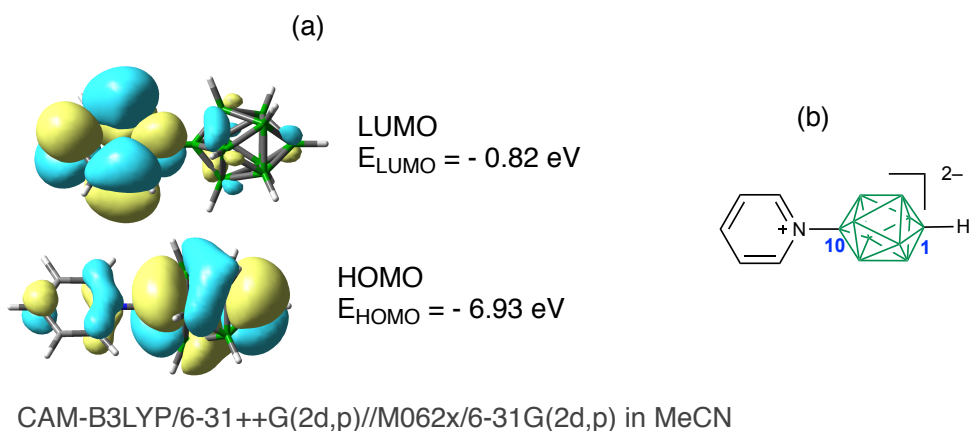


Figure 1.11. a) Frontier molecular orbitals of *closo*-B₁₀H₉-1-pyridinium showing the HOMO and LUMO energies b) structure of *closo*-B₁₀H₉-1-pyridinium showing positions 1 and 10 (apical positions).

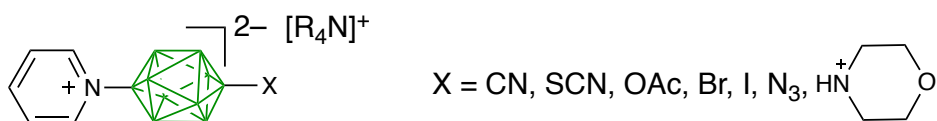
Is it possible to tune the absorption energies by modulating the energy gap between the HOMO and LUMO through:

- Modifying the energy of the HOMO via introduction of different substituents group to the boron atom of the cluster?
- Replacing pyridine with different azines such as pyrazine, pyridazine, pyrimidine, 4,4'-bipyridine and *p*-cyanopyridine?

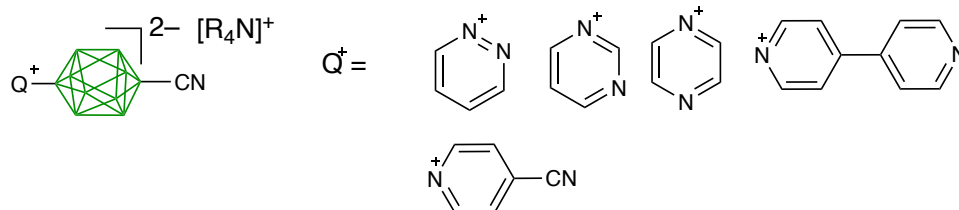
1.7 Research Objectives

In order to answer the research questions above, synthesis and photophysical measurements of the following compounds is planned:

Series 1: [*closo*-B₁₀H₈-1-X-10-NC₅H₅]⁻ [R₄N]⁺



Series 7: [*closo*-B₁₀H₈-1-CN-10-Q⁺]⁻ [R₄N]⁺



1.8 Thesis statement

The aim of this project is to a) synthesize and characterize, and b) investigate the photophysical properties of these derivatives and establish their absorption and emission energies with the ultimate goal of understanding the extent at which these properties can be tuned in our prototype system c) provide a predictive tool for the synthesis of compounds with desired colors based on *closo*-decaborane.

CHAPTER II

Tuning absorption energies via modifying the HOMO energies in [*closo*-B₁₀H₈-1-X-10-NC₅H₅]⁻ [R₄N]⁺

2.1 INTRODUCTION

The first objective of this thesis project as stated in Section 1.4, is to investigate the effect of nucleophilic substitution at the antipodal B1 boron (B-H) atom in the prototype system [*closo*-B₁₀H₉-NC₅H₅]⁻ anion (**1a**) on its HOMO energy. Controlling the HOMO energy invariably controls the HOMO – LUMO gap since the LUMO energy localized on the pyridine is relatively constant. To accomplish this aim, series **1** (Figure 2.1) were synthesized by attaching CN, OAc, N₃, I, SCN, Br and Morpholinium at the B1 position through nucleophilic substitution. Photophysical measurements were performed on pure compounds and correlated with Hammett parameters σ_p of the substituents. Structural properties were modeled with XRD and DFT calculations to augment experimental data. Most of the synthesis in these series were performed by me and Tegan Schafer with help from Dr. Szymon Kapuscinski who also synthesized a series **2** compound (details not discussed here) with the aim of perturbing the energy of the LUMO by introducing different substituent group to pyridine at the antipodal position. Dr Andrienne Friedli performed the photophysical measurements, Dr. Anna Pietrzak and Dr. Oleksandr Hietsoi collected and analyzed XRD data, while Dr. Piotr Kaszynski performed the computational modeling.

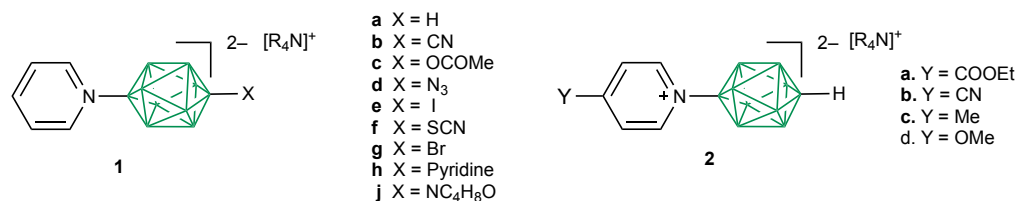


Figure 2.1. Series **1** and **2**

2.2 RESULTS AND DISCUSSION

2.2.1 Synthesis. Two synthetic approaches to series **1** were developed over the course of this research. The first method was inspired by previous work²⁸ that demonstrates that the monoiodonium derivative [*closo*-B₁₀H₉-1-IPh]⁻ (**3**[Et₄N]) undergoes nucleophilic substitution with pyridine to give **1a**[Et₄N], and with the CN⁻ anion giving [*closo*-B₁₀H₉-1-CN]²⁻ 2[Et₄N]⁺ (**4b**[Et₄N]) in good yields. This suggested a three-step method for the preparation of series **1** through the intermediate [*closo*-B₁₀H₈-1-IPh-10-X]⁻ (**5**, method A, Figure 2). The second method was also adopted from the same paper, it involves reacting bisiodonium [*closo*-B₁₀H₈-1,10-2(IPh)] (**6**) with AcO⁻ giving monosubstituted product **5c** with high selectivity,²⁸ suggesting the possibility of a two-step process leading to **1** as shown in Figure 2.2 (method B).

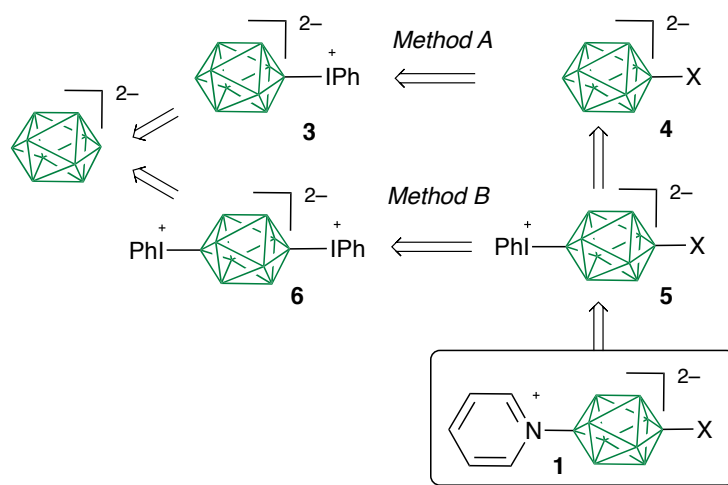
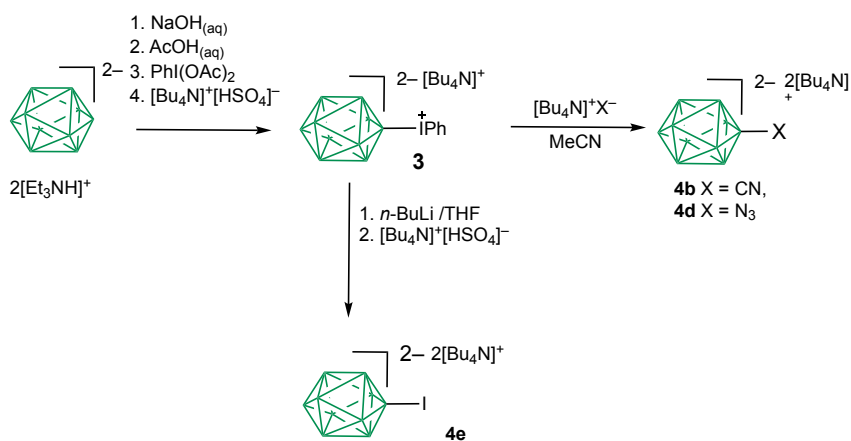


Figure 2.2. Two synthetic approaches to the preparation of series 1.

The initial synthesis of series 1 focused on the three-step method using **3**[Bu₄N], which is more convenient than the **3**[Et₄N] salt.²⁹ To determine the scope of the method, the reactivity of **3**[Bu₄N] with several nucleophiles X⁻ or XH (1:1.1 ratio in a 25 mM solution in MeCN at 60 °C) was screened in NMR tubes. The progress of each reaction was monitored with ¹¹B NMR spectroscopy as the rate of disappearance of the starting anion **3**. Results demonstrated that only the N₃⁻ nucleophile reacted cleanly to give the expected azide substitution product [*closo*-B₁₀H₉-1-N₃]²⁻ (**4d**). The reaction of **3** with the CN⁻ anion was slower and the expected product was contaminated with small amounts of a side product resulting from the decomposition of **3**, which is thermally unstable, and completely decomposes after 16 hr in MeCN at 55-60 °C in the absence of any nucleophile. Other nucleophiles, SCN⁻, AcO⁻, morpholine, pyridine, Br⁻ and I⁻, gave complex mixtures of products in which the desired product was either a minor component, or was not formed at all (pyridine, Br⁻, and I⁻). Consequently, method A could be practical for preparation of only **1d**. Thus, **3**[Bu₄N] was smoothly reacted with 1.1 eq of [Bu₄N]⁺N₃⁻ and the resulting

azide **4d**[Bu₄N] was isolated in 95% yield by column chromatography followed by recrystallization (Scheme 1). It was subsequently converted to phenyliodonium derivative **5d**[Bu₄N] by reacting with PhI(OAc)₂ in MeCN, and the resulting product was reacted with pyridine to give **1d**[Bu₄N] in 55% yield for the two step process (Scheme 2.1).

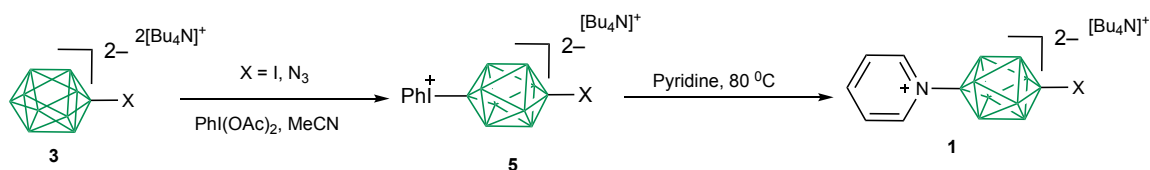


Scheme 2.1. Synthesis of intermediates **4**.

The iodo derivative **1e**[Bu₄N] was obtained in 29% overall yield by reacting iodide **4e**[Bu₄N], obtained from **3**[Bu₄N] according to a literature method (Scheme 2.1),²⁹ with PhI(OAc)₂ in MeCN followed by the reaction of the resulting [*clos*-B₁₀H₈-1-I-10-IPh]⁻ (**5e**[Bu₄N]) with pyridine (method A, Scheme 2.2). An alternative method for obtaining **5e**[Bu₄N] directly from bisiodonium **6** with controlled amounts of BuLi or NaOEt was much less efficient, and the desired product was isolated in 25% yield by column chromatography from a complex mixture of products.

The preparation of acetoxy, thiocyno, and bromo derivatives **1c**[Et₄N], **1f**[Et₄N] and **1g**[Et₄N] was accomplished using the bisiodonium derivative **6** according to method

B. Thus, acetate **5c**[Et₄N], prepared as described before from **6**,²⁸ was reacted with excess pyridine to yield the desired product **1c**[Et₄N] in 74% yield. A similar reaction of **6** with 1.5 eq of [Et₄N]⁺SCN⁻ in MeCN at 60 °C gave a mixture of products, from which **5f**[Et₄N] was isolated by column chromatography in 16% yield. The subsequent reaction of **5f**[Et₄N] with excess pyridine gave **1f**[Et₄N] in a nearly quantitative yield. Bromide **1g**[Et₄N] was obtained in 50% overall yield from **6** in the same sequence of reactions in 56% and 90% yield for **5g**[Et₄N] and **1g**[Et₄N], respectively (Method B, scheme 2.3). It was observed that chromatographic purification occasionally removes a portion of the [R₄N]⁺ counterion, presumably replacing it with a proton. To restore the correct ratio of [R₄N]⁺ these products were dissolved in CH₂Cl₂ and washed with a dilute aqueous solution of appropriate [R₄N]⁺OH⁻.

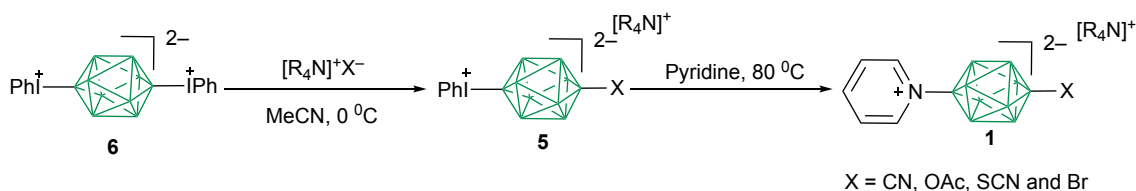


Scheme 2.2. Preparation of **1d** and **1e** using method A.

In an attempt to simplify the preparation of **1b**[Bu₄N], bisiodonium **6** was reacted with 1.1 eq of the [Bu₄N]⁺CN⁻ in MeCN at 55 °C. The resulting mixture contained the desired **5b**[Et₄N] as the main component, which was purified by column chromatography to give 53% yield of pure product.

This route to **5b**[Bu₄N] turned out to be more convenient, although poor solubility of the bisiodonium **6** in the reaction medium complicated the process (Scheme 2.3).

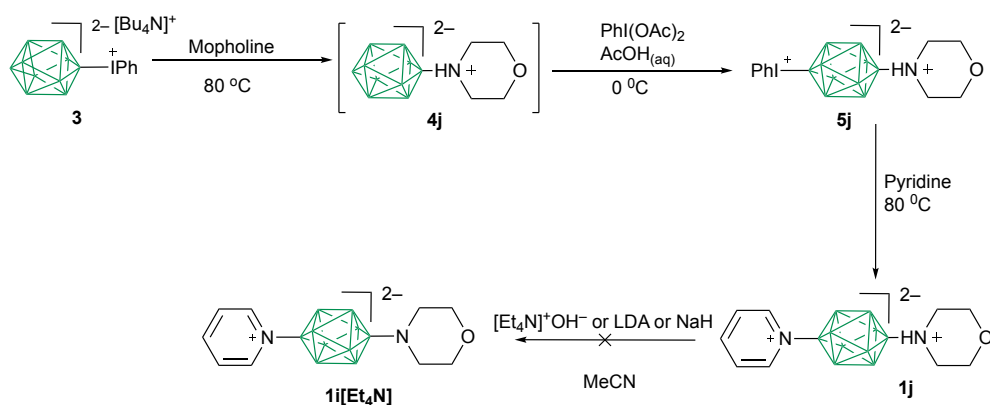
Method B was also tested for one-pot preparation of the azide **1d**[Bu₄N], yielding 70% of pure product based on **6** before recrystallization. Using Method B and partial purification (or one-pot reaction) of intermediates **5**, any unreacted **6** was converted to **1h** during the reaction with pyridine.



Scheme 2.3: Preparation of **1b**, **1c**, **1f** and **1g** from **6** via Method B

Preparation of the morpholine derivative **1i** required a different approach. Since morpholine did not react with **3**[Bu₄N] in MeCN solution (method A) and was not selective enough for method B, **3**[Bu₄N] was treated with neat morpholine at 85 °C in analogy to reactions with pyridine (Scheme 4). The resulting complex mixture of products was reacted with PhI(OAc)₂ in AcOH and the bis zwitterion **5j** was isolated in 32% yield by column chromatography. The subsequent reaction of **5j** with neat pyridine gave the morpholinium derivative **1j** in 32% yield. Deprotonation of the morpholinium group in **1j** with [Et₄N]⁺ OH⁻ in MeCN solutions turned out to be challenging and the formation of the expected **1i**[Et₄N] under these conditions was not confirmed by NMR or UV spectroscopy. Evidence

suggests quick decomposition of the anion, presumably due to basic attack on the pyridine ring.



Scheme 2.4. Preparation of **1j** and attempted deprotonation to **1i**.

2.2.2 Crystal and molecular structures

Yellow-greenish triclinic crystals of **1b**[Et₄N] and **1g**[Et₄N] and monoclinic crystals of **1c**[Et₄N] and **1j** were obtained from acetonitrile/ethanol solutions upon cooling. Monoclinic crystals of **1d**[Bu₄N] and **1e**[Et₄N] were grown from acetonitrile /ethyl acetate solutions. Orthorhombic crystals of **1f**[Et₄N] were obtained by slow evaporation of acetonitrile / CH₂Cl₂ solutions. Selected bond lengths and angles are collected in Table 2.1. Molecular structures for all eight new derivatives are shown in Figures 2.1 and 2.2.

Crystal systems of most salts **1** contain a single ion pair in the asymmetric unit, while **1f**[Et₄N] and the previously reported **1a**[Et₄N] contain two anions and two cations. Among the anions only the thiocyno derivative **1f** exhibits positional disorder of the SCN group in both unique molecules. In contrast, the [R₄N]⁺ cation is positionally disordered in

most salts with the exception of **1b**[Et₄N] and **1e**[Et₄N] and **1g**[Et₄N]. Additionally, **1g**[Et₄N] co-crystallizes with an acetonitrile molecule highly disordered around the special position. Therefore, the solvent molecule was removed from the model by the SQUEEZE tool.

The intracage dimensions of the anions, such as B–B bond distances and angles, are typical for {*closo*-B₁₀} derivatives (Table 2.1). In general, the more electron withdrawing the substituent, the more contracted the {*closo*-B₁₀} cage. This is evident from the comparison of the B(1)···B(10) distance in the parent anion [*closo*-B₁₀H₁₀]²⁻ (**A**, 3.717(4) Å, monopyridinium **1b**–**1g** (avg 3.636(14) Å) and bis-zwitterion **1j** (3.611(2) Å). The response to the substituent is largely localized at the substitution apex, which results in contraction of the square pyramid (distance from the equatorial belt). Thus, substitution of the parent anion **A** with pyridinium results in contraction of the pyramid from 1.100 Å to 1.056 Å in **1a**, which remains nearly constant in the series (Table 1). The pyramid height of the opposite apex is hardly affected by the substitution with the pyridinium, but responds to the presence of the substituent in a range from 1.095 Å for **1a** (X = H) to 1.060 for **1e** (X = I). An attempted correlation analysis of the substituent effect on the {*closo*-B₁₀} cluster geometry shows the trend mentioned above, but very poor correlation with Hammett σ_p parameters. As was noted previously,²⁹ iodine and CN have unusually strong effects on properties of boron cluster derivatives, qualitatively different from those in benzene derivatives.

TABLE 2.1. Selected Interatomic distances and angles for series **1**^a

	A[Q] ^b	1a[E ₄ N] ^{c,d} H	1b[E ₄ N] CN	1c[E ₄ N] AcO	1d[Bu ₄ N] N ₃	1e[E ₄ N] I	1f[E ₄ N] ^c SCN	1g[E ₄ N] Br	1j MrpH
B(10)–N	–	1.529(3)	1.524(2)	1.530(3)	1.527(2)	1.527(6)	1.528(13)	1.523(2)	1.523(2)
B(1)–Nu	–	–	1.543(2)	1.462(3)	1.510(2)	2.193(5)	1.879(11)	1.982(2)	1.547(2)
B(1)–B(6) avg	1.702 (3)	1.680(5)	1.682(4)	1.681(4)	1.684(5)	1.683(5)	1.681(5)	1.684(7)	1.677(4)
B(10)···B(6- 9) ^f	1.100	1.056	1.052	1.054	1.057	1.058	1.055(5)	1.055	1.049
B(6)–B(7) avg	1.835(9)	1.848(6)	1.856(14)	1.852(7)	1.854(5)	1.851(5)	1.851(15)	1.855(10)	1.850(7)
B(2)–B(6) avg	1.813(6)	1.809(6)	1.8011(6)	1.809(5)	1.808(6)	1.809(10)	1.8010(17)	1.810(4)	1.809(4)
B(2)–B(3) avg	1.835(9)	1.837(7)	1.853(2)	1.846(12)	1.848(5)	1.846(11)	1.851(5)	1.852(5)	1.846(7)
B(2)–B(1) avg	1.701(3)	1.699(6)	1.696(4)	1.698(6)	1.693(5)	1.682(10)	1.685(11)	1.689(5)	1.679(4)
B(1)···B(2- 5) ^f	1.100	1.095	1.077	1.086	1.076	1.060	1.061(1)	1.066	1.055
B(1)···B(10)	3.717(4)	3.660(4)	3.637(2)	3.647(3)	3.639(2)	3.624(7)	3.619(14)	3.628(3)	3.611(2)
B–B(10)–N	130.3(12)	129(2)	128.7(12)	128.8(4)	128.9(16)	129(2)	129.2(12)	128.9(14)	128.7(18)
B–B(1)–Nu	130.3(12)	130.1(2)	129(2)	130(5)	129.5(8)	129.1(13)	129(4)	129(2)	129(3)
Pyrr/{B1} ^g	–	24.0/34.0	1.2	14.3	27.8	19.5	4.6/10.8	14.4	6.2

^aExcept for unique interatomic distances, all parameters are average values and the esd refers to distribution of individual measurements. ^b Ref 30 ^c 2 molecules. ^d Ref 31. ^e {*c*-*loso*-B₁₀} treated as *D*_{4d} symmetric. ^f The height of the tetragonal pyramid. ^g Deviation (in °) from the ideal staggered orientation of pyridine.

The pyridine–B(10) distance is essentially the same in the entire series (within the experimental error) and 1.527(3) Å for all 8 derivatives. The orientation of the pyridine ring varies from nearly ideally staggered in **1b** to more than half way between staggered and eclipsed (34 ° off the staggered conformation in **1a**, Table 2.1). Orientation of functional groups, AcO, N₃ and SCN is about half way between staggered and eclipsed conformations, while the morpholinium group adopts a nearly ideal staggered orientation with respect to the {*closo*-B₁₀} cage (7.1 ° off the ideal staggered).

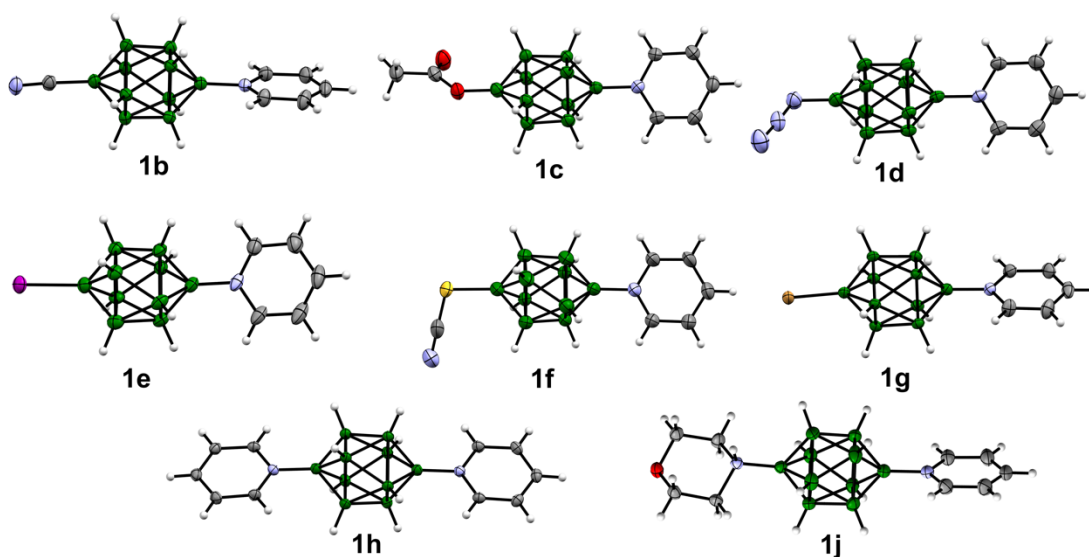


Figure 2.3. Atomic displacement ellipsoid representation of **1b–1h** and **1j** for geometrical dimensions see Table 1 and text. In **1b–1g** counterions are omitted for clarity and in **1f** only one unique molecule is shown. The corresponding ellipsoids are at the 50% probability level and the numbering system is according to the chemical structure.

The B(1)–X distances in derivatives **1** are typical for other derivatives of the [*closo*-B₁₀H₁₀]²⁻ anion containing B(1)–CN,³² B(1)–OCOR,³² B(2)–OCOR^{33,34} B(1)–I,^{29,35} B(1)–SCN, and B(2)–Br,³⁶ and B(1)–NH₃ substituents. The azido group in **1d** is the first example of such a *closo*-borane derivative. It is nearly linear with the angles $\alpha_{\text{N-N-N}} = 175.6(2)^\circ$ and $\alpha_{\text{B-N-N}} = 120.9(1)^\circ$. Interestingly, the N(1)–N(2) and N(2)–N(3) distances are similar (1.185(2) and 1.154(2) Å, respectively) and much different from those in typical organic azides (*e.g.* 1.247(2) and 1.120(2) Å). This is consistent with a significant shift in the negative charge to the terminal nitrogen atom (N3) and significant contribution from the second resonance structure ($\text{R-N}^--\text{N}^+\equiv\text{N} \leftrightarrow \text{R-N}=\text{N}^+=\text{N}^-$).

The supramolecular assembly of the cyano derivative **1b**[Et₄N] appears to be isostructural to that observed in bromo derivative **1g**[Et₄N] (Figure 2.4). The unit cell dimensions *c* are nearly the same for **1b**[Et₄N] and **1g**[Et₄N], while dimensions *a* and *b* are slightly different in the two structures. The resulting unit cell identity parameter³⁷ $\Pi = 0.0006$ indicates a strong resemblance between these two unit cells. Moreover, their crystal structures adopt similar molecular packing. In both structures, molecules of **1b** and **1g** are assembled in infinite chains running along the [100] direction. These chains are stabilized by C–H⋯B interactions between the pyridine C–H fragment and the boron cluster. The respective intermolecular contacts in **1b**[Et₄N] and **1g**[Et₄N] are 0.337 Å and 0.274 Å shorter than the vdW radii. Additionally, neighboring chains are associated through B⋯C interactions between a boron moiety and a fragment of the pyridine ring. These contacts for **1b**[Et₄N] and **1g**[Et₄N] are -0.181 Å and -0.127 Å inside the van der Waals separation, respectively. The resulting double chains running along the [100] direction are separated from each other by counterion molecules. Although iodine is regarded as an isomorphous

substituent for bromine, the crystal packing of **1e**[Et₄N] is completely different to those observed in **1b**[Et₄N] and **1g**[Et₄N]. However, the molecular assembly in **1e**[Et₄N] is affected by the presence of the solvent molecule in the crystal lattice.

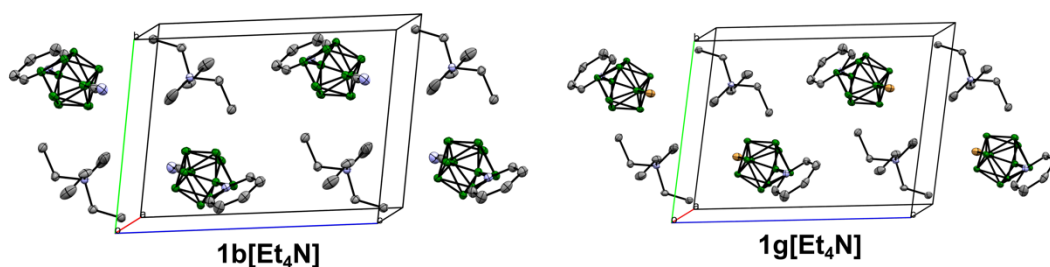


Figure 2.4. Packing diagram for **1b**[Et₄N] and **1g**[Et₄N]. Hydrogen atoms are omitted for clarity. The atomic displacement ellipsoid diagram is drawn at 50% probability.

2.2.3 Photophysical properties

Electronic absorption and emission spectra for selected pyridinium derivatives **1** were recorded in MeCN and results are shown in Table 2.2 and Figures 2.5 and 2.6.

Analysis of data in Figure 2.5 and Table 2.2 indicates that all eight derivatives exhibit two absorption bands. The bands with λ_{max} above 300 nm which corresponds to absorption energy around 4 eV have a narrow range of values (0.38 eV) with similar extinction coefficients ($-\log \varepsilon = 3.9$). These results are consistent with those for other derivatives of the [closo-B₁₀H₁₀]²⁻ anion.^{38,39,40,31} The absorption energy in series **1** depends on the substituents, and in general, the more electron donating the substituent, the lower the excitation energy in agreement with expectation (Table 2.2). The observed trend

in absorption energy correlates linearly with the Hammett parameter⁴¹ σ_p for the B(1) substituents, although several points lie off the trendline.

Solutions of the pyridinium derivatives **1** fluoresce weakly with the emission energy lower by about 1.4 eV (Figure 2.6, Table 2.2). This sizable Stokes shift is consistent with our previous findings.^{38,39}

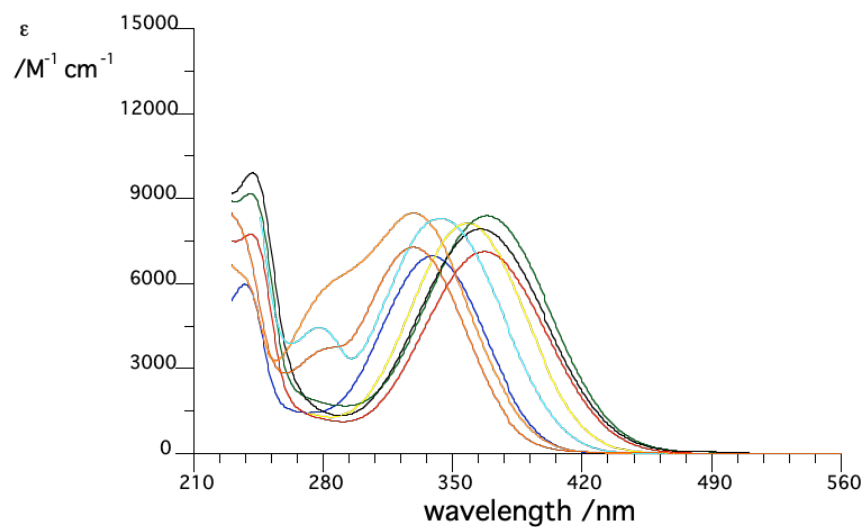


Figure 2.5. Electronic spectra of series **1** in MeCN. **1a** (red), **1b** (dark blue), **1c** (green), **1d** (black), **1e** (pink), **1f** (light blue), **1g** (yellow), **1j** (orange).

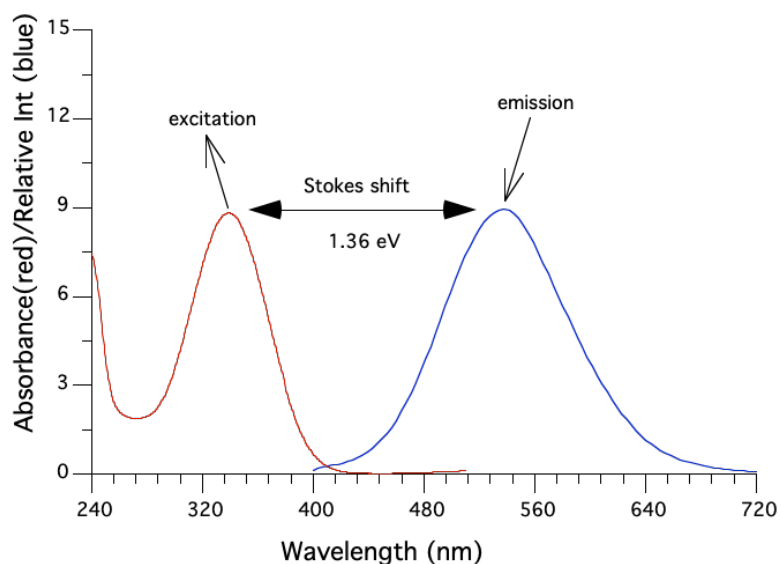


Figure 2.6. UV (red) and fluorescence (blue) spectra for **1b**

TD-DFT calculations in MeCN dielectric medium at the CAM-B3LYP/Def2TZVP // B3LYP/Def2TZVP level of theory reproduced the trend in experimental excitation energies, overestimated by an average of 0.56 eV. The lowest energy absorption bands involve a transition from the HOMO, localized primarily on the boron cluster and the B(1) substituent, to the LUMO, localized on the pyridinium fragment, as shown for **1b** in Figure 2.7.

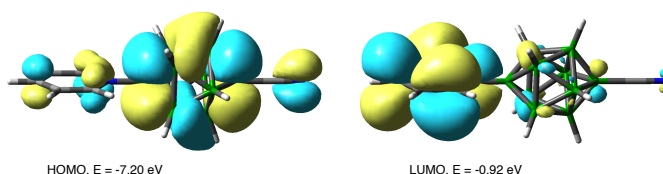


Figure 2.7. Frontier molecular orbitals of **1b** in MeCN dielectric medium relevant to the lowest-energy excitation. Derived from TD-DFT/CAM-B3LYP/Def2TZVP // B3LYP/Def2TZVP calculation.

Table 2.2. Selected experimental^a and calculated^b electronic transition energies and oscillator strength values.

Compound	X	Experimental ^a			Theoretical ^b	
		Absorption λ_{\max} /nm (log ϵ)	Absorption λ_{\max} /nm	Absorption Energy /eV ^c	Emission ^d λ_{\max} /nm (Stokes Shift /eV)	$\pi \rightarrow \pi^*$ /nm (<i>f</i>)
1a	H	366 (3.) ^e	241 ^e	3.39	569 (1.21)	312.5 (0.291)
1b	CN	339.5 (3.85)	237.5	3.65	540 (1.36)	295.7 (0.334)
1c	OAc	368.5 (3.92)	240.5	3.36	<i>n/a</i>	316.1(0.278)
1d	N ₃	344 (3.90)	238	3.60	554 (1.37)	322.6 (0.328)
1e	Br	358.5 (3.92)	241.5	3.45	<i>n/a</i>	306.8 (0.314)
1f	I	329.5 (3.93)	-	3.76	<i>n/a</i>	305.3 (0.332)
1g	SCN	344.5 (3.79)	239	3.59	555 (1.37)	306.6 (0.324)
1h	Pyr	358.5 (4.20)		3.45	527 (1.34)	
1j	Morph	329 (3.85)	218	3.77	530 (1.43)	

^aRecorded in MeCN. ^b Obtained with the TD CAM-B3LYP/6-31++G(2d,p)/B3LYP/TZVP method in MeCN dielectric medium and shifted by 0.56 eV. ^c Energy corresponding to charge transfer transition. ^dExcitation at the wavelength of maximum absorption. ^eRef. 39

Computational analysis of trends in series **1**, expanded to include the B(1)-OEt derivative **1k**, demonstrates that the DFT calculated excitation energies correlate linearly with the Hammett σ_p parameters⁴¹ for the B(1) substituent (Figure 2.8). Correlation is of high quality for most derivatives with the exception of the heavy halogens, Br and I. Different basis sets and pseudo potentials were used for compounds including halogens. It is unclear why the parent **1a** is also outside the correlation.

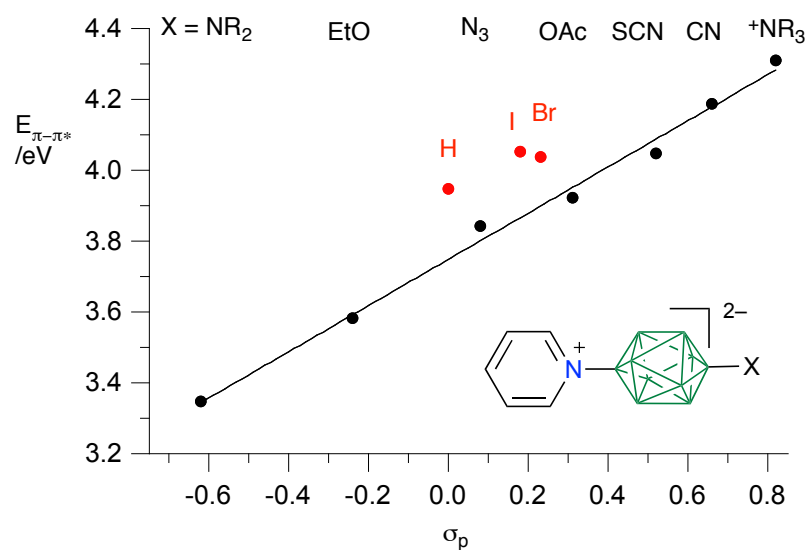


Figure 2.8. Correlation of DFT-calculated lowest excitation energy for series **1** with substituent parameter σ_p . Best fit line for black data points: $E_{\pi-\pi^*} = 3.75(1) + 0.651(26) \times \sigma_p$, $r^2 = 0.993$.

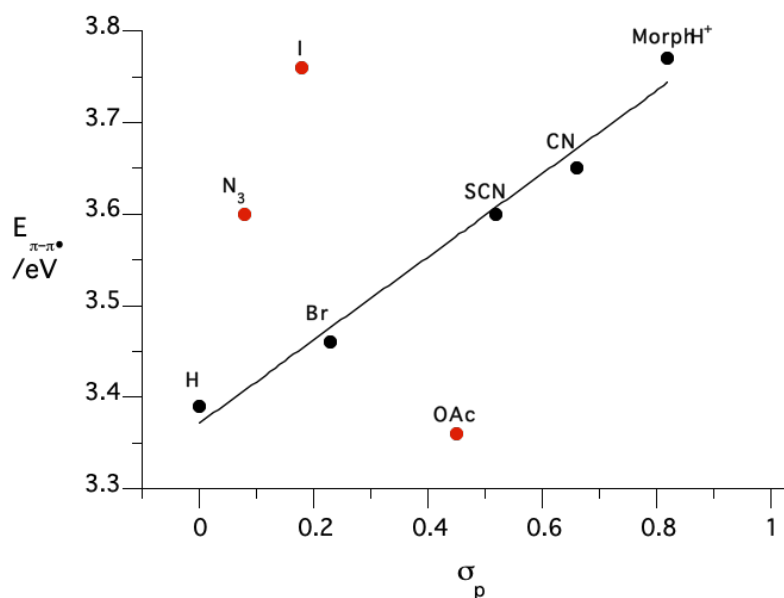


Figure 2.9. Correlation of experimental data for series **1** with substituents I, Br, CN, SCN, MorphH⁺. The Hammett parameter for NMe₃⁺ was used for **1j**. data points that do not fit the linear relationship are shown in red: N₃, I, and OAc. Best fit line for black data points: $E_{\pi-\pi^*} = 0.45378x + 3.716$; $R^2 = 0.9901$.

Inspection of the calculated FMO energies (Figure 2.10) reveals that the substituent effect on the excitation energy mainly affects the energy of the HOMO, which is 10 times more sensitive to the substituent than the energy of the LUMO. This is consistent with the distribution of the orbital density in the two FMO's and essentially electronic decoupling of the LUMO localized on the pyridine ring from the B(1) substituent, as shown in Figure 2.7. Consequently, the B(1) substituent controls energy of the HOMO and hence the HOMO–LUMO gap. Thus, the more electron donating the substituent, the higher the HOMO, the lower the HOMO–LUMO gap, and the larger the bathochromic shift.

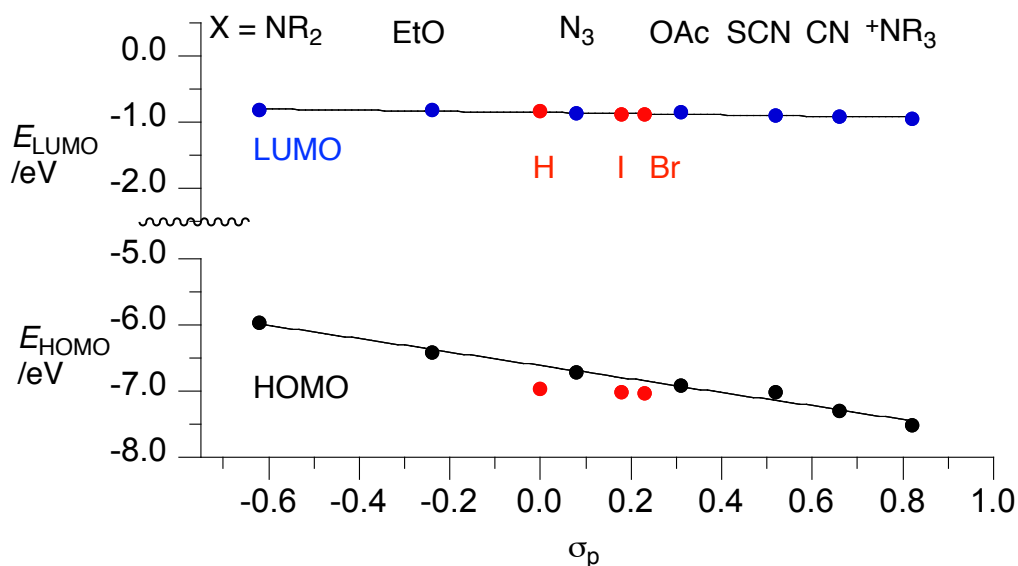


Figure 2.10. Correlation of the energy of the HOMO and the LUMO in series 1 with substituent parameter σ_p . Best fit line for black data points: $E_{\text{HOMO}} = -6.62(3) - 1.01(6) \times \sigma_p$, $r^2 = 0.985$; $E_{\text{LUMO}} = -0.859(8) - 0.086(16) \times \sigma_p$, $r^2 = 0.851$.

2.2 CONCLUSIONS

Functionalization of *closo*-decaborane through two synthetic strategies using phenyliodonium intermediates was demonstrated as an efficient method for synthesis of series **1**. The three-step approach starting from monoiodonium **3** was found to be suitable for X = N₃, I, and morpholinium derivatives, giving 29, 55, and 32 % yield of the respective products **1d**, **1e**, and **1j**. The two-step approach from the bisiodonium **6** was more efficient for X = CN, OAc, SCN, and Br in 55, 74, 16, and 50 % yield, respectively. Electronic absorption spectra revealed a significant shift in the wavelength of maximum absorption (λ_{max} 329.5 nm for X = MorphH⁺ to 368 nm for X = OAc) as more electron withdrawing substituents are attached to the cluster (hypsochromic shift). The observed trend in absorption energy correlates linearly with Hammett parameters with the exception of I, N₃, and OAc. Trends in calculated absorption energy are similar to the experimental trend with few exceptions. DFT calculations shows that variation in λ_{max} is related to the perturbation of HOMO energies (0.588 eV range) rather than the LUMO energies (0.059 eV range).

2.3 Computational Details

Quantum-mechanical calculations were carried out using Gaussian 09 suite of programs. Geometry optimizations were undertaken at the B3LYP/TZVP level of theory using tight convergence limits and appropriate symmetry constraints. All calculations were performed in PhCl dielectric medium (arbitrarily chosen) with the PCM model requested with SCRF(Solvent= C6H5Cl) keyword, since it was demonstrated that low dielectric medium is important for obtaining accurate geometry of zwitterions such as **1**. Calculations involving iodine and bromine used the LANL2DZdp effective core potential basis set (available from <http://www.emsl.pnl.gov/forms/-basisform.html>) and 6-31G (2d, p) for the remaining elements implemented with the GEN keyword. The ground state nature of stationary points for the obtained equilibrium geometry was confirmed with vibrational frequency calculations.

In order to use a uniform basis set for all elements, calculations of geometry, electronic excitations and NMR shielding constants were performed at the B3LYP/Def2TZVP level of theory taking molecular geometries obtained at the B3LYP/TZVP level as the starting points. All geometry optimizations were performed in PhCl dielectric medium using the PCM model requested with the SCRF(Solvent= C6H5Cl) keyword.

Electronic excitation energies for series **1** in MeCN dielectric medium were obtained at the CAM-B3LYP/Def2TZVP // B3LYP/Def2TZVP level of theory using the time-dependent DFT method supplied in the Gaussian package. The equilibrium geometry for each compound was obtained in PhCl dielectric medium (*vide supra*). The solvation model was implemented with the PCM model using SCRF(solvent=CH3CN) keyword.

Isotropic magnetic shielding factors for **A** and derivatives **1** and **4** were calculated at the CAM-B3LYP/Def2TZVP//B3LYP/Def2TZVP level of theory using the NMR=GIAO method in acetone dielectric medium requested with the SCRF(Solvent=Acetone) keywords (PCM model). The Chemical shifts were calculated using anion **A** (for ^{11}B) and benzene (for ^1H) as the reference.

2.4 EXPERIMENTAL SECTION

2.4.1 General. Reactions were carried out under Ar and subsequent manipulations were conducted in air. Literature procedures were used to synthesize [*closo*-B₁₀H₁₀]²⁻ 2[Et₃NH]⁺ (**A**[Et₃NH])⁴² and **3**[Bu₄N]²⁹ and [Et₄N]⁺SCN⁻ was synthesized by ion pair extraction to CH₂Cl₂ from an aqueous solution of equimolar [Et₄N]⁺ Cl⁻ and KSCN. NMR spectra were obtained at 500 MHz (^1H), 125 MHz (^{13}C) and 160.5 MHz (^{11}B) in acetone-*d*₆ unless otherwise indicated. Chemical shifts were referenced to the solvent (^1H and ^{13}C : 2.05 ppm and 29.84 ppm for acetone-*d*₆) or an external sample of neat BF₃•Et₂O in acetone-*d*₆ (^{11}B , $\delta = 0.0$ ppm). ^{11}B NMR chemical shifts are reported from { ^1H } decoupled spectra. IR spectra were recorded for neat samples using an ATR attachment. HR mass spectrometry was conducted with the TOF-MS ESI method in the negative mode at the Mass Spectrometry and Proteomics Facility at University of Notre Dame. Elemental analyses for C, H, N were run at Atlantic Microanalysis with V₂O₅ catalyst. UV-*vis* spectra were recorded in spectroscopic grade MeCN at concentrations in a range of 1–10 x 10⁻⁵ M. Molar extinction coefficients ϵ were obtained by fitting the maximum absorbance against concentration in agreement with Beer's law. Fluorescence was recorded using an Hitachi

F-4500 Fluorescence Spectrophotometer. The excitation wavelength was set to the absorbance λ_{max} and λ_{em} was scanned from $\lambda_{\text{max}} + 50$ nm to 900 nm.

2.3.2 X-Ray data collection. Single-crystal X-ray diffraction measurements were conducted at 100.0(2) K using the $\text{CuK}\alpha$ radiation ($\lambda = 1.54184$ Å). The data was integrated using CrysAlisPro program. Intensities for absorption were corrected using SCALE3 ABSPACK scaling algorithm implemented in CrysAlisPro program.⁴³

2.3.3. Synthetic Methods

General procedure for preparation of $[\textit{closo}\text{-B}_{10}\text{H}_8\text{-1-X-10-NC}_5\text{H}_5]^- [\text{R}_4\text{N}]^+$ (**1**[**R**,**N**]) from $[\textit{closo}\text{-B}_{10}\text{H}_8\text{-1-X-10-IPh}]^- [\text{R}_4\text{N}]^+$ (**5**[**R**,**N**]). Iodonium derivative **5**[**R**,**N**] (0.2 mmol) was dissolved in dry pyridine (1 mL) and heated at 80 °C overnight. Volatiles were removed in vacuum, the semisolid residue was washed with hexanes and then with dilute HCl, dried and then purified by column chromatography (SiO_2 , MeCN/ CH_2Cl_2) giving the desired product **1**[**R**,**N**] as the first main fraction.

$[\textit{closo}\text{-B}_{10}\text{H}_9\text{-1-NC}_5\text{H}_5]^- [\text{Bu}_4\text{N}^+]$ (**1a**[**Bu**,**N**]).²⁸ Starting with **5a**: 24 mg (51% yield); yellow powder, $R_f = 0.2$ (MeCN/ CH_2Cl_2 1:15); mp 167 °C; ^1H NMR (500 MHz, acetone- d_6) δ 0.03–1.22 (m, 8H), 0.97 (t, $J = 7.4$ Hz, 12H), 1.43 (sex, $J = 7.4$ Hz, 8H), 1.81 (quin, $J = 8.0$ Hz, 8H), 3.34 – 3.51 (m, 8H), 3.88 (br q, $J = 145.9$ Hz, 1H), 7.90 (t, $J = 7.2$ Hz, 2H), 8.35 (t, $J = 7.7$ Hz, 1H), 9.57 (d, $J = 5.4$ Hz, 2H); ^{13}C NMR (126 MHz, acetone- d_6) δ 13.9, 20.4, 24.5, 59.5, 126.5, 141.4, 148.8; ^{11}B NMR (160 MHz, acetone- d_6) δ -27.4 (d, $J = 135$ Hz, 4B), -23.4 (d, $J = 130$ Hz, 4B), 4.7 (d, $J = 146$ Hz, 1B), 13.9 (s, 1B); UV (MeCN)

λ_{\max} (log ϵ) 366; IR, ν 2966, 2930, 2876, 2467 (BH), 1470, 1160, 1007, 778, 692; HRMS (ESI, -) m/z calcd. for $C_5H_{14}B_{10}N$: 198.2062. Found: 198.2052.

Anal. Calcd. for $C_{21}H_{50}B_{10}N_2$: C, 57.49; H, 11.49; N, 6.39. Found: C, 57.70; H, 11.56; N, 6.29.

[*closo*-B₁₀H₈-1-CN-10-NC₅H₅]⁻[Bu₄N]⁺ (1b**[Bu₄N]).** Starting with **5b**: 56 mg (60% yield) pale yellow-green crystals from MeCN/EtOH; $R_f = 0.71$ (9% MeCN in CH₂Cl₂); mp 180 °C; ¹H NMR (500 MHz, acetone-*d*₆) δ 0.44-1.24 (br m, 8H), 0.97 (t, $J = 7.4$ Hz, 12H), 1.43 (sex, $J = 7.4$ Hz, 8H), 1.81 (quin, $J = 8.0$ Hz, 8H), 3.42 (m, 8H), 7.99 (t, $J = 7.1$ Hz, 2H), 8.45 (t, $J = 7.7$ Hz, 1H), 9.53 (d, $J = 5.3$ Hz, 2H); ¹³C NMR (126 MHz, acetone-*d*₆) δ 13.9, 20.4, 24.5, 59.5, 127.0, 142.6, 148.7; ¹¹B NMR (160 MHz, acetone-*d*₆) δ -24.5 (d, $J = 151$ Hz, 4B), -23.4 (d, $J = 142$ Hz, 4B), -4.9 (s, 1B), 19.0 (s, 1B); IR ν 3087, 2970, 2943, 2876, 2480 (B-H), 2188 (CN), 1483, 1460, 1209, 1155, 988, 894, 782, 687, 629 cm⁻¹; UV (MeCN) λ_{\max} (log ϵ) 339.5 (3.85); HRMS (ESI, -) m/z calcd. for $C_6H_{13}B_{10}N_2$: 223.2009. Found: 223.2038.

[*closo*-B₁₀H₈-1-OAc-10-NC₅H₅]⁻[Et₄N]⁺ (1c**[Et₄N]).** The product isolated from column chromatography was washed with a diluted solution of [Et₄N]⁺OH⁻. To balance the cation, solutions of **1**[R₄N] in CH₂Cl₂ was washed with an aqueous solution of [R₄N]⁺OH⁻ and recrystallized, typically from MeCN/EtOH. Starting with **5c**²⁸ 57 mg (74% yield); pale yellow-green crystals from MeCN/EtOH; $R_f = 0.32$ (30% MeCN in CH₂Cl₂); mp 253 °C; ¹H NMR (500 MHz, acetone-*d*₆) δ 0.44-1.10 (br m, 8H), 1.38 (tt, $J_1 = 7.2$ Hz, $J_2 = 1.9$ Hz, 12H), 2.31 (s, 3H), 3.48 (q, $J = 7.3$ Hz, 8H), 7.90 (t, $J = 7.2$ Hz, 2H), 8.37 (t, $J = 7.7$ Hz,

1H), 9.57 (d, $J = 5.3$ Hz, 2H); ^{13}C NMR (126 MHz, acetone- d_6) δ 7.8, 23.2, 53.1, 126.6, 141.7, 149.3, 172.9; ^{11}B NMR (160 MHz, acetone- d_6) δ -28.6 (d, $J = 127$ Hz, 4B), -26.5 (d, $J = 129$ Hz, 4B), 11.3 (s, 1B), 24.0 (s, 1B); IR, ν 3016, 2993, 2467 (BH), 1690 (C=O), 1452, 1371, 1285, 1178, 998, 778, 692 cm^{-1} ; UV (MeCN) λ_{max} (log ϵ) 368.5 (3.92); HRMS (ESI, -) m/z calcd. for $\text{C}_7\text{H}_{16}\text{B}_{10}\text{NO}_2$: 256.2112. Found: 256.2141. Anal. Calcd. for $\text{C}_{15}\text{H}_{36}\text{B}_{10}\text{N}_2\text{O}_2$: C, 46.85; H, 9.44; N, 7.28. Found: C, 46.78; H, 9.34; N, 7.17.

[*closo*- B_{10}H_8 -1- N_3 -10- NC_5H_5] $^-$ [Bu_4N] $^+$ (1d**[Bu_4N]).** Starting with **5d**: 80 mg (83% yield); pale yellow-green crystals from MeCN/EtOAc; $R_f = 0.90$ (9% MeCN in CH_2Cl_2); mp 156 $^\circ\text{C}$; ^1H NMR (500 MHz, acetone- d_6) δ 0.52–1.25 (m, 8H), 0.97 (t, $J = 7.4$ Hz, 12H), 1.43 (sex, $J = 7.4$ Hz, 8H), 1.81 (quin, $J = 7.7$ Hz, 8H), 3.36–3.49 (m, 8H), 7.92 (t, $J = 7.1$ Hz, 2H), 8.39 (t, $J = 7.7$ Hz, 1H), 9.55 (d, $J = 5.3$ Hz, 2H); ^{13}C NMR (126 MHz, acetone- d_6) δ 13.9, 20.4, 24.5, 59.4, 126.7, 141.9, 149.1; ^{11}B NMR (160 MHz, acetone- d_6) δ -27.8 (d, $J = 132.2$ Hz, 4B), -25.6 (d, $J = 131$ Hz, 4B), 12.0 (s, 1B), 18.4 (s, 1B); IR, ν 2966, 2944, 2876, 2476 (BH), 2112 (N_3), 1470, 1425, 1380, 1200, 1146, 998, 881, 773, 692 cm^{-1} ; UV (MeCN) λ_{max} (log ϵ) 344.0 (3.90); HRMS (ESI, -), calcd. for $\text{C}_5\text{H}_{13}\text{B}_{10}\text{N}_4$: $m/z = 239.2071$. Found: 239.2048. Anal. Calcd. for $\text{C}_{21}\text{H}_{49}\text{B}_{10}\text{N}_5$: C, 52.57; H, 10.30; N, 14.60. Found: C, 52.53; H, 10.37; N, 11.62.

[*closo*- B_{10}H_8 -1- I -10- NC_5H_5] $^-$ [Bu_4N] $^+$ (1e**[Bu_4N]).** Starting with **5e**: 36 mg (32% yield); pale yellow-green crystals from ACN/EtOAc; $R_f = 0.93$ (9% MeCN in CH_2Cl_2); mp 192 $^\circ\text{C}$; ^1H NMR (500 MHz, acetone- d_6) δ 0.40–1.20 (br m, 8H), 0.97 (t, $J = 7.4$ Hz, 12H), 1.43 (sex, $J = 7.2$ Hz, 8H), 1.82 (d, $J = 7.9$ Hz, 8H), 3.34–3.52 (m, 8H), 7.94 (t, $J = 6.6$ Hz, 2H),

8.42 (t, $J = 7.7$ Hz, 1H), 9.53 (d, $J = 6.0$ Hz, 2H); ^{13}C NMR (126 MHz, acetone- d_6) δ 13.9, 20.4, 24.5, 59.5, 126.8, 142.1, 148.8; ^{11}B NMR (160 MHz, acetone- d_6) δ -23.6 (d, $J = 112$ Hz, 8B), -1.7 (s, 1B), 17.1 (s, 1B); IR, ν 3151, 3061, 2966, 2935, 2876, 2467 (BH), 1492, 1474, 1389, 1214, 1115, 993, 881, 769, 688 cm^{-1} ; UV (MeCN) λ_{max} (log ϵ) 329.5 (3.93); HRMS (ESI, -) m/z calcd. for $\text{C}_5\text{H}_{13}\text{B}_{10}\text{NI}$: 324.1023. Found: 324.1027. Anal. Calcd. for $\text{C}_{15}\text{H}_{38}\text{B}_{10}\text{IN}_2$: C, 34.51; H, 7.50; N, 6.19. Found: C, 34.02; H, 6.85; N, 5.74.

[*closo*- B_{10}H_8 -1-*I*-10- NC_5H_5] $^-$ [Et_4N] $^+$ (1e**[Et_4N])** via cation exchange. Dowex-50 ion exchange resin was freshly washed with wet methanol until eluate was transparent, and then with small amounts of dry methanol. The resin was used as a stationary phase for ion exchange chromatography for compound **1e**[Bu_4N]. A solution of **1e**[Bu_4N] (36 mg, 0.064 mmol) in MeOH/ CH_2Cl_2 (5:1) solvent mixture was passed through the resin pad (6.5 g) using methanol. Then $\text{Et}_4\text{N}^+\text{OH}^-$ was added dropwise to the acidic eluate until solution reached neutral pH (monitored with pH paper indicator). Solvents were removed under reduced pressure and the crude product was washed with water and crystallized from EtOH/MeCN solvent mixture to give 25 mg (86% yield) of pure product **1e**[Et_4N] as pale-yellow crystals; $R_f = 0.33$ (9% MeCN in CH_2Cl_2); mp 237 $^\circ\text{C}$. ^1H NMR (500 MHz, acetone- d_6) δ 0.37 – 1.29 (br m, 8H), 1.37 (tt, $J_1 = 7.2$ Hz, $J_2 = 1.9$ Hz, 12H), 3.46 (q, $J = 7.2$ Hz, 8H), 7.95 (dd, $J_1 = 7.7$ Hz, $J_2 = 6.7$ Hz, 2H), 8.43 (tt, $J_1 = 7.8$ Hz, $J_2 = 1.4$ Hz, 1H), 9.53 (d, $J = 5.3$ Hz, 2H); ^{13}C NMR (126 MHz, acetone- d_6) δ 7.8, 53.2, 126.8, 142.2, 148.7; ^{11}B NMR (160 MHz, acetone- d_6) δ -23.1 (d, $J = 96$ Hz, 8B), -1.5 (s, 1B), 17.4 (s, 1B); IR, ν 3070, 2989, 2926, 2854, 2476 (BH), 1703, 1623, 1483, 1465, 1398, 1249, 1205, 1169, 1065, 998, 841, 773, 688 cm^{-1} .

[closo-B₁₀H₈-1-SCN-10-NC₅H₅]⁻ [Et₄N]⁺ (1f**[Et₄N]).** Starting from **5f**: 10 mg (78% yield); pale yellow-green crystals from MeCN/CH₂Cl₂; R_f = 0.42 (9% MeCN in CH₂Cl₂); mp 182 °C; ¹H NMR (500 MHz, acetone-*d*₆) δ 0.31–1.23 (br m, 8H), 1.37 (tt, *J*₁ = 7.3 Hz, *J*₂ = 1.9 Hz, 12H), 3.45 (q, *J* = 7.3 Hz, 8H), 7.98 (dd, *J*₁ = 7.7 Hz, *J*₂ = 6.7 Hz, 2H), 8.44 (t, *J* = 7.8 Hz, 1H), 9.53 (d, *J* = 5.3 Hz, 2H); ¹³C NMR (126 MHz, acetone-*d*₆) δ 7.8, 53.2, 119.1, 127.0, 142.6, 148.8; ¹¹B NMR (160 MHz, acetone-*d*₆) δ -24.3 (d, *J* = 107 Hz, 4B), -23.9 (d, *J* = 104 Hz, 4B), 9.2 (s, 1B), 16.6 (s, 1B); IR, ν 3070, 2984, 2917, 2854, 2481 (BH), 2139 (CN), 1627, 1465, 1389, 1182, 1007, 876, 769, 692 cm⁻¹; UV (MeCN) λ_{max} (log ε) 344.5 (3.79); HRMS (ESI, -) *m/z* calcd. for C₆H₁₃B₁₀N₂S: 255.1730. Found: 255.1749. Anal. Calcd. for C₁₄H₃₃B₁₀SN₃: C, 43.84; H, 8.67; N, 10.95. Found: C, 43.83; H, 8.54; N, 10.76.

[closo-B₁₀H₈-1-Br-10-NC₅H₅]⁻ [Et₄N]⁺ (1g**[Et₄N]).** Starting with **5g**: 61 mg (75% yield); pale yellow-green crystals from MeCN/EtOH; R_f = 0.37 (9% MeCN in CH₂Cl₂); mp 228 °C; ¹H NMR (500 MHz, acetone-*d*₆) δ 0.38 – 1.25 (br m, 8H), 1.38 (tt, *J*₁ = 7.3 Hz, *J*₂ = 1.9 Hz, 12H), 3.47 (q, *J* = 7.3 Hz, 8H), 7.93 (dd, *J*₁ = 7.7 Hz, *J*₂ = 6.8 Hz, 2H), 8.41 (t, *J* = 7.7 Hz, 1H), 9.54 (d, *J* = 5.3 Hz, 2H); ¹³C NMR (126 MHz, acetone-*d*₆) δ 7.8, 53.2, 126.7, 142.0, 149.0; ¹¹B NMR (160 MHz, acetone-*d*₆) δ -24.8 (d, *J* = 113 Hz, 4B), -24.2 (d, *J* = 108 Hz, 4B), 13.7 (s, 1B), 14.3 (s, 1B); IR, ν 3065, 2984, 2481 (BH), 1483, 1461, 1393, 1002, 876, 778, 629 cm⁻¹; UV (MeCN) λ_{max} (log ε) 358.5 (3.92); HRMS (ESI-) *m/z* calcd. for C₅H₁₃B₁₀NBr: 276.1162. Found: 276.1207. Anal. Calcd. for C₁₃H₃₃B₁₀BrN₂: C, 38.51; H, 8.20; N, 6.91. Found: C, 39.17; H, 8.21; N, 6.88.

[*closo*-B₁₀H₈-1,10-(NC₅H₅)₂] (1h). A solution of bis-iodonium derivative **6** (100 mg, 0.191 mmol) in dry pyridine (1 mL) was stirred at 80 °C for 12 h. Volatiles were removed in vacuum and the solid residue was washed with EtOH followed by hexane and recrystallized from EtOH to give 21 mg (40% yield) of **1h** as a pale yellow crystals; mp >260 °C ¹H NMR (500 MHz, acetone-*d*₆) δ 0.51 – 1.74 (br m, 8H), 8.06 (dd, *J*₁ = 7.6 Hz, *J*₂ = 6.7 Hz, 4H), 8.52 (t, *J* = 7.8 Hz, 2H), 9.57 (d, *J* = 5.3 Hz, 4H); ¹³C NMR (126 MHz, acetone-*d*₆) δ 127.3, 143.2, 149.0; ¹¹B NMR (160 MHz, acetone-*d*₆) δ -24.0 (d, *J* = 132.2 Hz, 8B), 18.6 (s, 2B); IR, ν 3110, 3088, 3065, 3043, 2485 (BH), 1623, 1488, 1461, 1245, 1200, 1002, 867, 854, 769, 679, 503 cm⁻¹; UV (MeCN) λ_{max} (log ε) 335.5 (4.20); HRMS (ESI-) *m/z* calcd. for C₁₀H₁₈B₁₀N₂: 276.2401. Found: 276.2365.

[*closo*-B₁₀H₈-1-(NHC₄H₈O)-10-(NC₅H₅)] (1j). Starting from **5j** using general procedure without acid wash: 18 mg (32% yield) of **1j** as a white solid. Product was recrystallized from MeCN/EtOH; R_f = 0.71 (30% MeCN in CH₂Cl₂); mp > 260 °C; ¹H NMR (500 MHz, acetone-*d*₆) δ 0.46 – 1.41 (m, 8H), 3.68 (ddd, *J*₁ = 13.8, *J*₂ = 11.4, *J*₃ = 3.6 Hz, 2H), 3.95 (d, *J* = 13.4 Hz, 2H) 4.10 (ddd, *J*₁ = 12.4 Hz, *J*₂ = 12.1 Hz, *J*₃ = 2.0 Hz, 2H), 4.20 (d, *J* = 12.4 Hz, 2H), 8.02 (t, *J* = 7.1 Hz, 2H), 8.48 (t, *J* = 7.8 Hz, 1H), 9.54 (d, *J* = 5.4 Hz, 2H); ¹³C NMR (126 MHz, acetone-*d*₆) δ 56.1, 65.9, 127.1, 143.0, 149.0; ¹¹B NMR (160 MHz, acetone-*d*₆) δ -27.3 (d, *J* = 134 Hz, 4B), -25.5 (d, *J* = 133 Hz, 4B), 17.4 (s, 2B); IR, ν 3088 (NH), 2975, 2926, 2872, 2472 (BH), 1623, 1483, 1461, 1254, 1119, 921, 854, 760, 688 cm⁻¹; UV (MeCN) λ_{max} (log ε) 329.0 (3.85); HRMS (ESI, -) *m/z* calcd. for C₉H₂₁B₁₀N₂O:

283.2590. Found: 283.2597. Anal. Calcd. for $C_9H_{22}B_{10}N_2O$: C, 38.28; H, 7.85; N, 9.92. Found: C, 39.45; H, 7.78; N, 9.03.

Method A. General procedure for preparation of $[closo-B_{10}H_8-1-X-10-IPh]^- [R_4N]^+$ (**5** $[R_4N]$) from $[closo-B_{10}H_9-1-IPh]^- [Bu_4N]^+$ (**3** $[Bu_4N]$). A solution of phenyliodonium **3** $[Bu_4N]$ (0.50 mmol) and freshly dried $[Bu_4N]^+X^-$ (0.75 mmol, 1.5 equiv) was stirred at 55 - 60 °C overnight. All volatiles were removed in vacuum and the crude brown product was chromatographed on silica gel ($CH_2Cl_2/MeCN$ 14:1 gradient to 5:1) the product, which was recrystallized from EtOH/MeCN mixtures giving pure **4** $[Bu_4N]$. The monosubstituted derivative **4** $[Bu_4N]$ was dissolved in MeCN (1.0 mL), cooled in an ice bath and $PhI(OAc)_2$ (1.2 equiv.) was added in 3 portions over 15 min. The reaction mixture was allowed to gradually reach ambient temperature and stirred overnight (16 – 20 h). Solvent was removed under reduced pressure at room temperature and the residue was chromatographed on silica gel ($MeCN/CH_2Cl_2$, 1:10). The isolated product **5** $[Bu_4N]$ was used without further purification.

Method B. General procedure for preparation of $[closo-B_{10}H_8-1-X-10-IPh]^- [R_4N]^+$ (**5** $[R_4N]$) from $[closo-B_{10}H_9-1,10-(IPh)_2]$ (**6**). A suspension of $[closo-B_{10}H_8-1,10-(IPh)_2]$ (**6**, 105 mg, 0.2 mmol) in dry MeCN (5 mL) and appropriate nucleophile salt $[R_4N]^+X^-$ ($X = CN^-$ (1.1 eq), OAc, SCN 1.1–2.5 eq) was stirred at 55 °C (**5b**) or 60 °C for 1 (CN), 2 or 3 days. Progress of the reaction was monitored with ^{11}B NMR using the supernatant liquid. When ^{11}B NMR demonstrated lack of reaction progress, the reaction mixture was filtered, and the solvent was removed from the brown filtrate under reduced pressure at ambient

temperature using a rotary evaporator and an oil pump. The resulting crude solid was passed through a short SiO₂ plug (MeCN/CH₂Cl₂, 1:9), the main fraction **5**[R₄N] was collected, and solvents were removed under vacuum avoiding excess heat.

One pot general procedure. A suspension of [*closo*-B₁₀H₈-1,10-(IPh)₂] (**6**, 210 mg, 0.4 mmol) in dry MeCN (10 mL) and appropriate nucleophile salt [R₄N]⁺X⁻, was stirred at 60 °C for 2 d or until a homogeneous solution was formed that contained at least 50% of the desired product by ¹¹B NMR. Volatiles were removed under vacuum, the residue was dissolved in dry pyridine (1 mL) and the resulting mixture was stirred at 80 °C for 12 h. The pure product was isolated by column chromatography and purified by recrystallization as described above.

[*closo*-B₁₀H₉-1-CN]²⁻ 2[Bu₄N]⁺ (**4b**[Bu₄N]).²⁸ Using Method A with [Bu₄N]⁺CN⁻ : 157 mg (50% yield) of the product as a gray-blue solid, which was recrystallized from EtOH/MeCN giving pure **4b**[Bu₄N] as a light gray microcrystals: R_f = 0.42 (17% MeCN in CH₂Cl₂); mp 216 °C; ¹H NMR (500 MHz, acetone-*d*₆) δ 0.05-0.73 (br m, 8H), 0.98 (t, *J* = 7.3 Hz, 24H), 1.45 (sex, *J* = 7.5 Hz, 16H), 1.80 (quin, *J* = 8.0 Hz, 16H), 3.42 (t, *J* = 8.6 Hz, 16H), 3.73 (br q, *J* = 145.9 Hz, 1H); ¹³C NMR (126 MHz, acetone-*d*₆) δ 14.0, 20.4, 24.6, 59.5; ¹¹B NMR (160 MHz, acetone-*d*₆) δ -27.3 (d, *J* = 148 Hz, 4B), -24.4 (d, *J* = 135 Hz, 4B), -10.0 (s, 1B), 6.71 (d, *J* = 152.2 Hz, 1B); IR, ν 2959, 2874, 2447 (B-H), 2175 (CN), 1480, 1473, 1380, 996, 882, 739 cm⁻¹. HRMS (ESI, -) *m/z* calcd. for CH₉B₁₀N: 145.1670. Found: 145.1671.

[*closo*-B₁₀H₉-1-N₃]²⁻ 2[Bu₄N]⁺ (4d**[Bu₄N]).** Using Method A and [Bu₄N]⁺ N₃⁻; chromatography using CH₂Cl₂/MeCN (10:1) to give 307 mg (95% yield) which was recrystallized from EtOH/MeCN to give pure **4d**[Bu₄N] as a white powder: mp 207 °C; R_f = 0.31 (9% MeCN in CH₂Cl₂); ¹H NMR (500 MHz, acetone-*d*₆) δ -0.08-0.78 (br m, 8H), 0.98 (t, *J* = 7.4 Hz, 24H), 1.44 (sex, *J* = 7.4 Hz, 16H), 1.79 (quin, *J* = 8.0 Hz, 16H), 3.35-3.48 (m, 16H); ¹³C NMR (126 MHz, acetone-*d*₆) δ 14.0, 20.4, 24.6, 59.4; ¹¹B NMR (160 MHz, acetone-*d*₆) δ -29.9 (d, *J* = 131 Hz, 4B), -28.2 (d, *J* = 121 Hz, 4B), -4.2 (d, *J* = 139.5 Hz, 1B), 12.7 (s, 1B); IR, ν 2960, 2873, 2451 (BH), 2095 (N₃), 1480, 1379, 1328, 1150, 1027, 997, 882, 739 cm⁻¹.

[*closo*-B₁₀H₈-1-CN-10-IPh]⁻ [Bu₄N]⁺ (5b**[Bu₄N]).** Method B using solvent was 1:1 THF/MeCN: 62-71 mg (53-60% yield); R_f = 0.82 (9% MeCN in CH₂Cl₂); mp 129 °C; ¹H NMR (500 MHz, acetone-*d*₆) δ 0.40-1.19 (br m, 8H), 0.97 (t, *J* = 7.4 Hz, 12H), 1.43 (sex, *J* = 7.4 Hz, 8H), 1.80 (quin, *J* = 8.0 Hz, 8H), 3.40 (t, *J* = 8.6 Hz, 8H), 7.46 (t, *J* = 7.8 Hz, 2H), 7.61 (t, *J* = 7.5 Hz, 1H), 8.18 (d, *J* = 8.5 Hz, 2H); ¹³C NMR (126 MHz, acetone-*d*₆) δ 13.9, 20.4, 24.5, 59.4, 104.6, 131.4, 132.1, 135.5; ¹¹B NMR (160 MHz, acetone-*d*₆) δ -24.0 (d, *J* = 143 Hz, 4B), -23.1 (d, *J* = 140 Hz, 4B), 0.8 (s, 1B), 2.7 (s, 1B); IR ν 2962, 2938, 2877, 2504 (B-H), 2192 (CN), 1477, 1443, 1383, 998, 884 cm⁻¹. HRMS (ESI, -) *m/z* calcd. for C₇H₁₂B₁₀IN: 347.0951. Found: 347.0958.

[*closo*-B₁₀H₈-1-OAc-10-IPh]⁻ [Et₄N]⁺ (5c**[Et₄N]).**²⁸ Method B: 46 mg (45% yield); pale grayish crystals from MeCN/EtOH; R_f = 0.55 (40% MeCN in CH₂Cl₂); mp 164 °C; ¹H NMR (500 MHz, acetone-*d*₆) δ 0.36-1.11 (br m, 8H), 1.35 (tt, *J*₁ = 7.3 Hz, *J*₂ = 1.9 Hz,

12H), 2.27 (s, 3H), 3.43 (q, $J = 7.3$ Hz, 8H), 7.45 (t, $J = 7.8$ Hz, 2H), 7.60 (t, $J = 7.4$ Hz, 1H), 8.20 (d, $J = 8.5$ Hz, 2H); ^{13}C NMR (126 MHz, acetone- d_6) δ 7.8, 23.3, 53.1, 104.0, 131.2, 131.9, 135.3, 172.2; ^{11}B NMR (160 MHz, acetone- d_6) δ -28.2 (d, $J = 133$ Hz, 4B), -26.4 (d, $J = 136$ Hz, 4B), -2.8 (s, 1B), 29.3 (s, 1B); IR, ν 3085, 2992, 2495 (BH), 1704 (C=O), 1278, 1185, 989, 745, 643 cm^{-1} . HRMS (ESI, -) m/z calcd. for $\text{C}_8\text{H}_{16}\text{B}_{10}\text{IO}_2$: 381.1131. Found: 381.1132.

[*closo*-B₁₀H₈-1-N₃-10-IPh]⁻ [Bu₄N]⁺ (5d[Bu₄N]). Method A: 40-47 mg (66-78% yield); yellowish oil which crystallizes slowly on standing; $R_f = 0.45$ (6% MeCN in CH_2Cl_2); mp 100 °C; ^1H NMR (500 MHz, acetone- d_6) δ 0.25–1.24 (br m, 8H), 0.98 (t, $J = 7.4$ Hz, 12H), 1.43 (sex, $J = 7.4$ Hz, 8H), 1.81 (quin, $J = 8.0$ Hz, 8H), 3.38–3.46 (m, 8H), 7.44 (t, $J = 7.8$ Hz, 2H), 7.60 (t, $J = 7.4$ Hz, 1H), 8.19 (d, $J = 8.2$ Hz, 2H); ^{13}C NMR (126 MHz, acetone- d_6) δ 13.9, 20.4, 24.5, 59.5, 104.1, 131.2, 132.0, 135.3; ^{11}B NMR (160 MHz, acetone- d_6) δ -27.5 (d, $J = 131$ Hz, 4B), -25.5 (d, $J = 138$ Hz, 4B), -2.0 (s, 1B), 23.3 (s, 1B); IR, ν 2975, 2939, 2872, 2494 (BH), 2117 (N₃), 1569, 1470, 1438, 1155, 998, 737 cm^{-1} .

[*closo*-B₁₀H₈-1-I-10-IPh]⁻ [Bu₄N]⁺ (5e[Bu₄N]). Method A: 63 mg (91% yield). Alternatively, the following approach gave 33 mg (25% yield or 38% yield relative to recovered starting material). To a solution of [*closo*-B₁₀H₈-1,10-(IPh)₂] (**6**, 100 mg, 0.191 mmol) in dry THF (8 mL) *n*-BuLi (2.5 M, 115 μL , 0.287 mmol, 1.5 equiv.) was added dropwise at -10 °C under argon atmosphere, and the resulting mixture was stirred for 30 min at -10 °C. Water (10 mL) was added and THF was thoroughly removed under reduced pressure forming aqueous solution of lithium salt. Then $\text{Bu}_4\text{N}^+\text{HSO}_4^-$ (97 mg, (0.287 mmol,

1.5 equiv.) was added at once at room temperature and the resulting white suspension was stirred overnight. The precipitate was filtered off and washed firstly with water, then with hexane, and dried under high vacuum. Resulting crude mixture was passed through short silica gel pad (CH₂Cl₂/MeCN), solvents were removed under reduced pressure and the crude product was used for the next step without further purification. pale yellow-green crystals from MeCN/EtOAc; R_f = 0.15 (30% MeCN in CH₂Cl₂); mp 70 °C; ¹H NMR (500 MHz, acetone-*d*₆) δ 1.19 – 0.28 (m, 8H), 0.97 (t, *J* = 7.3 Hz, 12H), 1.43 (d, *J* = 7.4 Hz, 8H), 1.81 (quin, *J* = 8.0 Hz, 8H), 3.45–3.37 (m, 8H), 7.45 (t, *J* = 7.9 Hz, 1H), 7.60 (t, *J* = 7.4 Hz, 1H), 8.18 (d, *J* = 8.4 Hz, 1H); ¹³C NMR (126 MHz, acetone-*d*₆) δ 13.9, 20.4, 24.5, 59.4, 104.0, 131.2, 132.0, 135.4; ¹¹B NMR (160 MHz, acetone-*d*₆) δ -23.3 (d, *J* = 135 Hz, 8B), 2.0 (s, 2B); IR, ν 2966, 2930, 2876, 2490 (BH), 1560, 1474, 1452, 1375, 993, 827, 755, 643 cm⁻¹. HRMS (ESI, -) *m/z* calcd. for C₆H₁₃B₁₀I₂: 449.0043. Found: 449.0043.

[*closo*-B₁₀H₈-1-SCN-10-IPh]⁻ [Et₄N⁺] (5f[Et₄N]). Method B: 16 mg (16% yield); pale yellow-green crystals from ACN/EtOH; R_f = 0.47 (9% MeCN in CH₂Cl₂); mp 62 °C; ¹H NMR (500 MHz, acetone-*d*₆) δ 0.27-1.16 (br m, 8H), 1.33 (tt, *J*₁ = 7.2 Hz, *J*₂ = 1.8 Hz, 12H), 3.39 (q, *J* = 7.3 Hz, 8H), 7.46 (t, *J* = 7.8 Hz, 2H), 7.62 (t, *J* = 7.4 Hz, 1H), 8.17 (d, *J* = 8.5 Hz, 2H); ¹³C NMR (126 MHz, acetone-*d*₆) δ 7.8, 53.1, 104.5, 118.5, 131.4, 132.1, 135.5; ¹¹B NMR (160 MHz, acetone-*d*₆) δ -23.5 (d, *J* = 84 Hz, 8B), 2.3 (s, 1B), 13.9 (s, 1B); IR, ν 2989, 2948, 2481 (BH), 2139 (CN), 1569, 1470, 1441, 989, 733, 647 cm⁻¹. HRMS (ESI, -) *m/z* calcd. for C₇H₁₂B₁₀INS: 379.0671. Found: 379.0680.

[*closo*-B₁₀H₈-1-Br-10-IPh]⁻ [Et₄N]⁺ (5g**[Et₄N])**. Method B: 80 mg (75% yield); pale yellow-green crystals from MeCN/EtOAc; R_f = 0.15 (30% MeCN in CH₂Cl₂); mp 165 °C; ¹H NMR (500 MHz, acetone-*d*₆) δ 0.34 – 1.23 (br m, 8H), 1.37 (tt, *J*₁ = 7.3 Hz, *J*₂ = 1.9 Hz, 12H), 3.46 (q, *J* = 7.3 Hz, 8H), 7.45 (t, *J* = 7.9 Hz, 2H), 7.60 (t, *J* = 7.4 Hz, 1H), 8.19 (d, *J* = 8.3 Hz, 2H); ¹³C NMR (126 MHz, acetone-*d*₆) δ 7.8, 53.1, 104.1, 131.2, 132.0, 135.4; ¹¹B NMR (160 MHz, acetone-*d*₆) δ -24.5 (d, *J* = 147 Hz, 8B), -0.5 (s, 1B), 17.3 (s, 1B); IR, ν 3085, 2985, 2486 (BH), 1571, 1447, 1185, 994, 829, 745, 656 cm⁻¹. HRMS (ESI, -) *m/z* calcd. for C₆H₁₂B₁₀BrI: 400.0103. Found: 400.0136.

[*closo*-B₁₀H₈-1-(NHC₄H₈O)-10-IPh] (5j**)**. A modification of method A was used. A mixture of phenyliodonium **3**[Bu₄N] (459 mg, 0.905 mmol) and morpholine (3 mL) was stirred overnight at 80 °C. Volatiles were removed under reduced pressure and the residue was washed with cold hexanes. The residue containing two major species in about equal amounts was dissolved in AcOH (25 mL) and water was added (5 mL). The yellowish mixture was cooled in an ice bath, solid PhI(OAc)₂ (310 mg, 0.96 mmol) was added in one portion and the resulting mixture was stirred for 1.5 h at 0 °C. Water (25 mL) was added and the resulting precipitation was filtered, washed with water, and dried giving 348 mg of a tan solid. The main fraction was separated by column chromatography (SiO₂, 5% gradient to 10% EtOAc in CH₂Cl₂) as the second fraction giving 111 mg (30% yield) of the iodonium derivative **5j** as a colorless powder: mp >260 °C; ¹H NMR (500 MHz, acetone-*d*₆) δ 0.32 – 1.47 (br m, 8H), 3.67 (ddd, *J*₁ = 13.8, *J*₂ = 11.1, *J*₃ = 3.8 Hz, 2H), 3.94 (d, *J* = 13.3 Hz, 2H), 4.10 (td, *J*₁ = 12.2 Hz, *J*₂ = 1.9 Hz, 2H), 4.19 (dd, *J*₁ = 12.5, *J*₂ = 1.6 Hz, 2H), 7.47 (t, *J* = 7.9 Hz, 2H), 7.63 (t, *J* = 7.4 Hz, 1H), 8.14 (s, 1H), 8.18 (dd, *J*₁ = 8.4, *J*₂ = 1.0

Hz, 2H); ^{13}C NMR (125 MHz, acetone- d_6) δ 56.0, 65.9, 104.6, 131.5, 132.2, 135.8; ^{11}B NMR (160 MHz, acetone- d_6) δ -25.7 (d, J = 137 Hz, 4B), -23.9 (d, J = 140 Hz, 4B), 2.9 (s, 1B), 22.5 (s, 1B); IR ν 3178 (NH), 2971, 2926, 2976, 2503, 2458 (BH), 1573, 1443, 1272, 1133, 1002, 755, 679 cm^{-1} . HRMS (ESI, -) m/z calcd. for $\text{C}_{10}\text{H}_{21}\text{B}_{10}\text{INO}$: 408.1604. Found: 408.1612.

CHAPTER III

Tuning absorption energies via modifying the LUMO energies in [*closo*-B₁₀H₈-1-CN-10-(Q⁺)]⁻[Bu₄N]⁺

3.1 INTRODUCTION

The photophysical properties of our prototype system [*closo*-B₁₀H₉-1-NC₅H₅] (**1a**), are dependent upon both the energy of the HOMO localized on the cluster and LUMO localized on the pyridine. In the previous chapter, we demonstrated the effect of eight different substituents attached at B1 on the HOMO of the {*closo*-B₁₀}. Similarly, DFT calculations suggest that perturbation of pyridine through different *para* substituents significantly changes the LUMO energy compared to the effects of substituents attached to the cluster on the HOMO (Figure 3.1).

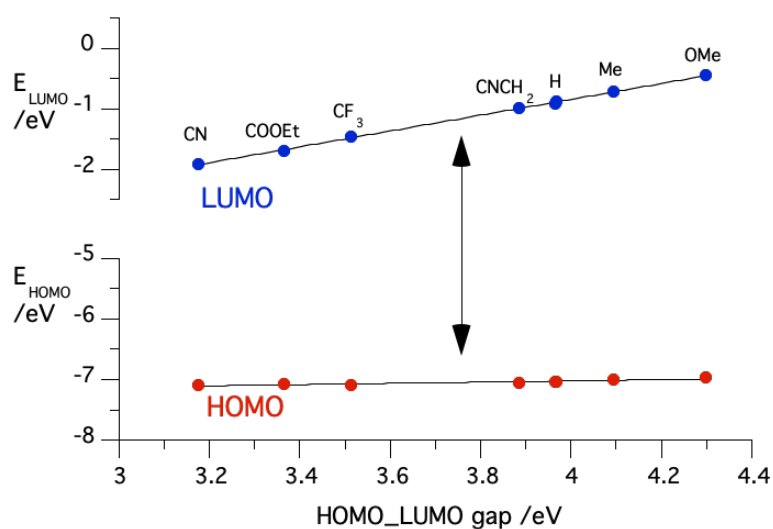


Figure 3.1: TD-DFT CAM-B3LYP/TVZP calculations showing the effect of substituents on pyridine on the HOMO and LUMO of our prototype system (**1a**).

In this chapter, we discuss a simple synthetic variation (series **7**), designed to keep the HOMO relatively constant, while varying the LUMO (CN attached at an antipodal boron atom position relative to the azine). Series **7** compounds have possible applications as ditopic ligands in metal organic frameworks as well as in supramolecular structures via co-crystallization with organic acids. To achieve the latter, **8a** and **8b** were synthesized to serve as model compounds. The synthesis of these compounds was performed by me. Dr. Friedli performed the photophysical measurements, Dr. Hietsoi collected and analyzed XRD data, while Dr. Piotr Kaszynski performed the computational modeling.

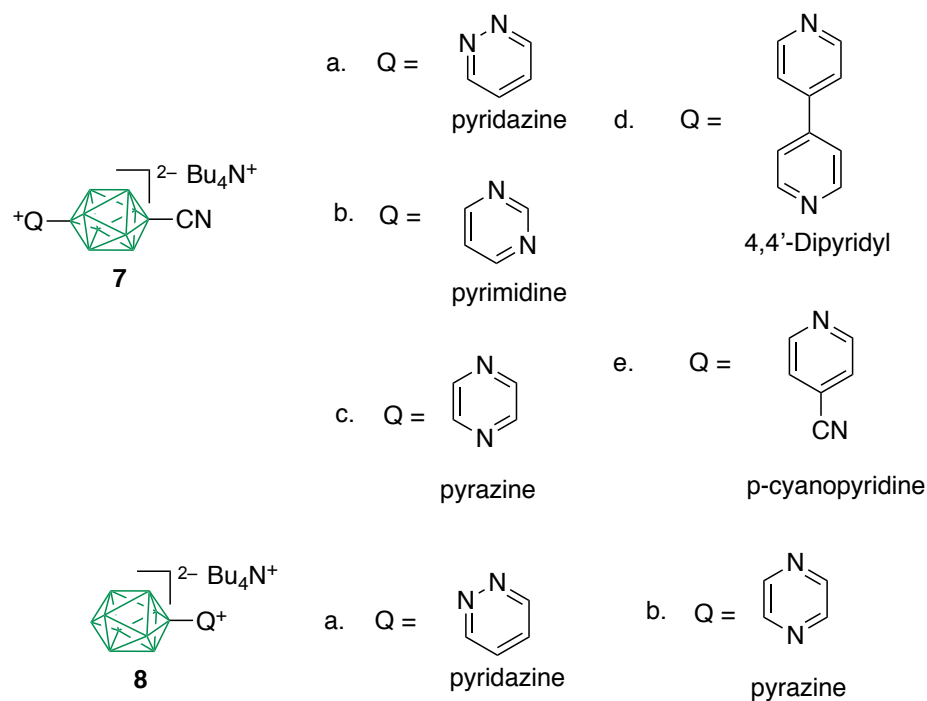
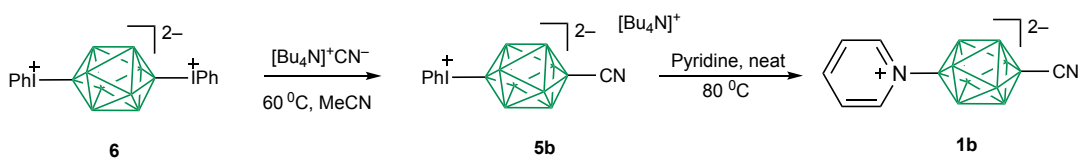


Figure 3.2: Target azine structures **7** and **8**.

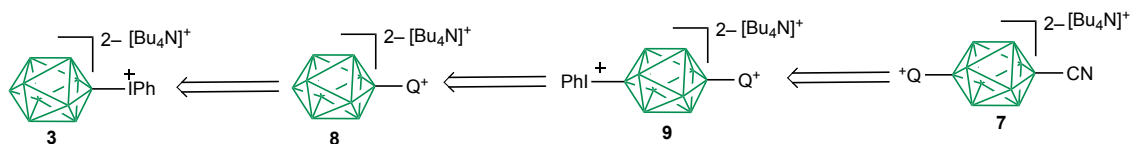
3.2 RESULTS AND DISCUSSIONS

3.2.1 Synthesis

In the previous chapter, we demonstrated a two-step approach for the successful synthesis of **1b**. In this method, [*closo*-B₁₀H₈-1,10-(IPh)₂] (**6**) undergoes selective nucleophilic substitution with 1 eq of [Bu₄N]⁺CN⁻ to give the monocyano derivative (**5b**[Et₄N]) in 50-55% yield after column chromatography. Subsequent treatment of **5b** in excess pyridine at 80 °C gives **1b**[Bu₄N] (Scheme 3.1).

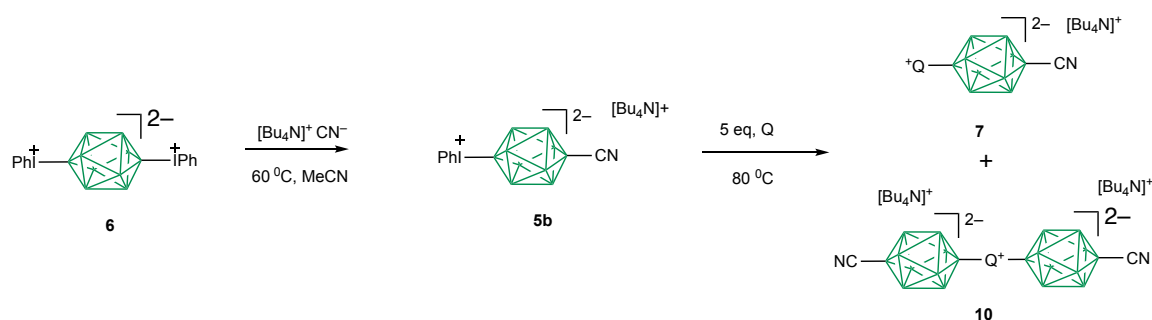


Scheme 3.1. Synthesis of **1b**[Bu₄N] from **6**.



Scheme 3.2. Three step approach to synthesis of **7** through intermediate **8**

This suggests the feasibility of either method to obtain **7**. To optimize the synthesis for a representative target azine **7a**, an NMR experiment was done to investigate the relative reactivities of pyridazine with monoiodonium derivative **3** and **5b** by varying the concentration of **3** (or **5b**) relative to pyridazine (1:5, 1:10 and 1:20 ratio in 50 mM MeCN at 80 °C) and monitoring the progress of the reaction using ^{11}B NMR. After 3 hours, **3** reacts completely with pyridazine to give **8a** whereas **5b** reacts completely after 18 h to give **7a**. To improve the overall yield of target molecules, series **7a–7e** was synthesized from **5b**[**Bu₄N**] using 5 eq of each azine in a minimum of MeCN at 80 °C for 18 hours. We chose to use tetrabutyl- rather than tetraethyl ammonium cyanide due to better solubility of **7a**[**Bu₄N**] as compared to **7a**[**Et₄N**]. The products **7a–7e** were obtained in 50 to 78% yield. Synthesis of **7c** produced an unexpected double substituted side product **10** in a paltry 5 % yield. Attempts to increase the yield of **10** using a 2:1 ratio of **5b** to pyridazine resulted in low yield as well. (Scheme 3.3).



Scheme 3.3: Synthesis of series **7** and **10** side product from **6**.

Products **8a** and **8b** were obtained by treating **3** with 5.0 equivalents of pyridazine or pyrazine, respectively, at 80 °C in MeCN and stirring for 3 h. Yields were 55 and 25% yield, respectively, after column chromatography. These compounds are possible precursors for synthesis of series **7** using a three-step approach from **3** (Scheme 3.2).

3.2.2 Crystal and molecular structures

All new materials formed monoclinic crystals. Yellow **7a**[Bu₄N] crystallized upon slow cooling from MeCN/EtOH), yellow **7c**[Bu₄N] crystallized from hot EtOH, dark red crystals of **8a** [Bu₄N] grew from MeCN/EtOH. Compounds **7b**, **7d** and **7e** did not crystallize from any available solvent mixture.

Selected bond lengths and angles are collected in Table 3.1. Molecular structures for three new derivatives are shown in Figure 3.3.

Crystal systems of most salts **7** contain a single ion pair in the asymmetric unit, while **7a**[Bu₄N] contains eight molecules in the unit cell, four anions and four cations. The large [Bu₄N] cation is positionally disordered in most salts. The intracage dimensions of the anions, such as B–B bond distances and angles, are typical for {*closo*-B₁₀} derivatives (Table 3.1). The cage is contracted in **7** derivatives relative to **8** derivatives due to the highly electron withdrawing CN substituent, as discussed in Ch 2. The monopyridinium **1a** intracage distance is slightly shorter (3.637(2) Å) than monopyrazinium **8b** (3.644(2) Å) but longer than compounds **7**. For compounds with a CN substituent at B1, the azine does not have much effect on square pyramid (distance from the equatorial belt) **1b** < **7c** < **7b**. Thus, from **1b** the pyramid increases from 1.052 Å to 1.057 Å in **7b**. (Table 3.1)

TABLE 3.1. Selected Interatomic distances and angles for selected derivatives **7** and **8^a**

Q ⁺	Pyridine (1a) ^{c,d} (X = H)	Pyridine (1b) (X = CN)	Pyridazine (7a) (X = CN)	Pyrazine (7c) (X = CN)	Pyrazine (8a) (X = H)
B(10)–N	1.529(3)	1.524(2)	1.525(2)	1.528(2)	1.525(2)
B(1)–X		1.543(2)	1.539(2)	1.540(3)	1.10(2)
B(1)–B(2) avg	1.699(6)	1.696(4)	1.697	1.684	1.701
B(1)···B(2-5)	1.095	1.077	1.079	1.075	1.097
B(2)–B(3) avg	1.848(6)	1.853(2)	1.853(0)	1.856	1.839
B(2)–B(6) avg	1.809(6)	1.811(6)	1.810(0)	1.811	1.813
B(6)–B(7) avg	1.837(6)	1.856(14)	1.856(0)	1.852	1.852
B(6)–B(10) avg	1.680(5)	1.682(4)	1.685(0)	1.689	1.681
B(10)···B(6-9) <i>e</i>	1.056	1.052	1.057(0)	1.053	1.054
B(1)···B(10)	3.660(4)	3.637(2)	3.644(2)	3.638(3)	3.664(2)
B–B(10)–N	129(2)	128.7(1)	128.9(1)	128.8(1)	128.8(4)
B–B(1)–X	130.1(2)	129.4(2)	129.5(1)	129.4(1)	

^aExcept for unique interatomic distances, all parameters are average values and the esd refers to distribution of individual measurements. ^b Ref 30 ^c 2 molecules. ^d Ref 31. ^e The height of the tetragonal pyramid.

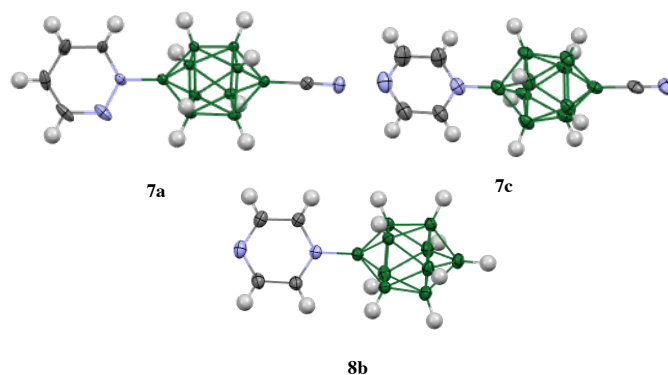


Figure 3.3: Atomic displacement ellipsoid representation of **7a**, **7c** and **8b**. For geometrical dimensions see Table 3.1 and the text. The corresponding counterions are omitted for clarity, ellipsoids are at the 50% probability level and the numbering system according to the chemical structure.

The azine N–B(10) distance is essentially the same in entire series (within the experimental error) and 1.527 Å for all 4 derivatives in Table 3.1. B(1)–CN distances are typical for other derivatives of the [*closo*-B₁₀H₁₀]²⁻ anion,³² containing CN substituents.

The supramolecular assembly of the cyano derivatives **7a**, and **7c** are isostructural, with four anions and four cations in the unit cell (Figure 3.4). Compound **1b** has only two of each ion in the structural unit. The anions are arranged centrosymmetrically so that the end of one molecule with the azine (net positive charge) overlaps with the end of a neighboring molecule containing the {*closo*-B₁₀}.

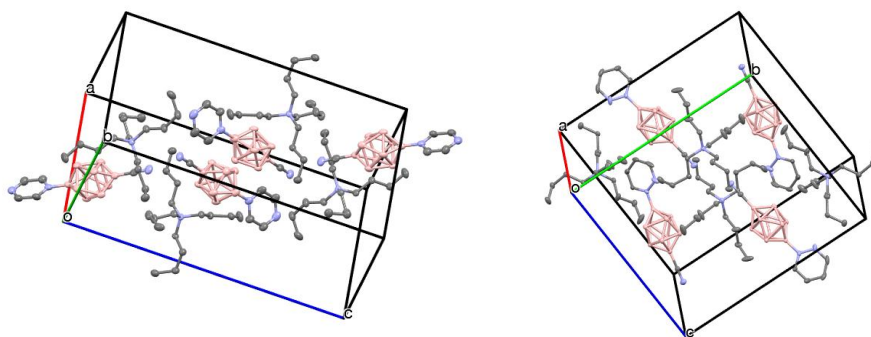


Figure 3.4. Packing diagram for **7a** and **7c**. Hydrogen atoms omitted for clarity. Atomic displacement ellipsoid diagrams are drawn at 50% probability.

3.2.3 Photophysical properties

Electronic absorption and emission data for compounds **7a-e**, **8a**, and **1b** are shown in Figures 3.5 and 3.6, and Tables 3.2 and 3.3. Azine derivatives **7** have a broad band with λ_{max} ranging between 339.5 and 409 nm (Figure 3.5). This is characteristic of a charge transfer transition from cluster to azine (HOMO–LUMO gap).

Each compound also has a higher energy peak with λ_{\max} between 230 nm and 260 nm corresponding to the $\pi - \pi^*$ transition of the azine. The strength of these absorption bands is an indicator of the ability of $\{closo-B_{10}\}$ to couple strongly with π symmetry substituents.

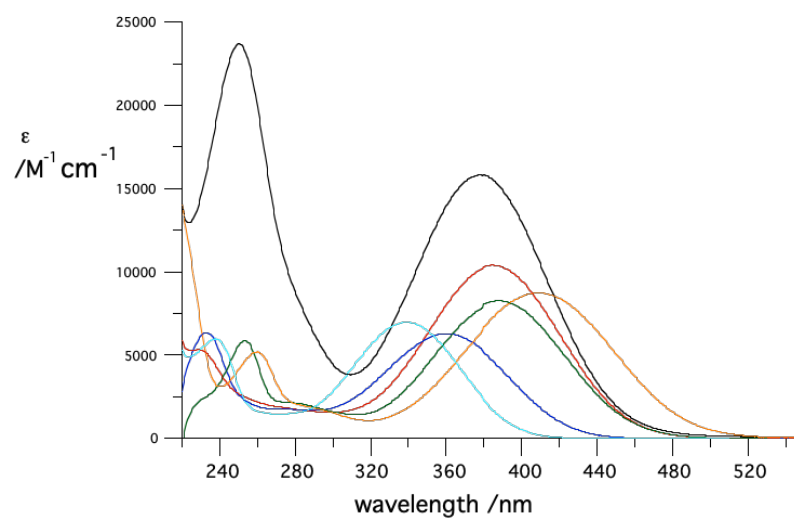
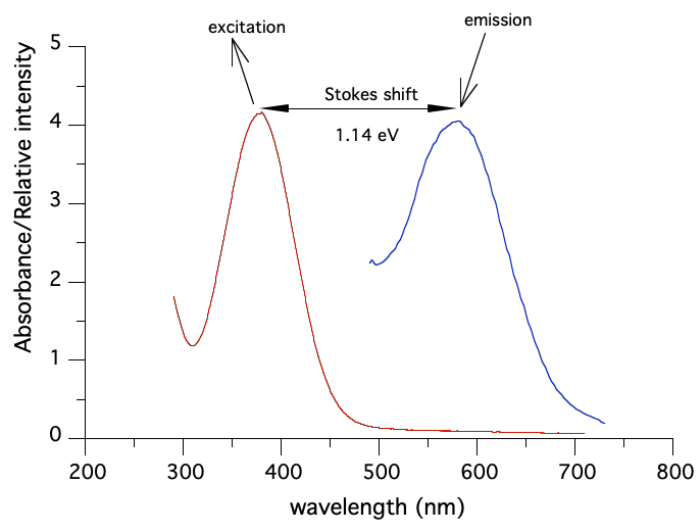


Figure 3.5. Electronic spectra of series 7: **7a** (red); **7b** (blue); **7c** (green); **7d** (black); **7e** (orange); **1b** (light blue).

Table 3.2. Selected experimental and theoretical electronic transition energies and oscillator strength values

Compound	Q	Experimental ^a			Theoretical ^b	
		Absorption λ_{\max} /nm (log ϵ)	Absorption λ_{\max} /nm (log ϵ)	Absorption Energy /eV ^c	Emission λ_{\max} /nm (Stokes shift /eV)	$\pi \rightarrow \pi^*$ /eV (<i>f</i>)
7a	Pyridazine	384.5 (4.08)	229	3.22	None	3.62 (0.378)
7b	Pyrimidine	360 (3.79)	232	3.44	554 (1.21)	3.94 (0.323)
7c	Pyrazine	388 (3.93)	255	3.20	n/a	3.60 (0.353)
7d	Dipyridyl	379 (4.19)	250.5	3.35	581(1.14)	3.82 (0.579)
7e	<i>p</i> -cyanopyridine	409 (3.96)	259.5	3.03	n/a	3.41 (0.454)
8b^d	Pyrazine	425 (4.52)	258	2.92	n/a	-
1a^d	Pyridine	366 ^e		3.39	569	
1b	Pyridine	339.5 (3.88)	237.5	3.65	540 (1.36)	4.19 (0.341)

^aRecorded in MeCN. ^b Obtained with the TD CAM-B3LYP/6-31++G(2d,p)//B3LYP/TZVP method in MeCN dielectric medium and shifted by 0.56 eV. ^c Energy corresponding to charge transfer transition ^d H in place of CN. ^e Ref 39

**Figure 3.6.** UV (red) and fluorescence spectra (blue) of **7d** showing the Stokes shift.

Upon excitation at the λ_{\max} , fluorescence is observed only in **1b**, **7b** and **7d**. (Table 3.3) The Stokes shift for **7d** is characteristically large (1.14 eV), yet not as large as for **7b** (1.21 eV) or **1b** (1.36 eV). Compared to the pyridine derivative **1b**, the two fluorescent azine derivatives have very low relative fluorescence intensities. It is not immediately clear why the other compounds do not fluoresce.

The HOMO-LUMO energy (column 5, Table 3.2) is significantly reduced in all azine compounds with respect to the pyridine derivative (**1b**, 3.65 eV) in the order **1b** > **7b** > **7d** > **7a** > **7c** > **7e**. The highest observed bathochromic shift in **7e** (3.03 eV) can be attributed to a reduction in the energy of the LUMO because the HOMO in each case is localized on the [*closo*-B₁₀H₈-1-CN]⁻ fragment. Although an electron withdrawing group such as CN is expected to lower the LUMO energy of the 4-cyanopyridinium in **7e**, a reduction in the LUMO energy is also observed when a CH fragment is replaced by a N atom, as in pyridazine (**7a**), pyrimidine (**7b**), pyrazine (**7c**), and dipyrityl (**7d**) also reduces the energy of the LUMO relative to **1b**, this fact is corroborated by DFT calculations as shown in Figure 3.7. The above trend can be explained in terms of resonance and inductive arguments.

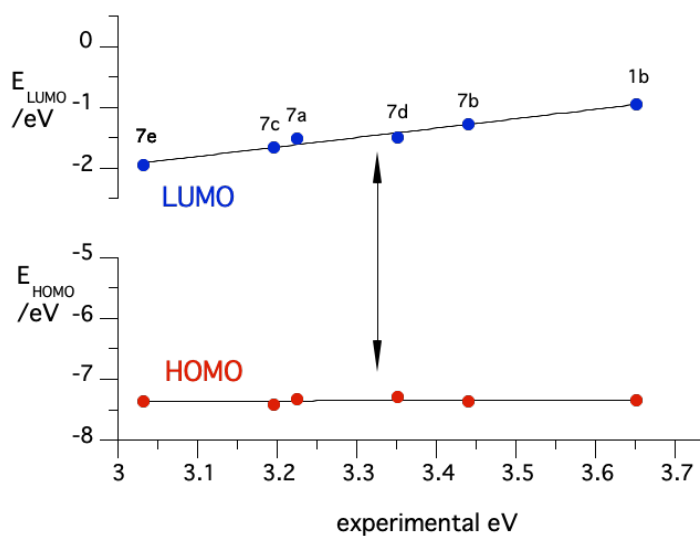


Figure 3.7. Correlation of HOMO and LUMO energies of series **7** vs experimental absorption energies in eV. Energies calculated using TD-DFT CAM-B3LYP/TVZP.

The CN group is electron withdrawing, therefore it enhances the electron affinity of pyridine in **7e**, reducing the LUMO energy. In **7a**, **7b**, **7c** and **7d**, addition of a N atom, which is more electronegative than a C, enhances the electron affinity of the azines.⁴⁴ An extra N atom in *ortho* (**7a**) or *para* (**7c**) position in an azine has more effect on the LUMO than N in a *meta* position (**7b**).

The same trend is observed when comparing parent pyrazinium derivative **8b** with parent pyridinium derivative **1a**. The HOMO of this system is higher for compounds with H at B1 than for those with CN at B1, yet for reasons given above, the pyrazine is better at stabilizing the LUMO, resulting in the smallest observed H-L gap (2.92 eV, Table 3.2).

3.2.4 IR spectroscopy.

The stretching vibration of the nitrile group in series **7** compounds ranges between 2183-2188 cm⁻¹(Table 3.3), consistent with a report for the di-cyano derivative of [*closo*-B₁₀H₁₀]³² as nitrile groups attached to a *closo*-{B₁₀} group have lesser bond order due to the resonance effect of the electron-rich cluster as compared to their benzene (2228 cm⁻¹, Table 3.3) and [*closo*-CB₉H₁₀]- (2201 cm⁻¹, Table 3.3) analog. This suggest a significant electronic interaction between the cage and the nitrile group, and also further confirm the fact that binary boranes such as *closo*-decaborane have better interactions with π systems than the corresponding carboranes.

Table 3.3. IR CN stretching vibration of **7a-7e** and similar derivatives.^a

Compound	7a	7b	7c	7d	7e
CN ν /cm ⁻¹	2188	2188	2186	2183	2183
Compound	1b	[<i>closo</i> -1-CB ₉ H ₉ -10-CN] ^{-b}	[<i>closo</i> -B ₁₀ H ₈ -1,10-(CN) ₂] ^{2-c}	Ph-CN ^c	<i>t</i> -Bu-CN ^c
CN ν /cm ⁻¹	2188	2201	2183	2228	2235

^a Measured neat ^b Ref. 45 ^c Ref. 32

3.3 CONCLUSIONS

Nucleophilic substitution of *closo*-decaborane via bis-phenyliodonium **6** proved to be an efficient strategy in synthesizing series **7** in terms of yield, although the rate of reaction of **3** with azines is faster than **5b** with azines. Compounds **7a-e** were obtained from **5b** in 78, 57, 53, 50, and 55% yield, respectively. Electronic absorption spectra show a significant shift in the wavelength of maximum absorption (from 339.5 nm for Q = pyridine to 409 nm for Q = *para*-cyanopyridine) as more electronegative atom or group is attached and/or introduced to the ring (bathochromic shift). Trends in experimental and calculated absorption energies does not seem to correlate with any relevant properties of the azines, however it can be deduced from DFT calculations that the variation in λ_{\max} is related to the perturbation of the LUMO energies (1.00 eV range) rather than the HOMO energies (0.12 eV range).

3.4 Experimental Section

General experimental information is the same as that described in Chapter II.

General Procedure for Synthesis of Series 7

Compound **6** (524 mg, 1.00 mmol) was dissolved in MeCN (5 mL) and $[\text{Bu}_4\text{N}]^+\text{CN}^-$ (295.4 mg, 1.10 mmol) was added and stirred at 55-60 °C overnight. MeCN was removed via rotary evaporator under reduced pressure, compound **5b** was purified using gradient flash chromatography (1:150 w/w SiO_2) starting with 12:1 $\text{CH}_2\text{Cl}_2/\text{MeCN}$. Compound **5b** (60 mg, 0.10 mmol) was dissolved in MeCN (0.1 mL) and azine (5 eq) was added and stirred at 80 °C overnight. The volatiles were removed under vacuum, the crude mixture was washed with hexanes and 10% HCl. The residue was purified using gradient flash column chromatography (1:200 w/w SiO_2) starting with 9:1 $\text{CH}_2\text{Cl}_2/\text{MeCN}$, followed by recrystallization with using EtOH or CH_2Cl_2 / EtOH, to obtain analytical samples of compound **7a-7e**. When **7b** was prepared from **5b** and pyrazine, and purified as described above, a small amount of **10** was obtained.

[closo-B₁₀H₈-1-CN-10-pyridazine]⁻ [Bu₄N]⁺ (7a): 36.6 mg (78% yield) of pale yellow-green crystals from $\text{CH}_2\text{Cl}_2/\text{EtOH}$. $R_f = 0.55$ (5:1 $\text{CH}_2\text{Cl}_2/\text{MeCN}$); mp 181 °C; ¹H NMR (500 MHz, acetone-*d*₆) δ 0.39-1.20 (br m, 8H), 0.91 (t, $J = 7.4$ Hz, 12H) 1.37 (sex, $J = 7.4$ Hz, 8H), 1.62-1.88 (m, 8H), 3.34-3.40 (m, 8H), 8.28 (ddd, $J_1 = 8.3$, $J_2 = 5.1$, $J_3 = 1.5$ Hz, 1H), 8.35 (ddd, $J_1 = 8.0$ Hz, $J_2 = 5.8$ Hz, $J_3 = 2.0$ Hz, 1H), 9.36 (d, $J = 5.0$ Hz, 1H), 10.21 (d, $J = 5.8$ Hz, 1H); ¹³C NMR (126 MHz, acetone-*d*₆) δ 13.0, 19.5, 23.6, 58.6, 131.8, 132.3,

150.8, 152.7; ^{11}B NMR (160 MHz, acetone- d_6) δ -23.4 (d, J = 136 Hz, 4B), -21.8 (d, J = 133 Hz, 4B), -2.3 (s, 1B), 19.4 (s, 1B); IR ν 3098, 3075, 2963, 2873, 2499 (BH), 2188 (CN), 1586, 1469, 1425, 1166, 889 cm^{-1} ; HRMS (ESI, -) m/z calcd. for $\text{C}_5\text{H}_{12}\text{B}_{10}\text{N}_3$: 224.1967. Found: 224.1972. Anal. Calcd. for $\text{C}_{21}\text{H}_{48}\text{B}_{10}\text{N}_4$: C, 54.27; H, 10.41; N, 12.06. Found: C, 53.58; H, 10.28; N, 11.70.

[*closo*- B_{10}H_8 -1-CN-10-pyrimidine] $^-$ [Bu_4N] $^+$ (7b): 26 mg (57% yield) of light orange powder from hot EtOH. R_f = 0.58 (5:1 $\text{CH}_2\text{Cl}_2/\text{MeCN}$); mp 145 $^\circ\text{C}$; ^1H NMR (500 MHz, acetone- d_6) δ 0.43-1.21 (br m, 8H), 0.94 (t, J = 7.4 Hz, 12H), 1.40 (sex, J = 7.4 Hz, 8H), 1.78 (quin, J = 16.1, 8.0 Hz, 8H), 3.37-3.43 (m, 8H), 8.13 (t, J = 5.5 Hz, 1H), 9.35 (d, J = 5.0 Hz, 1H), 9.75 (d, J = 5.7 Hz, 1H), 10.12 (s, 1H); ^{13}C NMR (126 MHz, acetone- d_6) δ 13.0, 19.5, 23.6, 58.5, 122.6, 154.4, 155.7, 161.3; ^{11}B NMR (160 MHz, acetone- d_6) δ -23.43 (d, J = 155 Hz, 4B), -22.48 (d, J = 149 Hz, 4B), -2.77 (s, 1B), 17.46 (s, 1B); IR ν 3109, 3082, 2970, 2873, 2491 (BH), 2188 (CN), 1608, 1477, 1413, 1174, 893, 698 cm^{-1} ; HRMS (ESI, -) m/z calcd. for $\text{C}_5\text{H}_{12}\text{B}_{10}\text{N}_3$: 224.1967. Found: 224.1969. Anal. Calcd. for $\text{C}_{21}\text{H}_{48}\text{B}_{10}\text{N}_4$: C, 54.27; H, 10.41; N, 12.06. Found: C, 54.27; H, 10.20; N, 11.27.

[*closo*- B_{10}H_8 -1-CN-10-pyrazine] $^-$ [Bu_4N] $^+$ (7c): 23.8 mg (53% yield) of compound **7c** as bright yellow crystals from $\text{CH}_2\text{Cl}_2/\text{EtOH}$. R_f = 0.60 (5:1 $\text{CH}_2\text{Cl}_2/\text{MeCN}$); mp 173 $^\circ\text{C}$; ^1H NMR (500 MHz, acetone- d_6) δ 0.40-1.26 (br m, 8H), 0.95 (t, J = 7.4 Hz, 12H) 1.41 (sex, J = 7.4 Hz, 8H), 1.81 (quin, J = 16.1, 8.0 Hz, 8H), 3.40-3.45 (m, 8H), 9.22 (dd, J = 3.1, J_2 = 1.2 Hz, 2H), 9.48 (d, J = 3.8 Hz, 2H); ^{13}C NMR (126 MHz, acetone- d_6) δ 13.0, 19.5, 23.6,

58.6, 140.6, 148.4; ^{11}B NMR (160 MHz, acetone- d_6) δ -22.91 (d, J = 137 Hz, 4B), -21.30 (d, J = 135 Hz, 4B), -0.77 (s, 1B), 18.57 (s, 1B); IR ν 3609, 3410, 3104, 2968, 2872, 2485 (BH), 2186 (CN), 1607, 1482, 1426, 1168, 829, 633 cm^{-1} ; HRMS (ESI, -) m/z calcd. for $\text{C}_5\text{H}_{12}\text{B}_{10}\text{N}_3$: 224.1967. Found: 224.1969. Anal. Calcd. for $\text{C}_{21}\text{H}_{48}\text{B}_{10}\text{N}_4$: C, 54.27; H, 10.41; N, 12.06. Found: C, 51.77; H, 9.20 ; N, 11.04.

[*closo*- B_{10}H_8 -1-CN-10-(4,4'-bipyridyl)] $^-$ [Bu_4N] $^+$ (7d**):** 22 mg (50% yield) of compound **7c** as light-yellow powder from $\text{Et}_2\text{O}/\text{CH}_2\text{Cl}_2$. R_f = 0.35 (5:1 $\text{CH}_2\text{Cl}_2/\text{MeCN}$); mp 80 $^\circ\text{C}$; ^1H NMR (500 MHz, acetone- d_6) δ 0.46-1.29 (br m, 8H), 0.98 (t, J = 7.4 Hz, 12H) 1.44 (sex, J = 7.5 Hz, 8H), 1.83 (quin, J = 7.5 Hz, 8H), 3.42-3.47 (m, 8H), 8.01 (dd, J_1 = 4.5 Hz, J_2 = 1.7 Hz, 2H), 8.36 (dd, J_1 = 5.5 Hz, J_2 = 1.5 Hz, 2H), 8.87 (dd, J_1 = 4.6 Hz, J_2 = 1.6 Hz, 2H), 9.60 (dd, J_1 = 5.6 Hz, J_2 = 1.2 Hz, 2H); ^{13}C NMR (126 MHz, acetone- d_6) δ 13.9, 20.4, 24.5, 59.5, 122.5, 124.6, 143.7, 149.1, 151.1, 152.0; ^{11}B NMR (160 MHz, acetone- d_6) δ -23.7 (d, J = 162 Hz, 4B), -22.7 (d, J = 160 Hz, 4B), -3.6 (s, 1B), 19.0 (s, 1B); IR ν 3109, 3044, 2962, 2876, 2485 (BH), 2183 (CN), 1632, 1595, 1485, 1212, 825, 633 cm^{-1} ; HRMS (ESI, -) m/z calcd. for $\text{C}_{11}\text{H}_{16}\text{B}_{10}\text{N}_3$: 300.2280. Found: 300.2290; Anal. Calcd. for $\text{C}_{27}\text{H}_{52}\text{B}_{10}\text{N}_4$: C, 59.96; H, 9.69; N, 10.36. Found: C, 59.66; H, 10.08; N, 9.77.

[*closo*- B_{10}H_8 -1-CN-10-(4-cyanopyridine)] $^-$ [Bu_4N] $^+$ (1e**):** 40 mg (55% yield) of compound **7c** as an orange powder from hot EtOH. R_f = 0.70 (5:1 $\text{CH}_2\text{Cl}_2/\text{MeCN}$); mp 81 $^\circ\text{C}$; ^1H NMR (500 MHz, acetone- d_6) δ 0.47-1.28 (br m, 8H), 0.98 (t, J = 7.4 Hz, 12H) 1.44 (sex, J = 7.5 Hz, 8H), 1.83 (quin, J = 7.5 Hz, 8H), 3.41-3.48 (m, 8H), 8.37 (dd, J_1 = 5.5, J_2 = 1.3 Hz, 2H), 9.74 (d, J = 6.7 Hz, 2H); ^{13}C NMR (126 MHz, acetone- d_6) δ 13.9, 20.4,

24.5, 59.5, 116.3, 125.2, 129.5, 149.6; ^{11}B NMR (160 MHz, acetone- d_6) δ -22.6 (d, J = 137 Hz, 4B), -21.02 (d, J = 134 Hz, 4B), -1.1 (s, 1B), 19.8 (s, 1B); IR ν 3109, 2962, 2876, 2485 (BH), 2183 (CN), 1494, 1428, 1232, 837, 735 cm^{-1} ; HRMS (ESI, -) m/z calcd. for $\text{C}_7\text{H}_{12}\text{B}_{10}\text{N}_3$: 248.1967. Found: 248.1987. Anal. Calcd. for $\text{C}_{21}\text{H}_{48}\text{B}_{10}\text{N}_4$: C, 56.52; H, 9.90; N, 11.46. Found: C, 55.75; H, 9.49; N, 11.04.

1,4-Bis-[*closo*- B_{10}H_8 -10-CN-1-pyrazine-1,4-diium] [2Bu $_4$ N] $^+$ (10): 4.2 mg (5% yield) of compound **10** as a dark purple solid from EtOH. R_f = 0.25 (5:1 $\text{CH}_2\text{Cl}_2/\text{MeCN}$); ^1H NMR (500 MHz, acetone- d_6) δ 0.60-1.21 (br m, 16H), 0.98 (t, J = 7.4 Hz, 24H) 1.44 (sex, J = 7.5 Hz, 16H), 1.83 (quin, J = 7.5 Hz, 16H), 3.42-3.48 (m, 16H), 9.83 (s, 4H); ^{13}C NMR (126 MHz, acetone- d_6) δ 13.9, 20.4, 24.5, 9.5, 144.2; ^{11}B NMR (160 MHz, acetone- d_6) δ -23.5 (d, J = 137 Hz, 4B), -21.0 (d, J = 134 Hz, 4B), 2.0 (s, 1B), 17.6 (s, 1B).

[*closo*- B_{10}H_9 -1-pyridazine] $^-$ [Bu $_4$ N] $^+$ (8a): 24.2 mg (55% yield) of compound **8a** as bright yellow powder from hot EtOH. R_f = 0.53 (5:1 $\text{CH}_2\text{Cl}_2/\text{MeCN}$); ^1H NMR (500 MHz, acetone- d_6) δ 0.17-1.24 (br m, 8H), 0.97 (t, J = 7.4 Hz, 12H) 1.43 (sex, J = 7.4 Hz, 8H), 1.80 (quin, J = 7.5 Hz, 8H), 3.38-3.46 (m, 8H), , 4.08 (q, J = 143.5 Hz, 1H) 8.23 (ddd, J_1 = 8.1, J_2 = 5.0, J_3 = 1.2 Hz, 1H), 8.30 (ddd, J_1 = 7.9 Hz, J_2 = 5.9 Hz, J_3 = 2.0 Hz, 1H), 9.33 (d, J = 4.9 Hz, 1H), 10.29 (d, J = 5.8 Hz, 1H); ^{13}C NMR (126 MHz, acetone- d_6) δ 13.9, 20.4, 24.5, 59.5, 131.4, 132.5, 151.2, 153.1; ^{11}B NMR (160 MHz, acetone- d_6) δ -25.0 (d, J = 128 Hz, 4B), -20.3 (d, J = 134 Hz, 4B), 8.8 (d, J = 149 Hz 1B), 16.9 (s, 1B); IR ν 3098, 3075, 2963, 2873, 2499 (BH), 2188 (CN), 1586, 1469, 1425, 1166, 889 cm^{-1} .

[*closo*-B₁₀H₉-1-pyrazine]⁻ [Bu₄N]⁺ (8b**):** 32.3 mg (25% yield) of compound **8c** as light green powder from hot EtOH. R_f = 0.53 (5:1 CH₂Cl₂/MeCN); mp 153 °C; ¹H NMR (500 MHz, acetone-*d*₆) δ 0.17-1.28 (br m, 8H), 0.97 (t, *J* = 7.4 Hz, 12H) 1.43 (sex, *J* = 7.5 Hz, 8H), 1.82 (quin, *J* = 8.0 Hz, 8H), 3.41-3.46 (m, 8H), 4.16 (q, *J* = 148.0 Hz, 1H) 9.12 (dd, *J*₁ = 3.1, *J*₂ = 1.0 Hz, 2H), 9.51 (dd, *J*₁ = 3.0, *J*₂ = 0.9 Hz, 2H); ¹³C NMR (126 MHz, acetone-*d*₆) δ 13.9, 20.4, 24.5, 59.5, 141.7, 148.6; ¹¹B NMR (160 MHz, acetone-*d*₆) δ -24.9 (d, *J* = 131 Hz, 4B), -20.3 (d, *J* = 134 Hz, 4B), 9.4 (d, *J* = 145 Hz, 1B), 16.0 (s, 1B); IR ν 3101, 2966, 2888, 2468 (BH), 1604, 1420, 1171, 820, 727 cm⁻¹; HRMS (ESI, -) *m/z* calcd. for C₄H₁₃B₁₀N₂: 199.2015. Found: 199.2021.

References

- (1) Ray, S.; Widom, J. R.; Walter, N. G. Life under the Microscope: Single-Molecule Fluorescence Highlights the RNA World. *Chem. Rev.* **2018**, *118* (8), 4120–4155. <https://doi.org/10.1021/acs.chemrev.7b00519>.
- (2) Gunnlaugsson, T.; Ali, H. D. P.; Glynn, M.; Kruger, P. E.; Hussey, G. M.; Pfeffer, F. M.; Dos Santos, C. M. G.; Tierney, J. Fluorescent Photoinduced Electron Transfer (PET) Sensors for Anions; From Design to Potential Application. *J. Fluoresc.* **2005**, *15* (3), 287–299. <https://doi.org/10.1007/s10895-005-2627-y>.
- (3) Wu, D.; Sedgwick, A. C.; Gunnlaugsson, T.; Akkaya, E. U.; Yoon, J.; James, T. D. Fluorescent Chemosensors: The Past, Present and Future. *Chem. Soc. Rev.* **2017**, *46* (23), 7105–7123. <https://doi.org/10.1039/c7cs00240h>.
- (4) Kitai, A., (Ed). *Luminescent Materials and Applications*, Wiley, 2008.
- (5) Lipscomb, W. N. *Boron Hydrides*, Dover; Courier Corporation, 2013, 1963.
- (6) Alexandrova, A. N.; Boldyrev, A. I.; Zhai, H. J.; Wang, L. S. All-Boron Aromatic Clusters as Potential New Inorganic Ligands and Building Blocks in Chemistry. *Coord. Chem. Rev.* **2006**, *250* (21–22), 2811–2866. <https://doi.org/10.1016/j.ccr.2006.03.032>.
- (7) Housecroft, C. E.; Sharpe, A. G. *Inorganic Chemistry 5th Ed.* Pearson; 2005.
- (8) Aihara, J. Three-Dimensional Aromaticity of Polyhedral Boranes. *J. Am. Chem. Soc.* **1978**, *100* (11), 3339–3342. <https://doi.org/10.1021/ja00479a015>.
- (9) King, R. B. Three-Dimensional Aromaticity in Polyhedral Boranes and Related Molecules. *Chem. Rev.* **2001**, *101* (5), 1119–1152. <https://doi.org/10.1021/cr000442t>.
- (10) Grimes, R. N. Viewpoints : Chemists on Chemistry Boron Clusters Come of Age. *J. Chem. Educ.* **2004**, *81* (5), 657–672.
- (11) Hey-Hawkins, E.; Teixidor, C. V. (Eds) *Boron-Based Compounds: Potential and Emerging Applications in Medicine*, Wiley; 2018.
- (12) Kokado, K.; Chujo, Y. Emission via Aggregation of Alternating Polymers with O-Carborane and p-Phenylene-Ethynylene Sequences. *Macromolecules* **2009**, *42* (5), 1418–1420. <https://doi.org/10.1021/ma8027358>.
- (13) P. Kaszynski, in: N. Hosmane (Ed.), *closo*-Boranes as Structural Elements for

Liquid Crystals” in Boron Science: New Technologies & Applications, CRC *Boron Science*; 2016. <https://doi.org/10.1201/b11199>.

- (14) Hajhusein, A. N.; Abuzahra, L. S.; Pietrzak, A.; Sadek, M. F.; Ali, M. O.; Wojciechowski, J.; Friedli, A. C.; Kaszyński, P. Synthesis of 4-Alkoxy pyridines as Intermediates for Zwitterionic Liquid Crystals. *Arkivoc* **2018**, 2018 (7), 225–235. <https://doi.org/10.24820/ark.5550190.p010.700>.
- (15) Dash, B. P.; Satapathy, R.; Maguire, J. A.; Hosmane, N. S. Polyhedral Boron Clusters in Materials Science. *New J. Chem.* **2011**, 35 (10), 1955–1972. <https://doi.org/10.1039/c1nj20228f>.
- (16) Tsuboya, N.; Lamrani, M.; Hamasaki, R.; Ito, M.; Mitsuishi, M.; Miyashita, T.; Yamamoto, Y. Nonlinear Optical Properties of Novel Carborane-Ferrocene Conjugated Dyads. Electron-Withdrawing Characteristics of Carboranes. *J. Mater. Chem.* **2002**, 12 (9), 2701–2705. <https://doi.org/10.1039/b202236b>.
- (17) Dash, B. P.; Satapathy, R.; Gaillard, E. R.; Norton, K. M.; Maguire, J. A.; Chug, N.; Hosmane, N. S. Enhanced π -Conjugation and Emission via Icosahedral Carboranes: Synthetic and Spectroscopic Investigation. *Inorg. Chem.* **2011**, 50 (12), 5485–5493. <https://doi.org/10.1021/ic200010q>.
- (18) Dash, B. P.; Satapathy, R.; Gaillard, E. R.; Maguire, J. A.; Hosmane, N. S. Synthesis and Properties of Carborane-Appended C₃-Symmetrical Extended π Systems. *J. Am. Chem. Soc.* **2010**, 132 (18), 6578–6587. <https://doi.org/10.1021/ja101845m>.
- (19) Kokado, K.; Nagai, A.; Chujo, Y. Poly(γ -Glutamic Acid) Hydrogels with Water-Sensitive Luminescence Derived from Aggregation-Induced Emission of *o*-Carborane. *Macromolecules* **2010**, 43 (15), 6463–6468. <https://doi.org/10.1021/ma100792z>.
- (20) Lerouge, F.; Ferrer-Ugalde, A.; Viñas, C.; Teixidor, F.; Sillanpää, R.; Abreu, A.; Xochitiotzi, E.; Farfán, N.; Santillan, R.; Núñez, R. Synthesis and Fluorescence Emission of Neutral and Anionic Di- and Tetra-Carboranyl Compounds. *Dalt. Trans.* **2011**, 40 (29), 7541–7550. <https://doi.org/10.1039/c1dt10309a>.
- (21) Kokado, K.; Chujo, Y. Multicolor Tuning of Aggregation-Induced Emission through Substituent Variation of Diphenyl-*o*-Carborane. *J. Org. Chem.* **2011**, 76 (1), 316–319. <https://doi.org/10.1021/jo101999b>.
- (22) Tominaga, M.; Naito, H.; Morisaki, Y.; Chujo, Y. Colour-Tunable Aggregation-Induced Emission of Trifunctional *o*-Carborane Dyes. *New J. Chem.* **2014**, 38 (12), 5686–5690. <https://doi.org/10.1039/c4nj00955j>.
- (23) Ferrer-Ugalde, A.; González-Campo, A.; Viñas, C.; Rodríguez-Romero, J.;

- Santillan, R.; Farfán, N.; Sillanpää, R.; Sousa-Pedrares, A.; Núñez, R.; Teixidor, F. Fluorescence of New *O*-Carborane Compounds with Different Fluorophores: Can It Be Tuned? *Chem. - A Eur. J.* **2014**, *20* (32), 9940–9951. <https://doi.org/10.1002/chem.201402396>.
- (24) Mukherjee, S.; Thilagar, P. Boron Clusters in Luminescent Materials. *Chem. Commun.* **2016**, *52* (6), 1070–1093. <https://doi.org/10.1039/c5cc08213g>.
- (25) Il'inchik, E. A.; Volkov, V. V.; Dunaev, S. T. Structural Effects in the Electron Absorption and Luminescence Spectra of Decaborane Derivatives B₁₀H₁₂L₂) *J. Struct. Chem.* **1996**, *37* (1), 51–57.
- (26) Pakhomov, S.; Kaszynski, P.; Young, V. G. 10-Vertex *Closo*-Boranes as Potential π Linkers for Electronic Materials. *Inorg. Chem.* **2000**, *39* (10), 2243–2245. <https://doi.org/10.1021/ic991350t>.
- (27) Sivaev, I. B.; Bregadze, V. I.; Sjöberg, S. Chemistry of *Closo*-Dodecaborate Anion [B₁₂H₁₂]²⁻; A Review. *Collect. Czechoslov. Chem. Commun.* **2002**, *67* (6), 679–727. <https://doi.org/10.1135/cccc20020679>.
- (28) Kaszyński, P.; Ringstrand, B. Functionalization of *Closo*-Borates via Iodonium Zwitterions. *Angew. Chemie - Int. Ed.* **2015**, *54* (22), 6576–6581. <https://doi.org/10.1002/anie.201411858>.
- (29) Rzeszotarska, E.; Novozhilova, I.; Kaszyński, P. Convenient Synthesis of [*Closo*-B₁₀H₉-1-I]²⁻ and [*Closo*-B₁₀H₈-1,10-I₂]²⁻ Anions. *Inorg. Chem.* **2017**, *56* (22), 14351–14356. <https://doi.org/10.1021/acs.inorgchem.7b02477>.
- (30) Mebs, S.; Kalinowski, R.; Grabowsky, S.; Förster, D.; Kickbusch, R.; Justus, E.; Morgenroth, W.; Paulmann, C.; Luger, P.; Gabel, D.; *et al.* Real-Space Indicators for Chemical Bonding. Experimental and Theoretical Electron Density Studies of Four Deltahedral Boranes. *Inorg. Chem.* **2011**, *50* (1), 90–103. <https://doi.org/10.1021/ic1013158>.
- (31) Tokarz, P.; Kaszyński, P.; Domagała, S.; Woźniak, K. The [*Closo*-B₁₂H₁₁-1-IAr]-Zwitterion as a Precursor to Monosubstituted Derivatives of [*Closo*-B₁₂H₁₂]²⁻. *J. Organomet. Chem.* **2015**, *798*, 70–79. <https://doi.org/10.1016/j.jorganchem.2015.07.035>.
- (32) Jacob, L.; Rzeszotarska, E.; Pietrzak, A.; Young, V. M.; Kaszyński, P. Synthesis, structural analysis and functional group interconversion in the [*closo*-B₁₀H₈-1,10-2X]²⁻ (X = CN, [OCRNMe₂]⁺, OCOR, and [OH₂]⁺) derivatives. *Eur. J. Inorg. Chem.* **2020**, *in press*.

- (33) Avdeeva, V. V.; Polyakova, I. N.; Churakov, A. V.; Vologzhanina, A. V.; Malinina, E. A.; Zhizhin, K. Y.; Kuznetsov, N. T. Complexation and Exopolyhedral Substitution of the Terminal Hydrogen Atoms in the Decahydro-*Closo*-Decaborate Anion in the Presence of Cobalt(II). *Polyhedron* **2019**, *162*, 65–70. <https://doi.org/10.1016/j.poly.2019.01.051>.
- (34) Avdeeva, V. V.; Polyakova, I. N.; Goeva, L. V.; Malinina, E. A.; Kuznetsov, N. T. [2,7(8)-B₁₀H₈(OC(O)CH₃)₂]²⁻ Derivatives in Synthesis of Position Isomers of the [B₁₀H₈(OC(O)CH₃)(OH)]²⁻ Anion with the 2,6(9)- and 2,7(8)-Arrangement of Functional Groups. *Russ. J. Inorg. Chem.* **2014**, *59* (11), 1247–1258. <https://doi.org/10.1134/S0036023614110047>.
- (35) Nachtigal, C.; Preetz, W. Dipyridiniomethane 1-Iodo-*Closo*-Decaborate, [(C₅H₅N)₂CH₂][1-B₁₀H₉]. *Acta Crystallogr. Sect. C Cryst. Struct. Commun.* **1996**, *52* (2), 453–455. <https://doi.org/10.1107/S0108270195012340>.
- (36) Haeckel, O.; Preetz, W. Darstellung Und Kristallstrukturen von Dipyridiniomethan-Monohalogenohydro-*closo*-Dodecaboraten(2-), [(C₅H₅N)₂CH₂][B₁₂H₁₁X]; X = Cl, Br, I. *J. Inorg. Gen. Chem.* **1995**, *621* (9), 1454–1458. <https://doi.org/10.1002/zaac.19956210903>.
- (37) Kálmán, A.; Párkányi, L.; Argay, G. Classification of the Isostructurality of Organic Molecules in the Crystalline State. *Acta Crystallogr. Sect. B* **1993**, *49* (6), 1039–1049. <https://doi.org/10.1107/S010876819300610X>.
- (38) Kaszynski, P.; Huang, J.; Jenkins, G. S.; Bairamov, K. A.; Lipiak, D. Boron Clusters in Liquid Crystals. *Mol. Cryst. Liq. Cryst. Sci. Technol. Sect. A Mol. Cryst. Liq. Cryst.* **1995**, *260* (pt 1), 315–332. <https://doi.org/10.1080/10587259508038705>.
- (39) Jankowiak, A.; Baliński, A.; Harvey, J. E.; Mason, K.; Januszko, A.; Kaszyński, P.; Young, V. G.; Persoons, A. [*Closo*-B₁₀H₁₀]²⁻ as a Structural Element for Quadrupolar Liquid Crystals: A New Class of Liquid Crystalline NLO Chromophores. *J. Mater. Chem. C* **2013**, *1* (6), 1144–1159. <https://doi.org/10.1039/c2tc00547f>.
- (40) Kaszynski, P. *Closo* Boranes As π Structural Elements for Advanced Anisotropic Materials. *ACS Symp. Ser.* **2001**, *798*, 68–82. <https://doi.org/10.1021/bk-2001-0798.ch005>.
- (41) Hansch, C.; Leo, A.; Taft, R. W. A Survey of Hammett Substituent Constants and Resonance and Field Parameters. *Chem. Rev.* **1991**, *91* (2), 165–195. <https://doi.org/10.1021/cr00002a004>.
- (42) Hawthorne, M. F.; Pilling, R. L.; Knoth, W. H. Bis-(triethylammonium) decahydrodeca-borate(2-). *Inorg. Synth.* **1967**, *9*, 16–19.

- (43) *CrysAlisPro*. Rigaku Oxford Diffraction: Oxford 2017.
- (44) Nenner, I.; Schulz, G. J. Temporary Negative Ions and Electron Affinities of Benzene and N-Heterocyclic Molecules: Pyridine, Pyridazine, Pyrimidine, Pyrazine, and *s*-Triazine. *J. Chem. Phys.* **1975**, *62* (5), 1747–1758. <https://doi.org/10.1063/1.430700>.
- (45) Zurawiński, R.; Jakubowski, R.; Domagała, S.; Kaszyński, P.; Woźniak, K. Regioselective Functionalization of the [*Closo*-1-CB₉H₁₀]⁻ Anion through Iodonium Zwitterions. *Inorg. Chem.* **2018**, *57* (16), 10442–10456. <https://doi.org/10.1021/acs.inorgchem.8b01701>.

APPENDIX: Table of Contents

Appendix I: NMR Spectra for Series 1 (Chapter 2)

Figures S1-S27 77

Appendix II: NMR Spectra for Series 7, 8 and 10 (Chapter 3)

Figures S28-S52 103

Appendix III: Copyright permissions. 118

APPENDIX I: NMR Spectra of Series 1

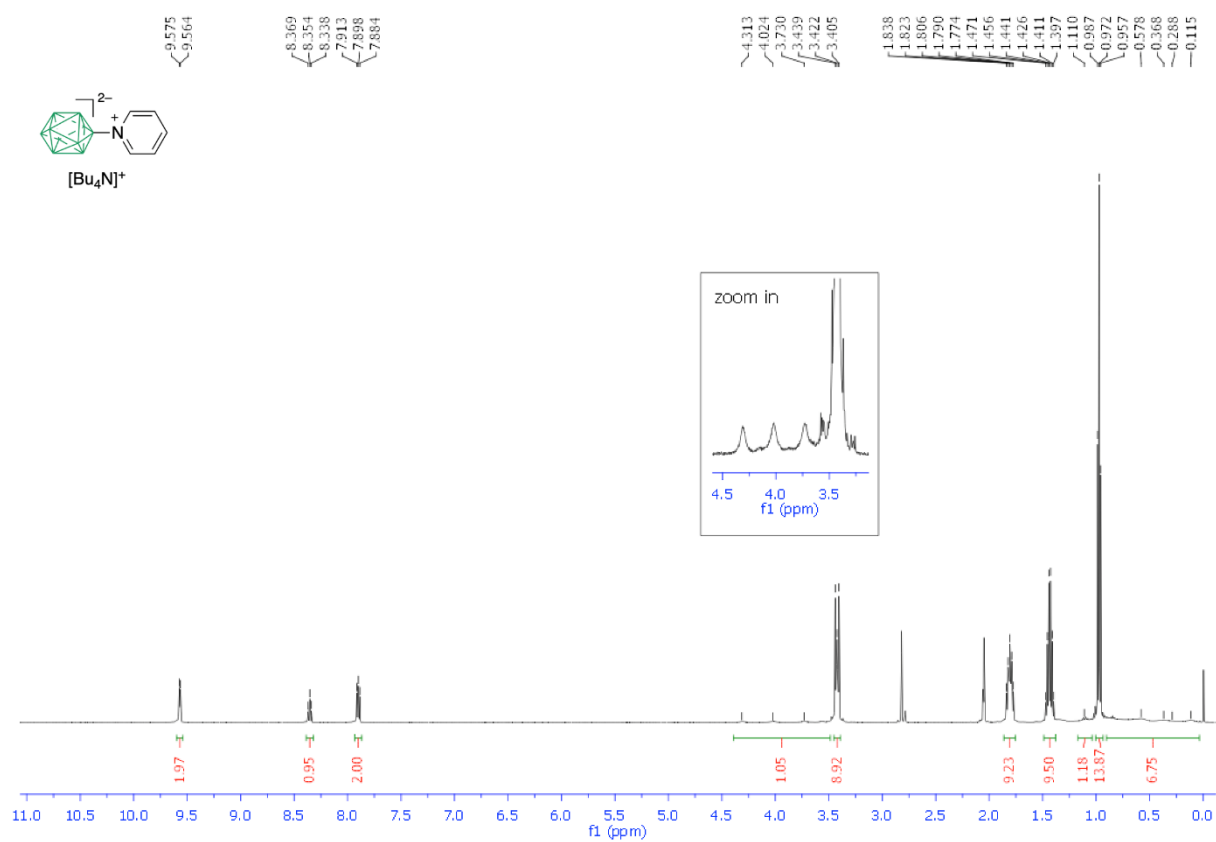


Figure S1. ^1H NMR spectrum for compound **1a**[Bu₄N].

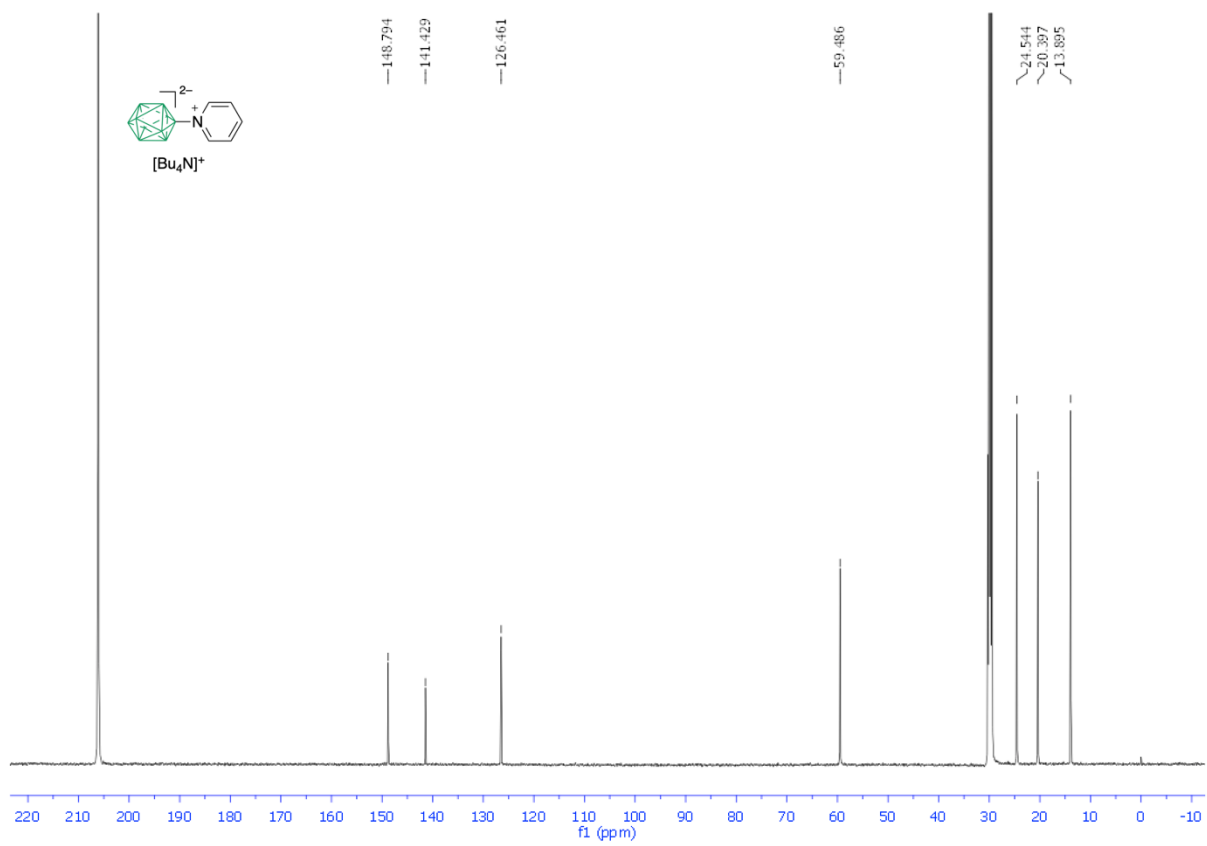


Figure S2. ^{13}C NMR decoupled spectrum for compound **1a**[Bu_4N].

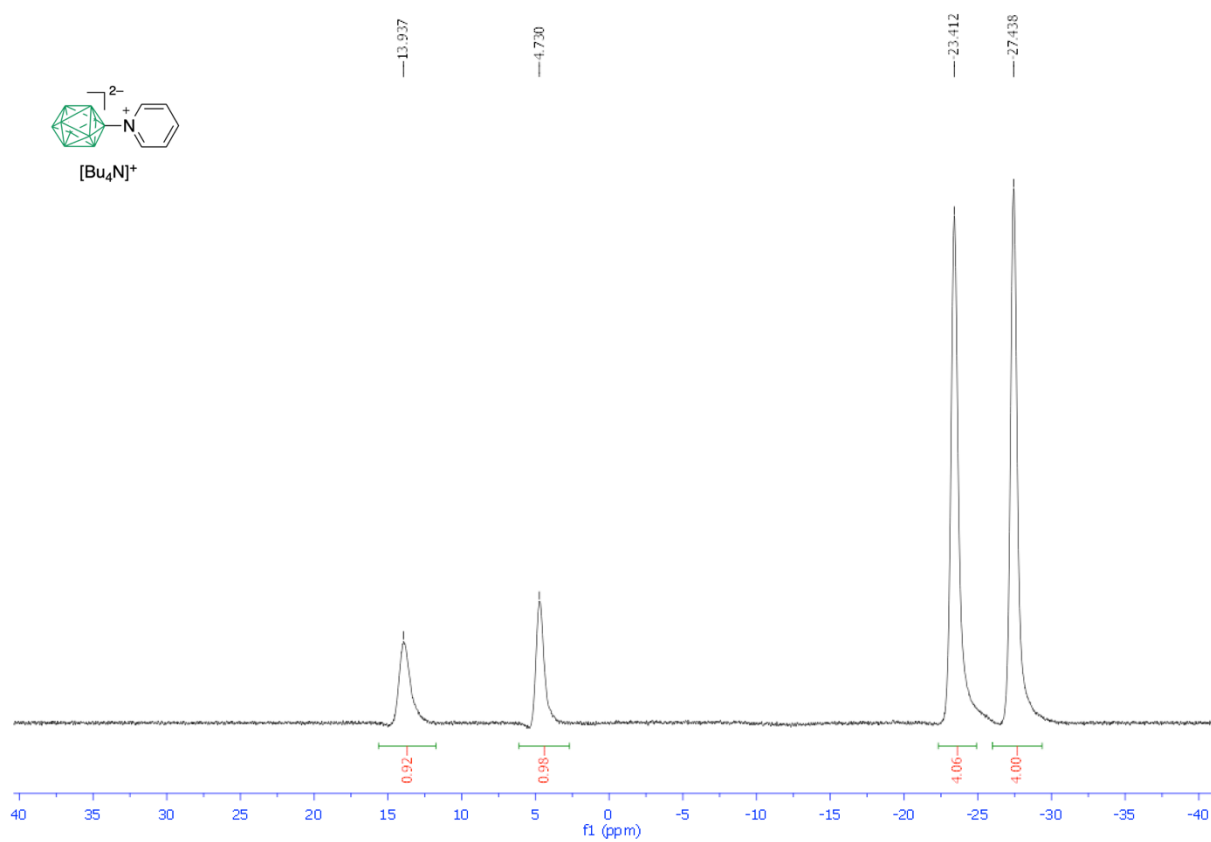


Figure S3. ^{11}B NMR decoupled spectrum for compound **1a**[Bu_4N].

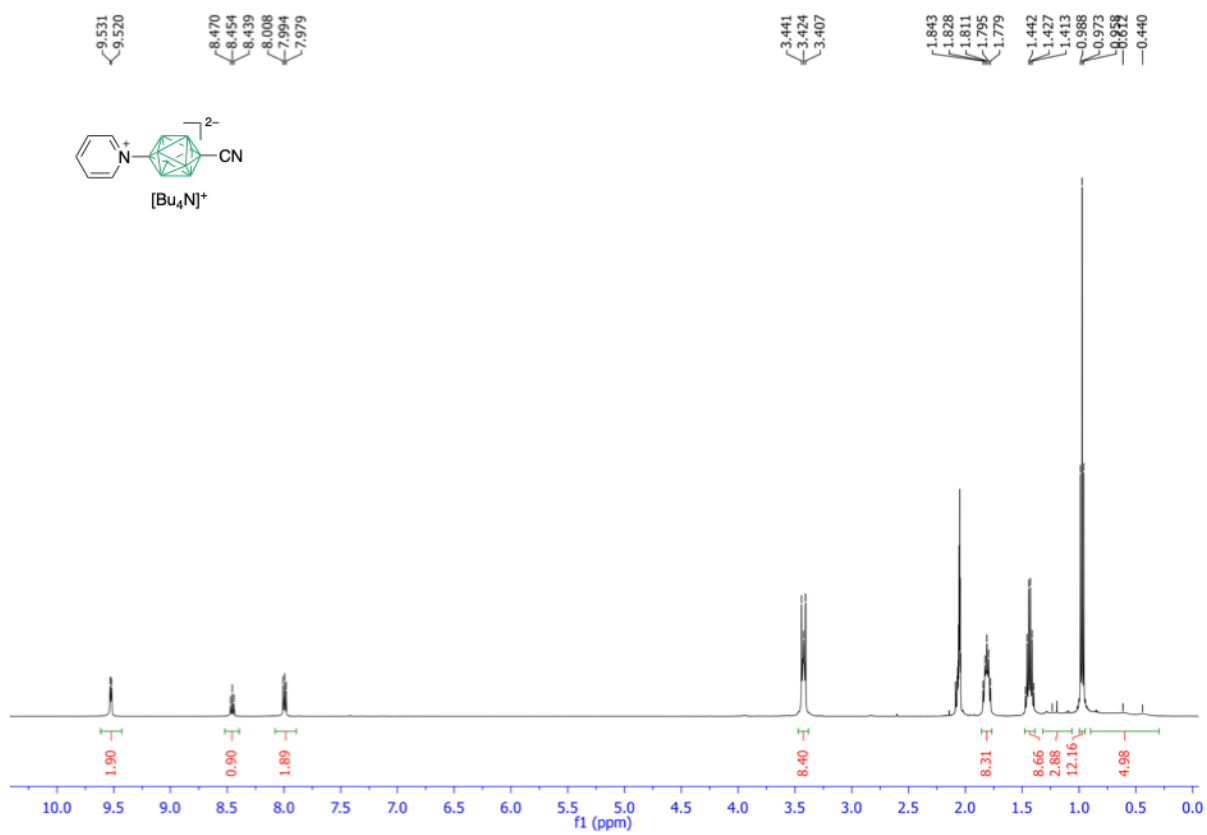


Figure S4. ¹H NMR spectrum for compound **1b**[Bu₄N].

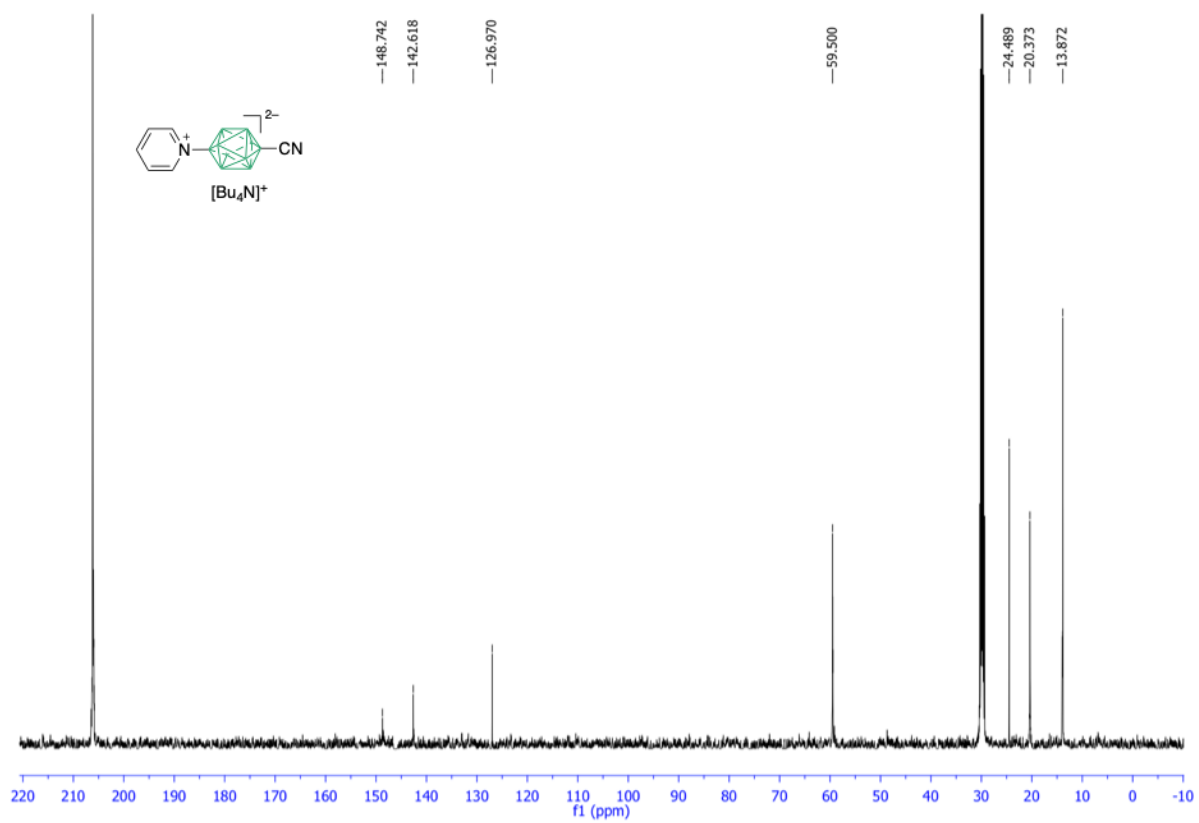


Figure S5. ^{13}C NMR spectrum for compound **1b**[Bu_4N].

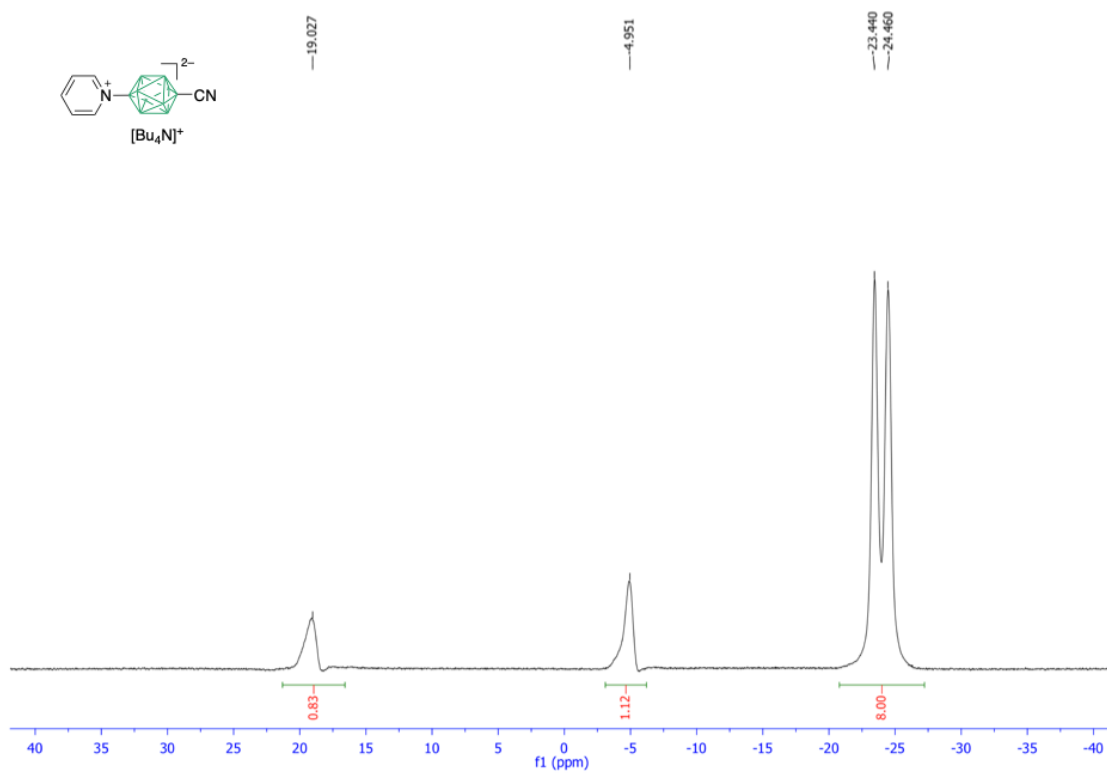


Figure S6. ^{11}B NMR decoupled spectrum for compound **1b**[Bu_4N].

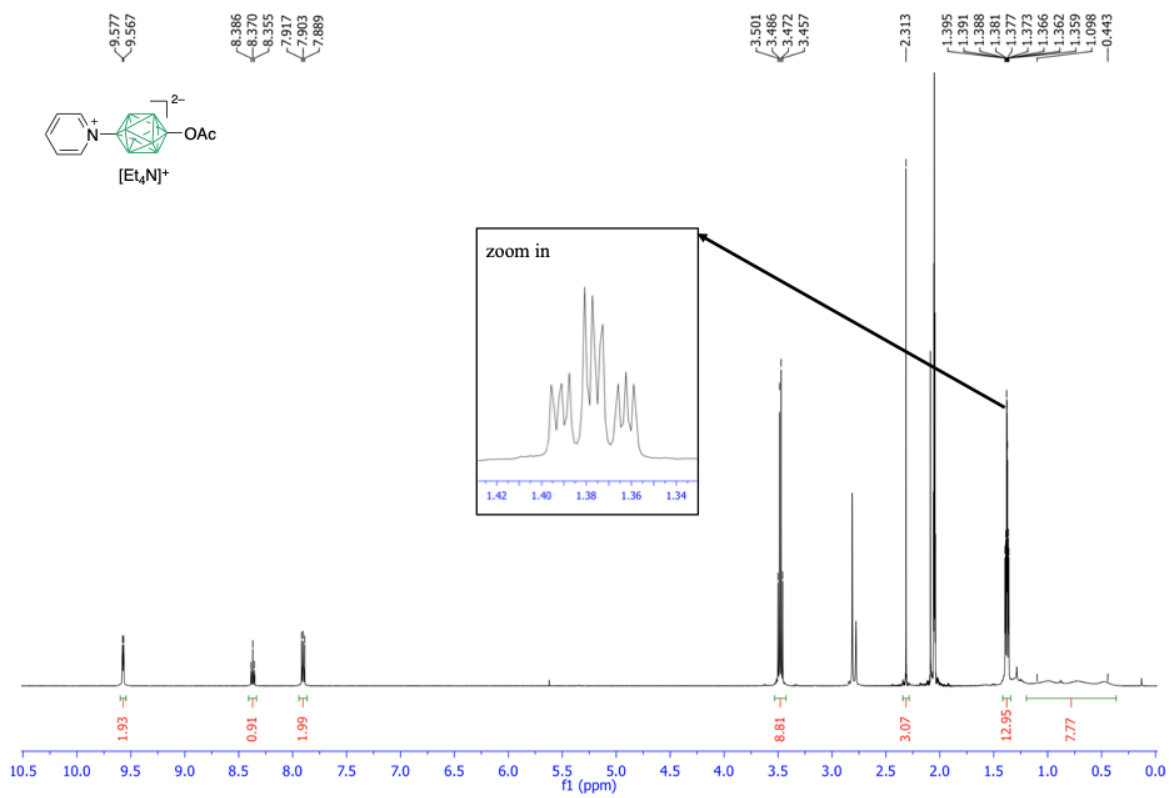
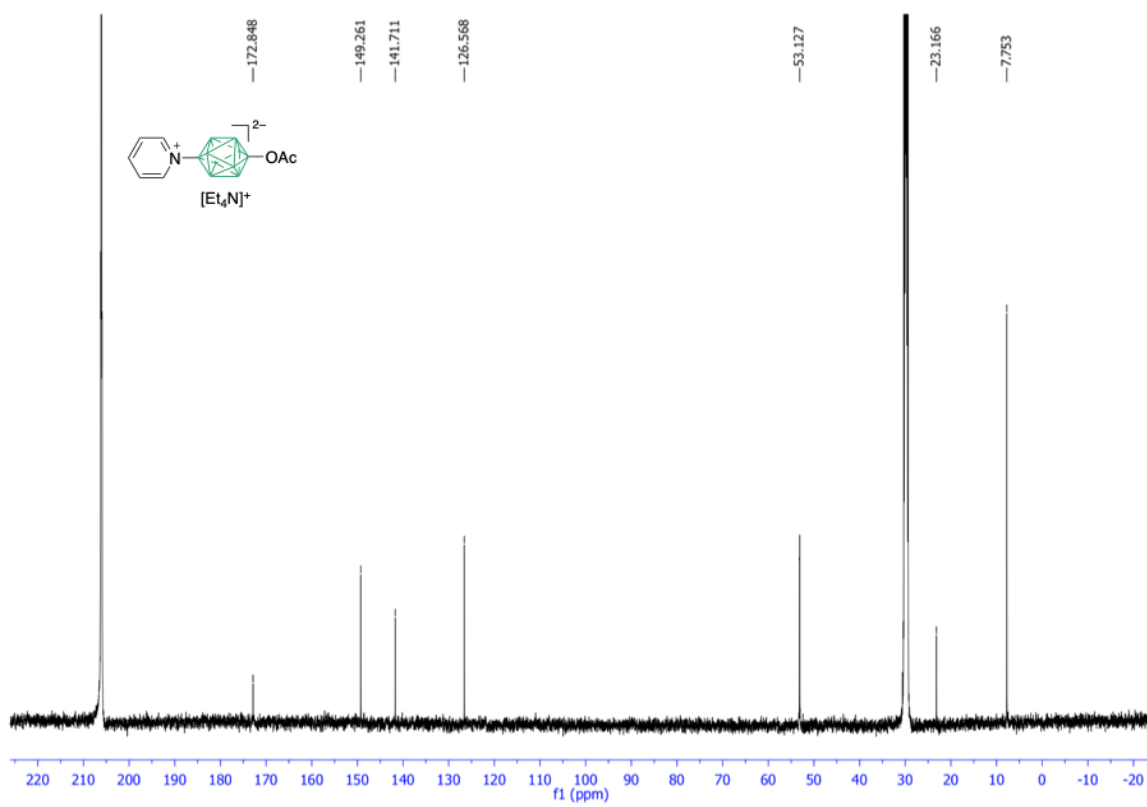


Figure S7. ^1H NMR spectrum for compound **1c**[Et₄N].



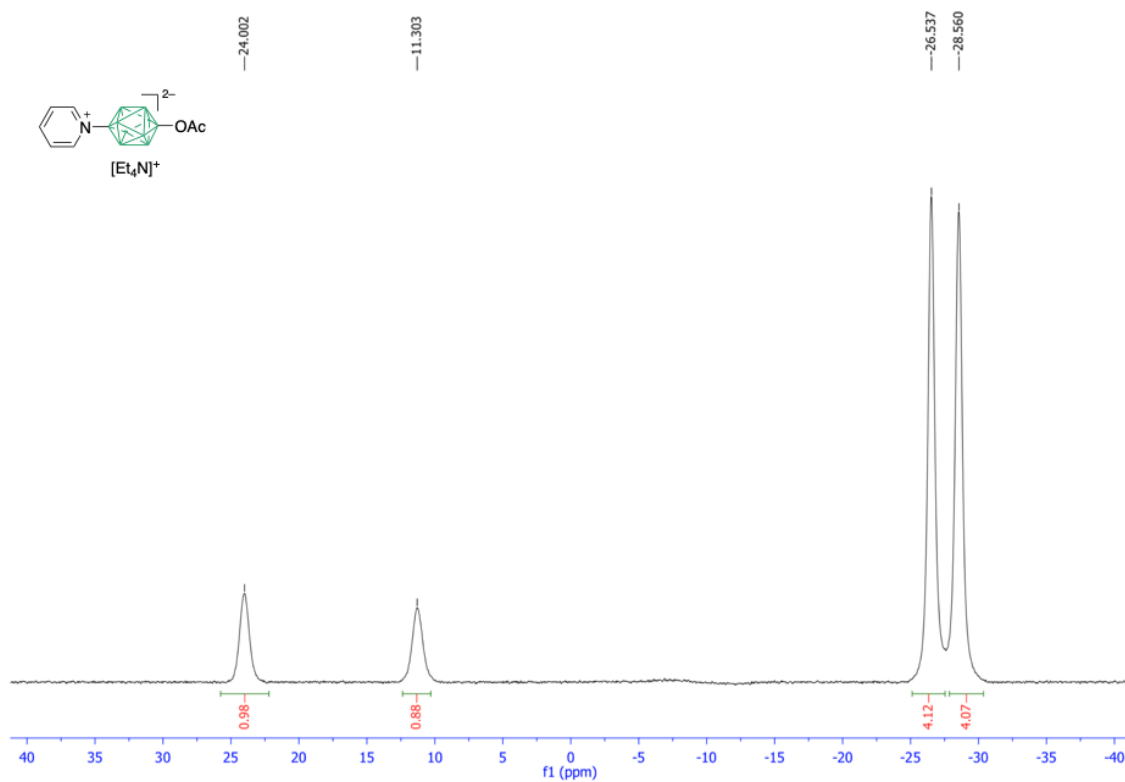


Figure S9. ^{11}B NMR decoupled spectrum for compound **1c** $[\text{Et}_4\text{N}]$.

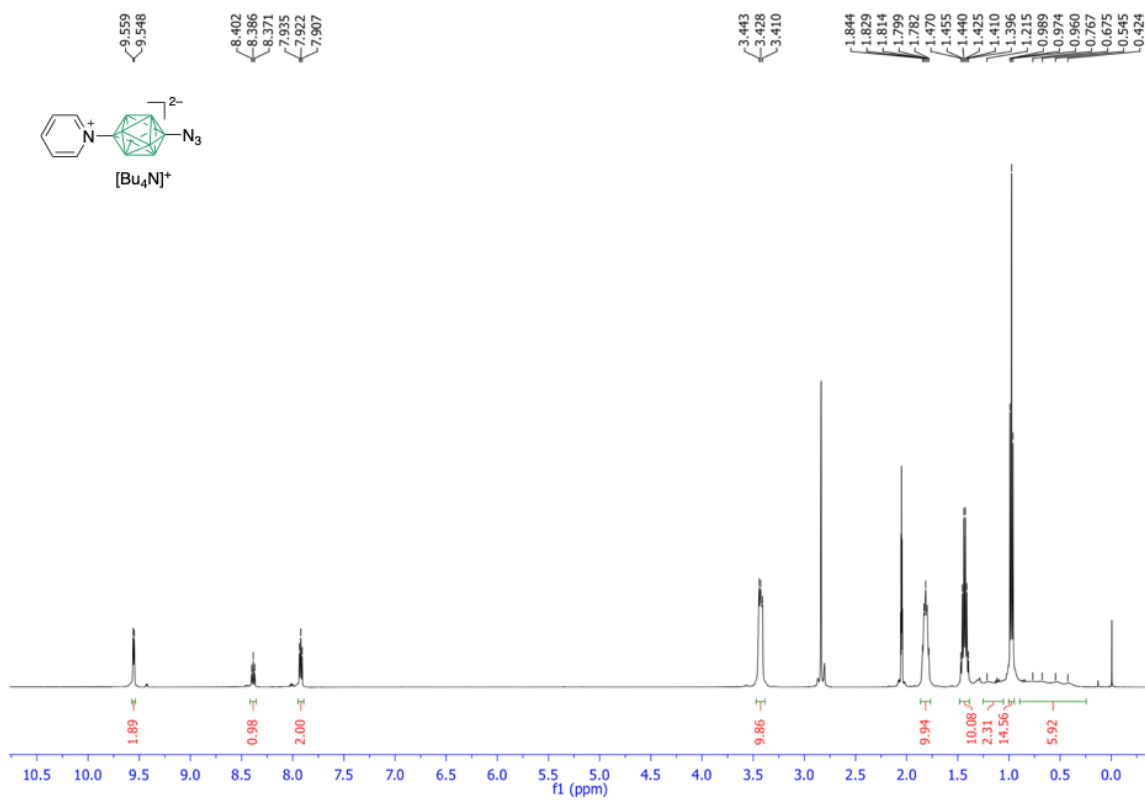


Figure S10. ^1H NMR spectrum for compound **1d**[Bu_4N].

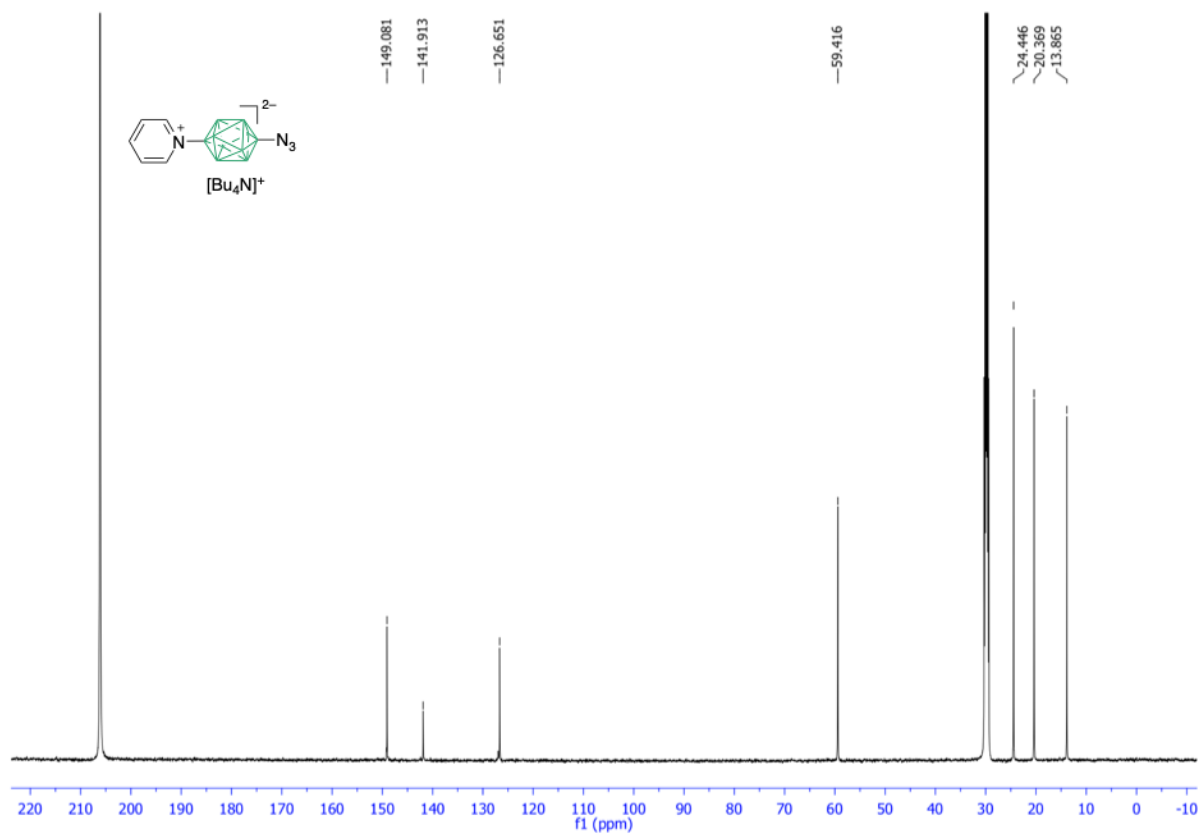


Figure S11. ^{13}C NMR spectrum for compound **1d**[Bu_4N].

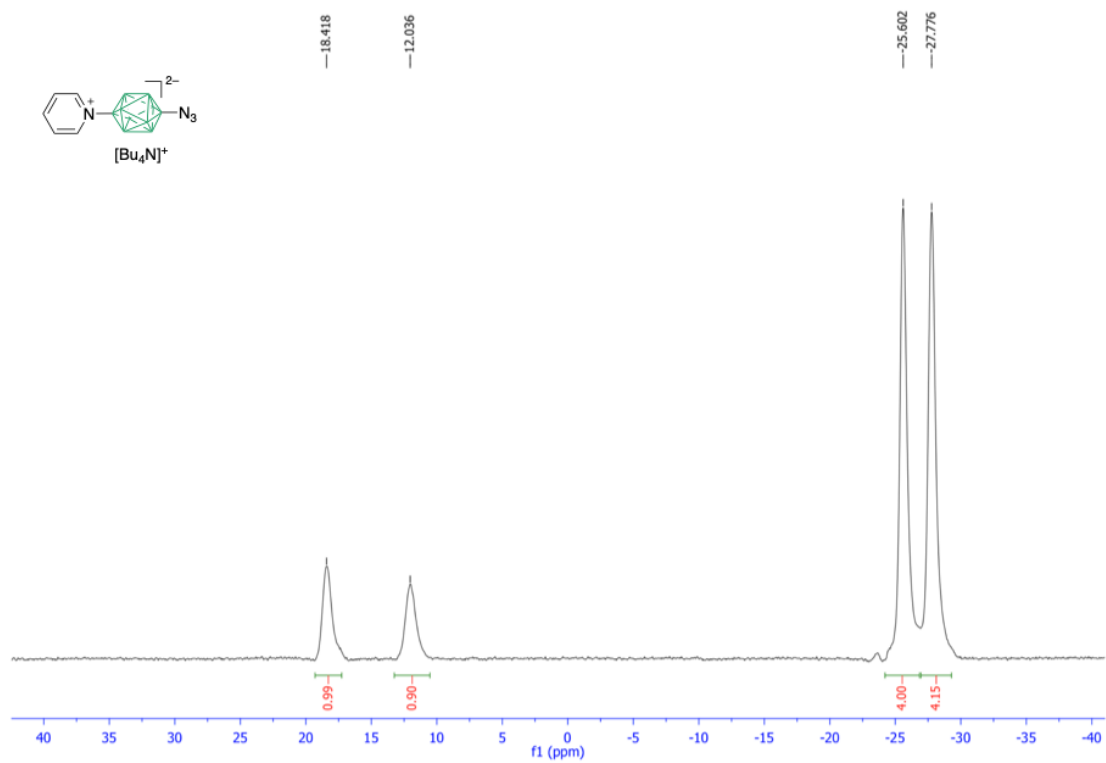


Figure S12. ^{11}B NMR decoupled spectrum for compound **1d** $[\text{Bu}_4\text{N}]$.

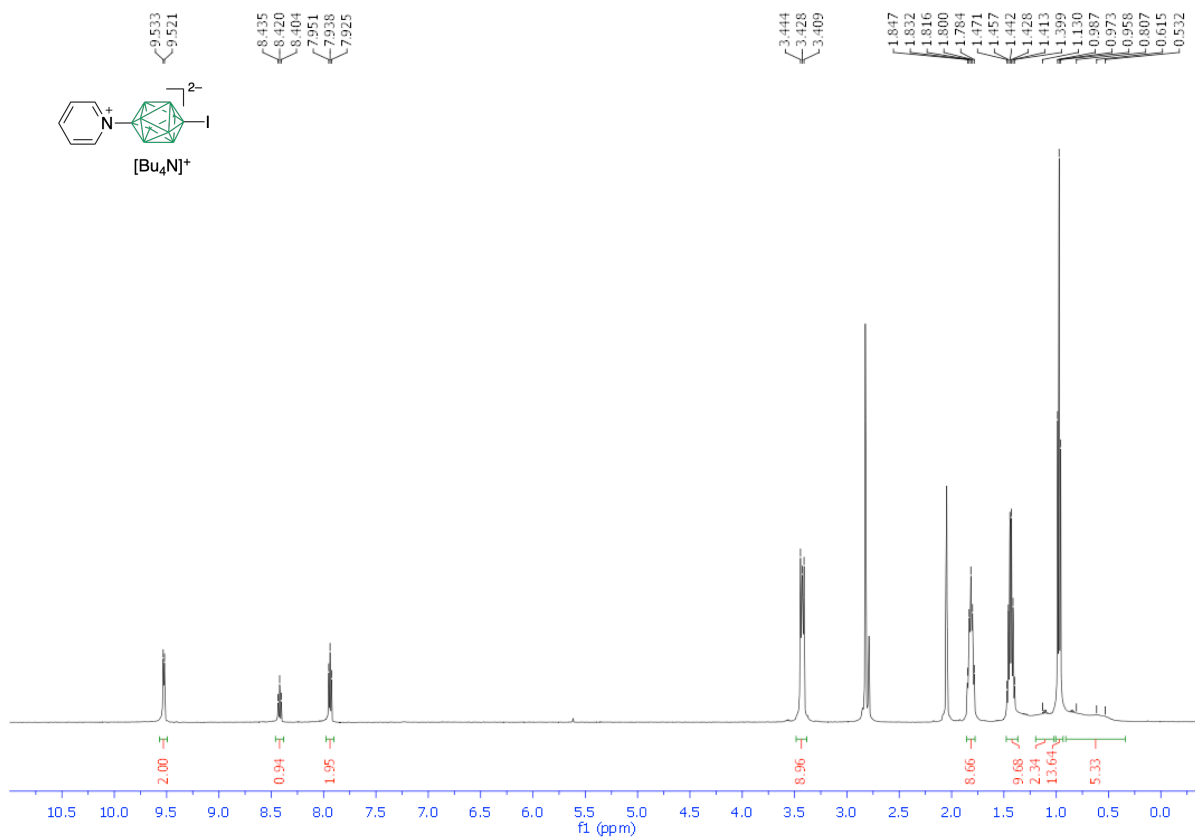


Figure S13. ¹H NMR spectrum for compound **1e**[Bu₄N].

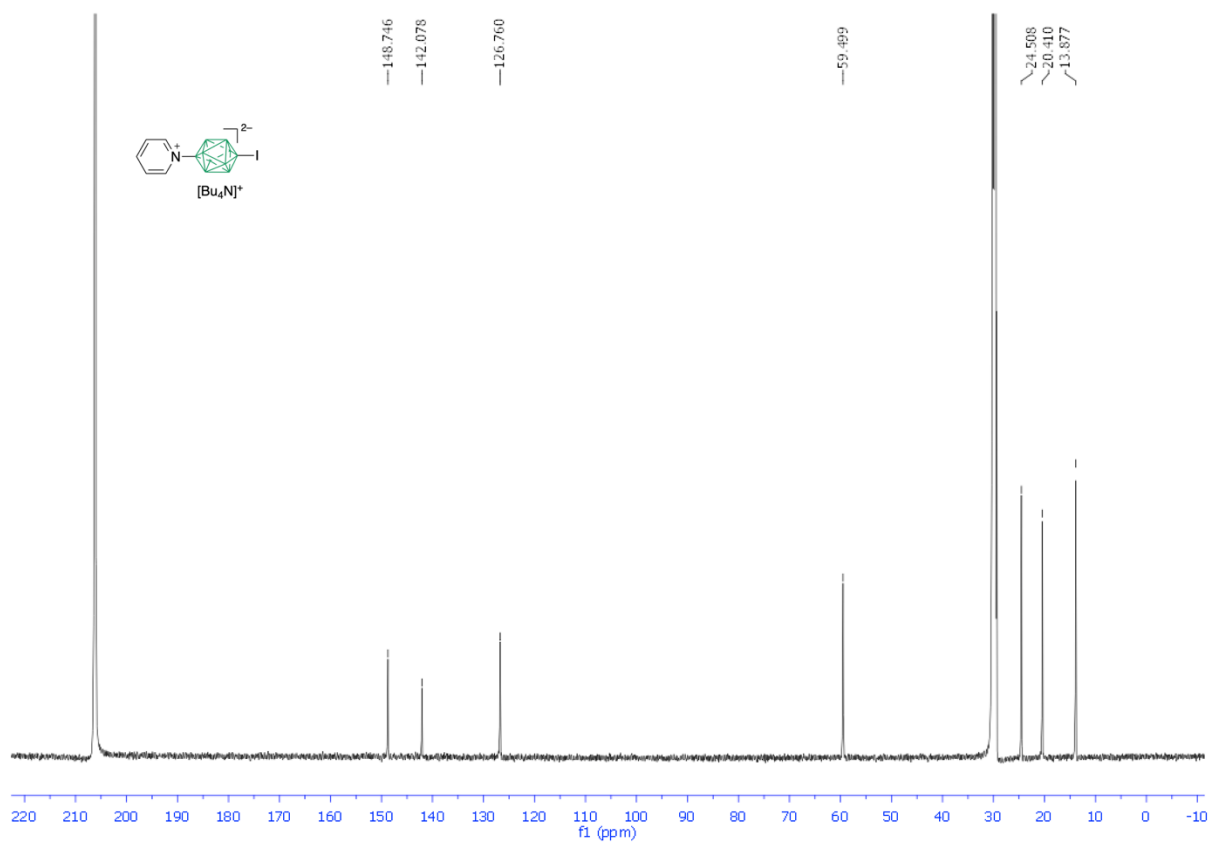


Figure S14. ^{13}C NMR spectrum for compound **1e** $[\text{Bu}_4\text{N}]$.

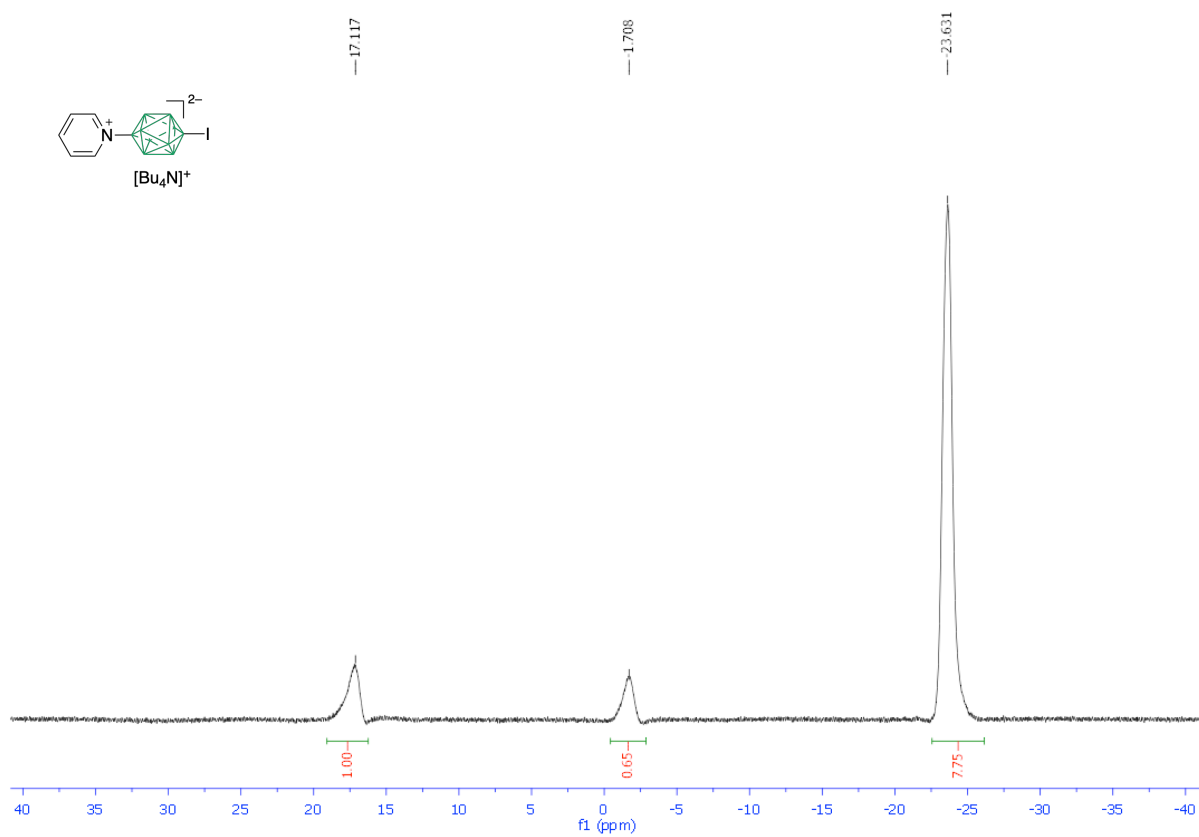


Figure S15. ^{11}B NMR spectrum for compound **1e** $[\text{Bu}_4\text{N}]$.

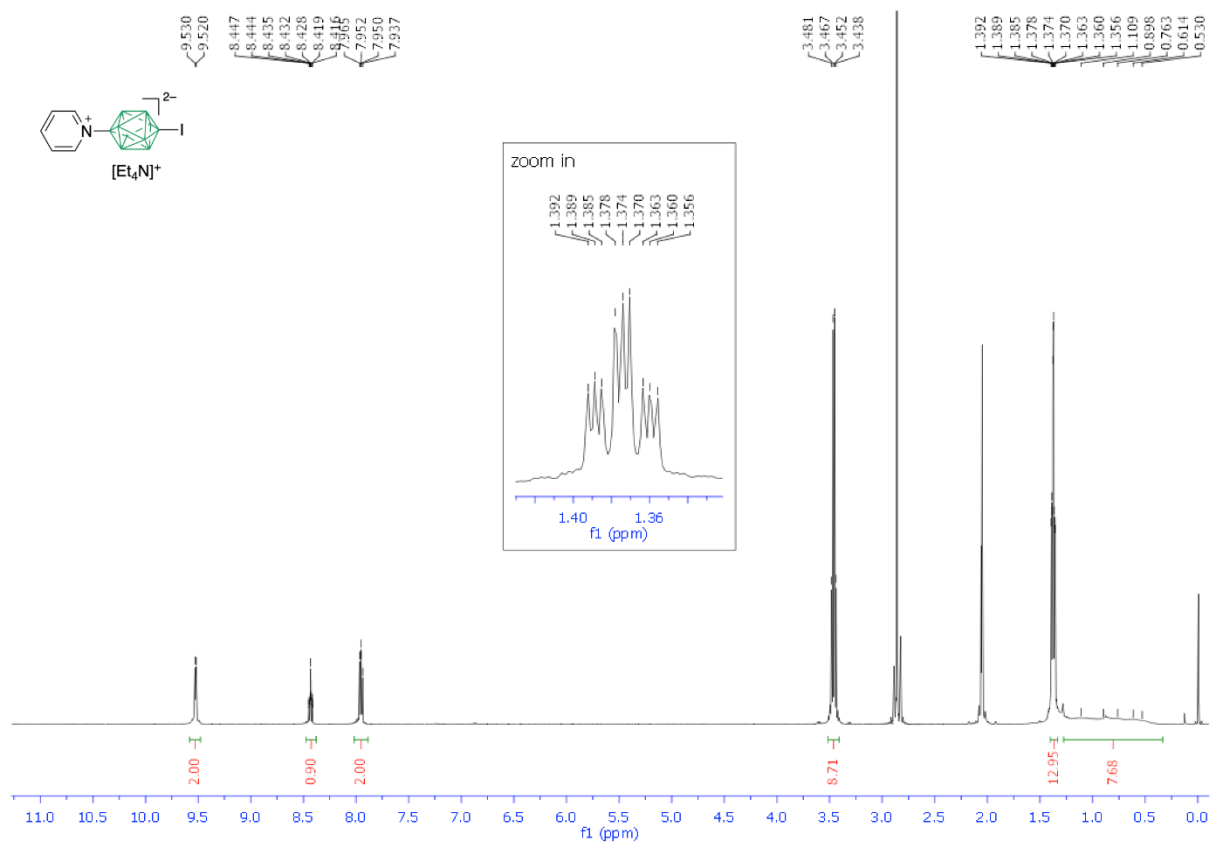


Figure S16. ^1H NMR spectrum for compound **1e**[Et₄N].

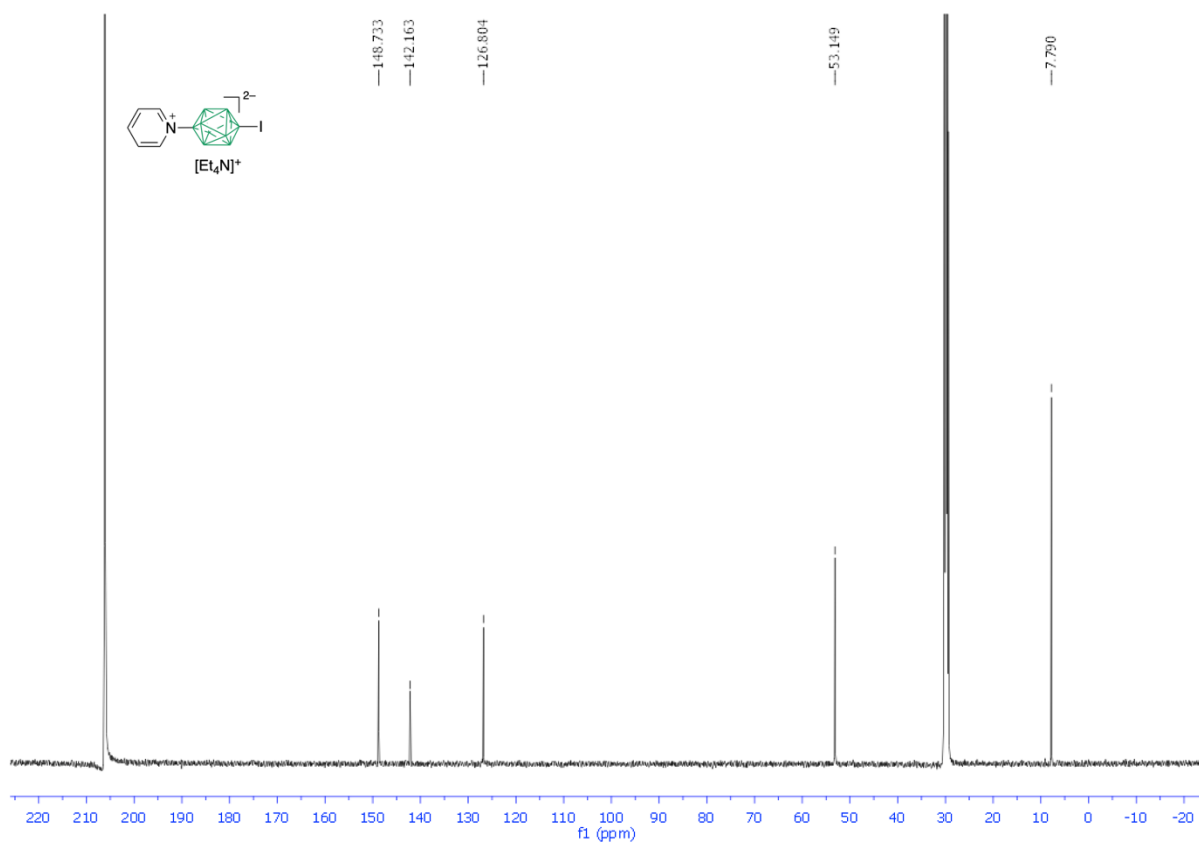


Figure S17. ^{13}C NMR spectrum for compound **1e** $[\text{Et}_4\text{N}]$.

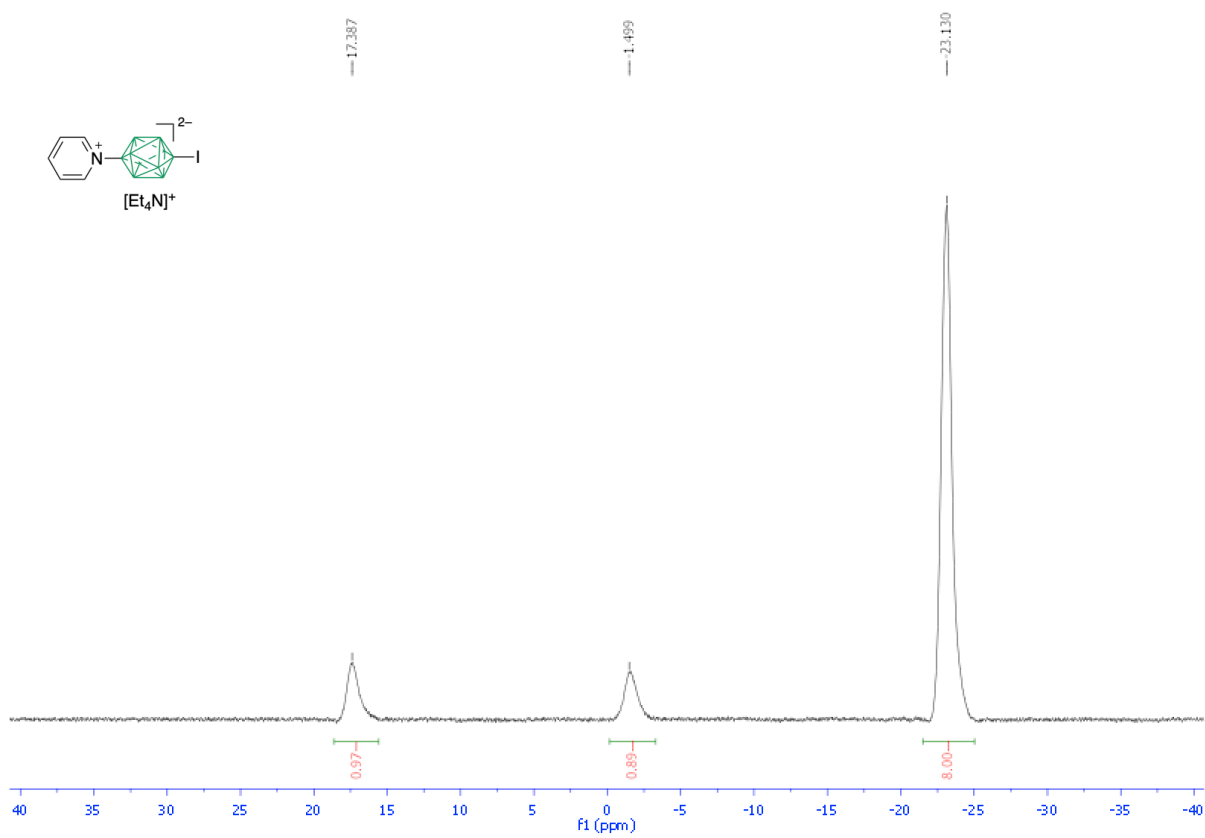


Figure S18. ^{11}B NMR spectrum for compound **1e** $[\text{Et}_4\text{N}]$.

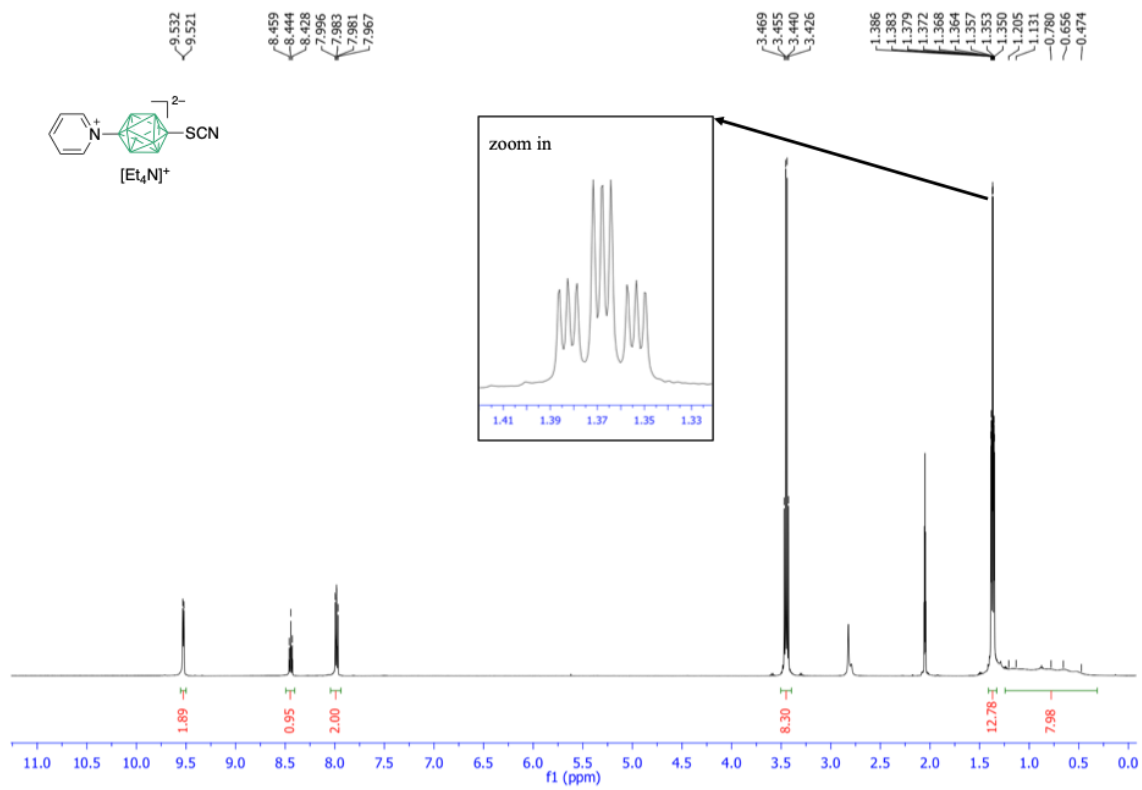


Figure S19. ^1H NMR spectrum for compound **1f**[Et_4N].

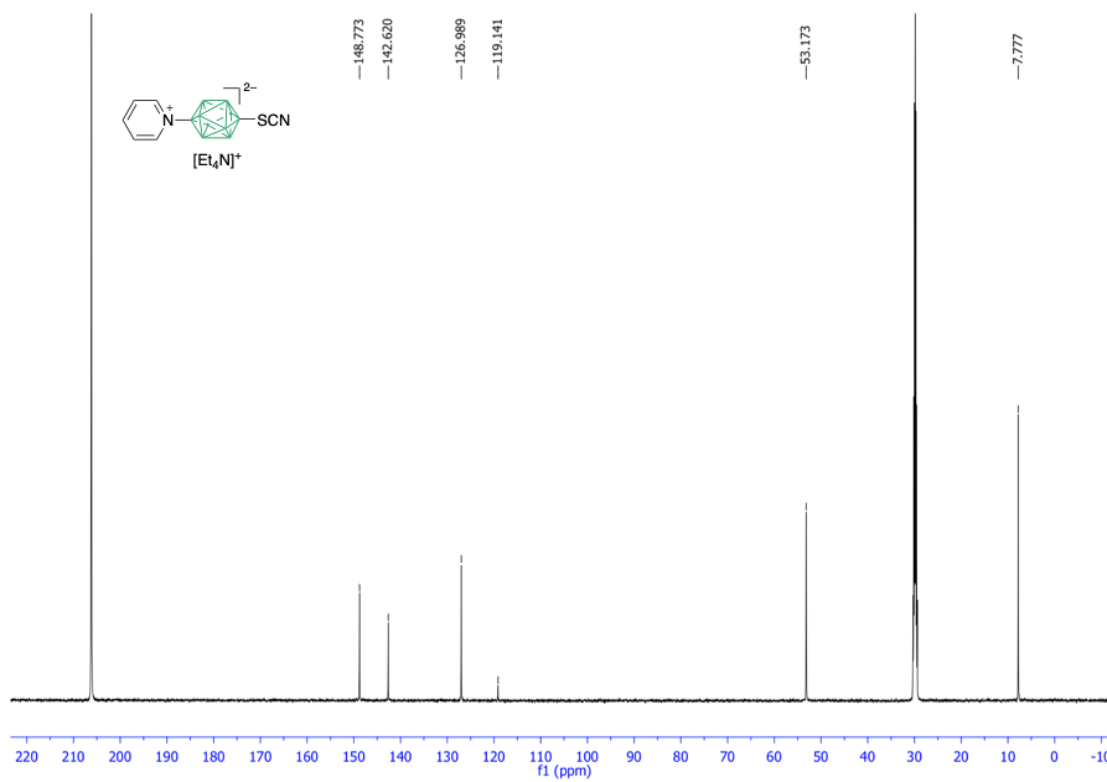


Figure S17. ^{13}C NMR spectrum for compound **1f**[Et₄N].

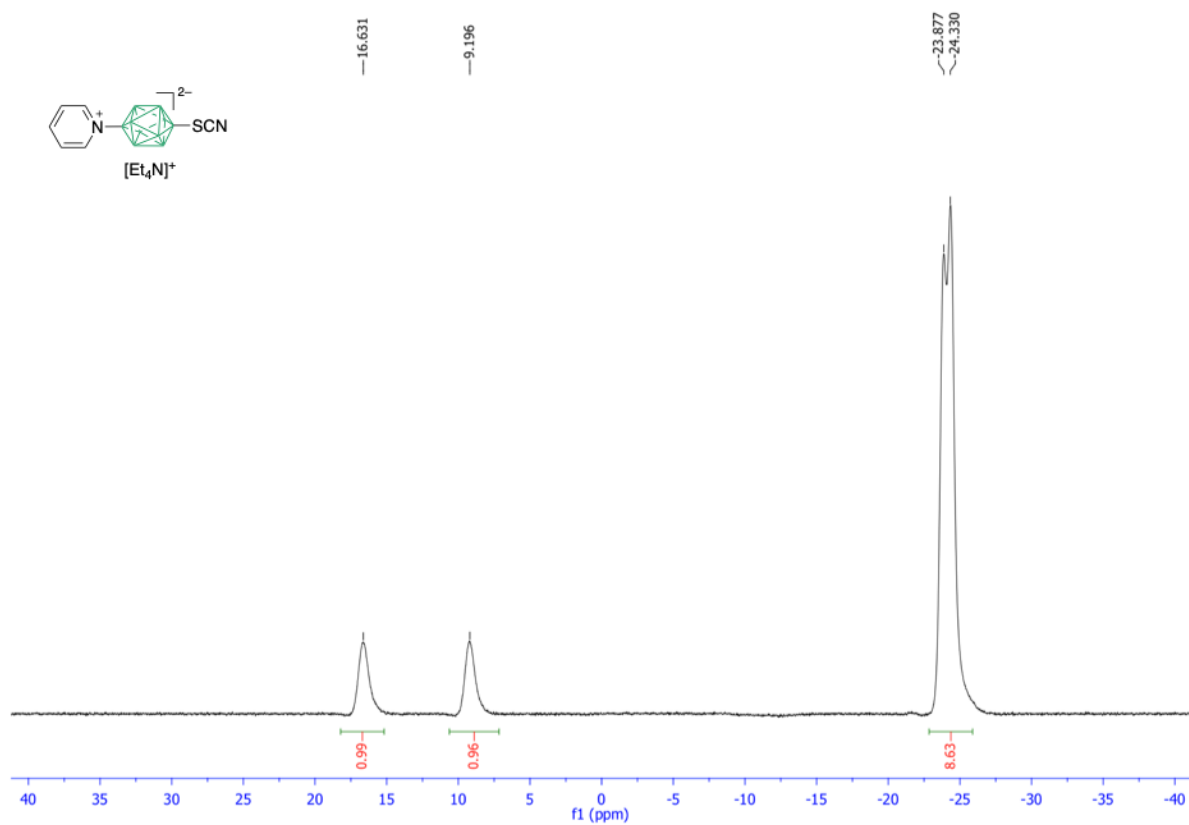


Figure S18. ^{11}B NMR decoupled spectrum for compound **1f**[Et₄N].

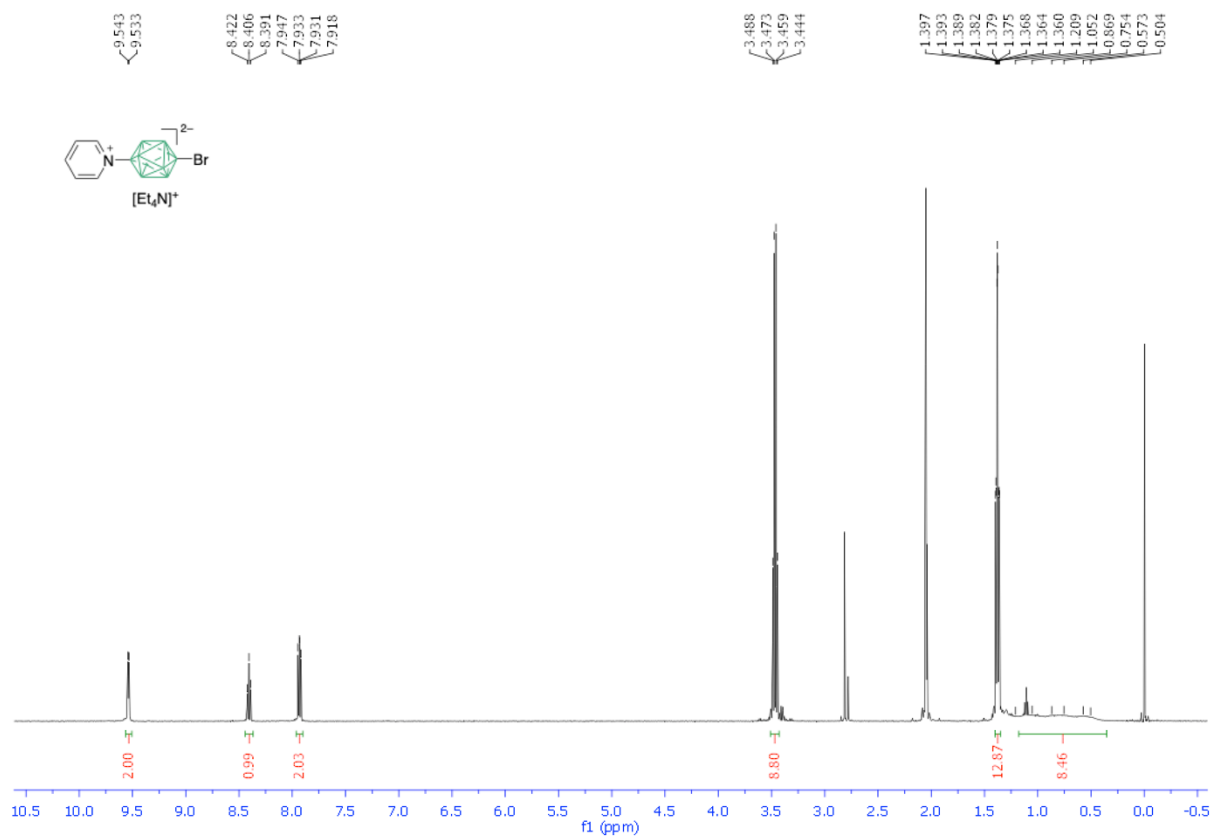


Figure S19. ¹H NMR spectrum for compound **1g**[Et₄N].

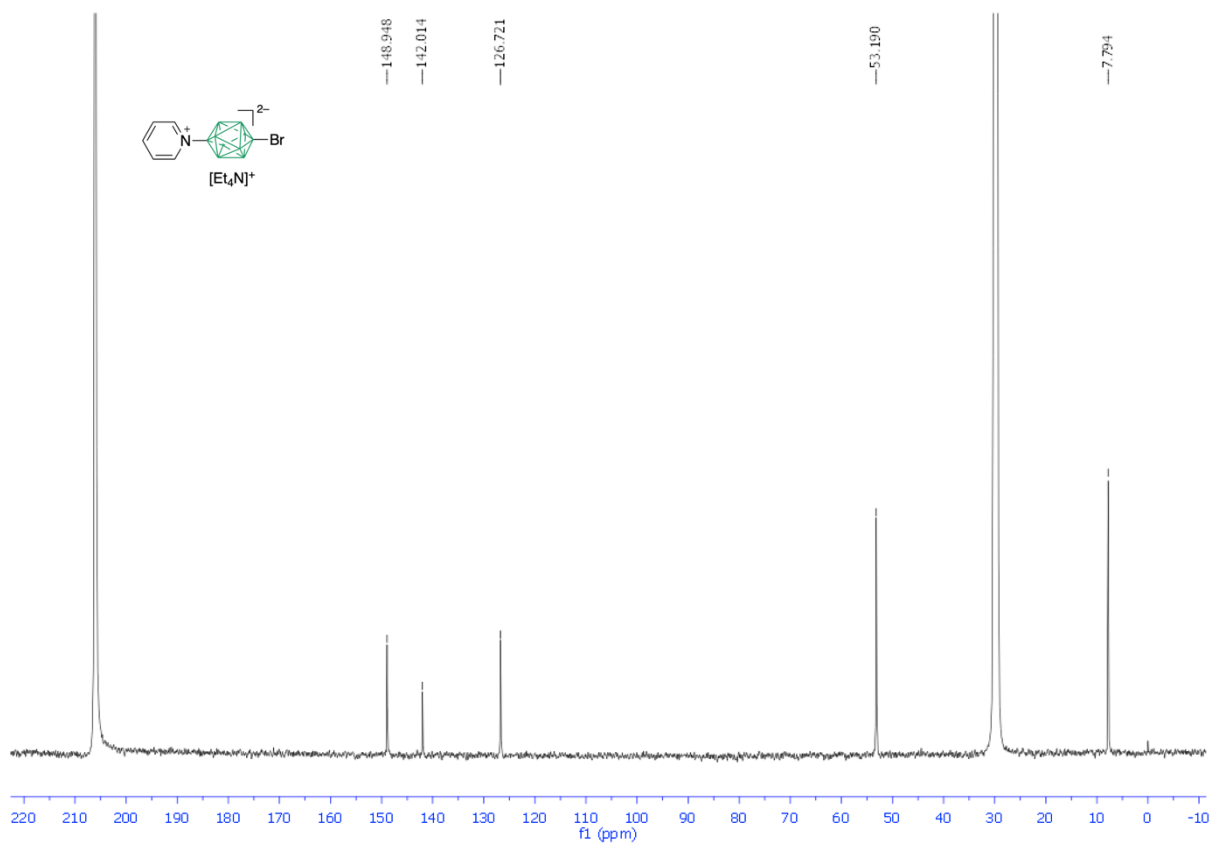


Figure S20. ^{13}C NMR spectrum for compound **1g**[Et₄N].

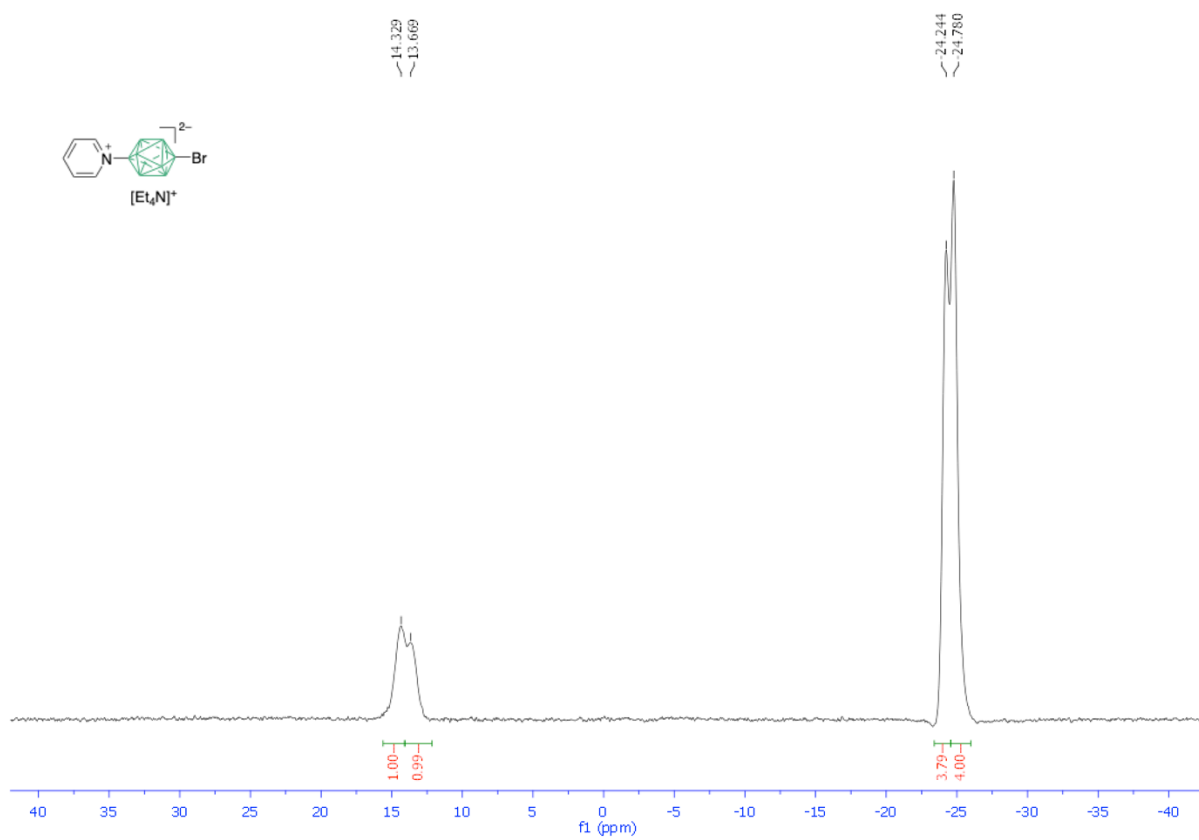


Figure S21. ^{11}B NMR spectrum for compound **1g**[Et_4N].

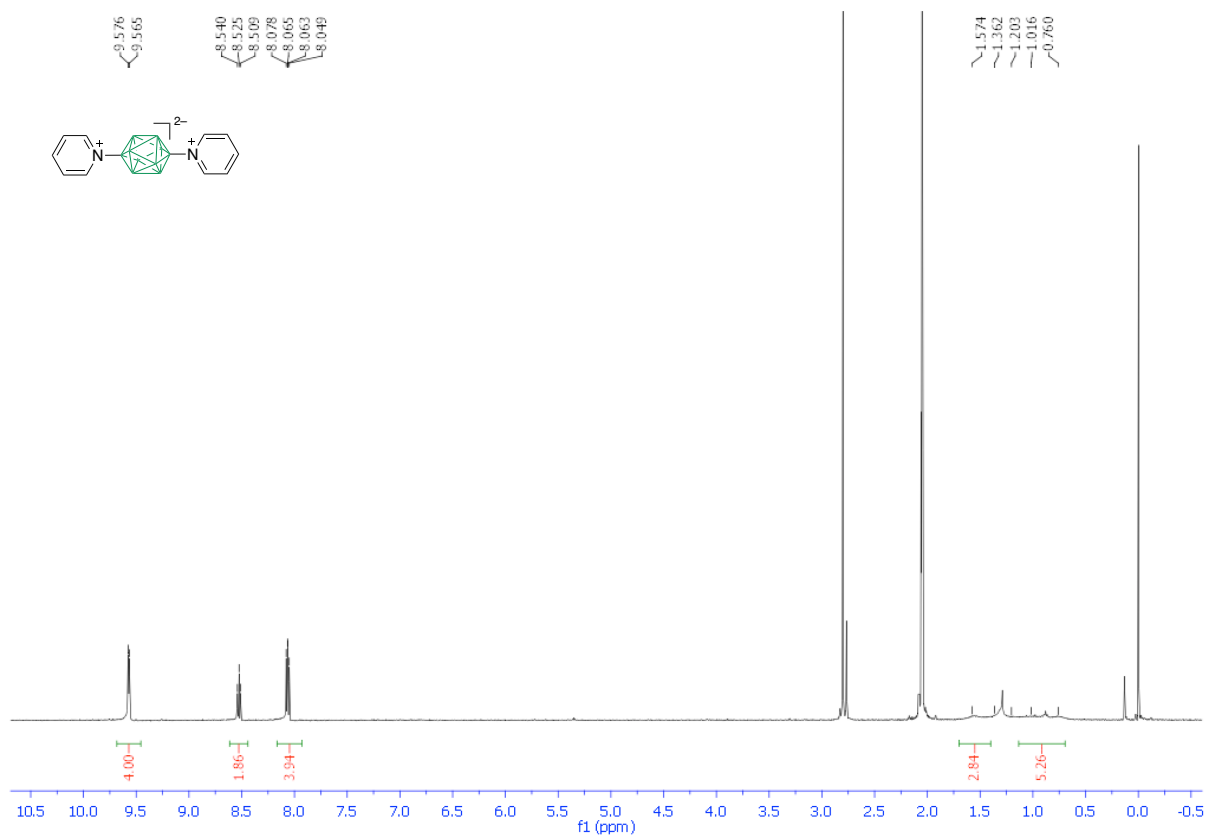


Figure S22. ¹H NMR spectrum for compound **1h**.

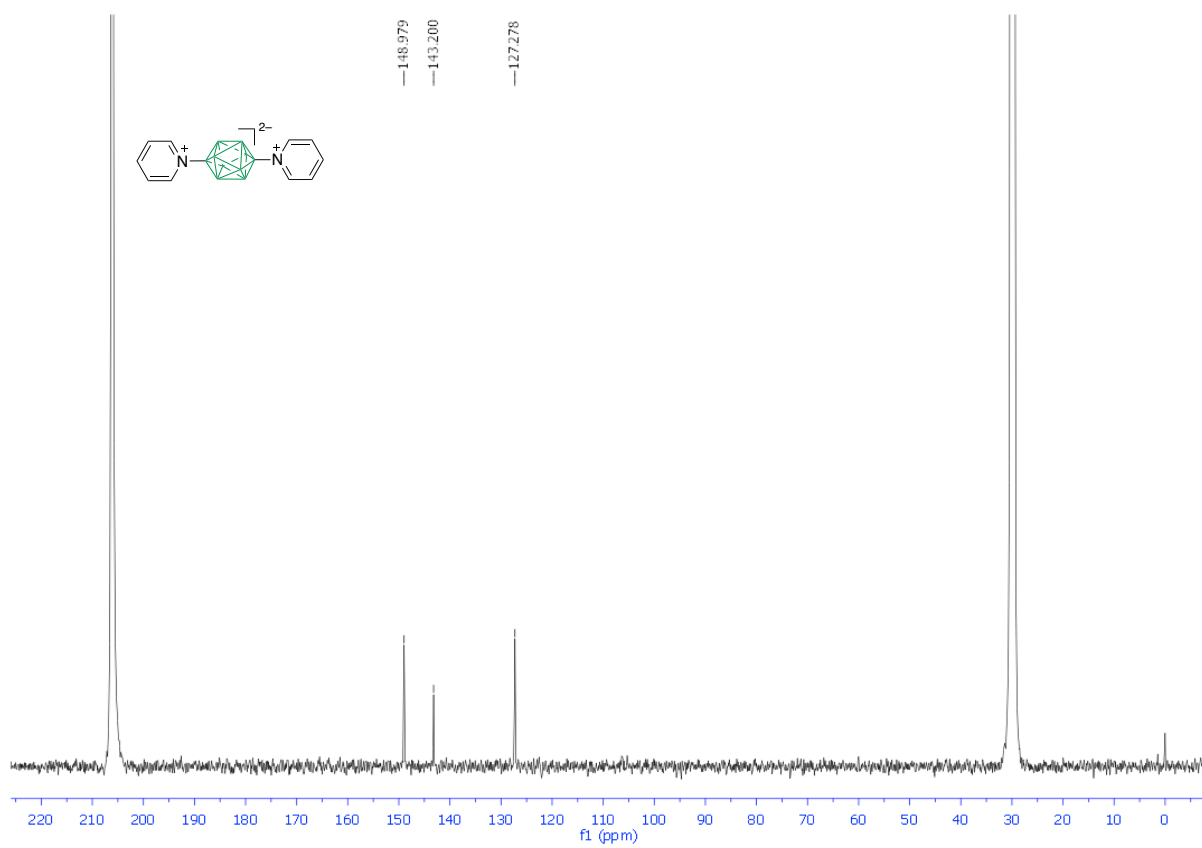


Figure S23. ^{13}C NMR spectrum for compound **1h**.

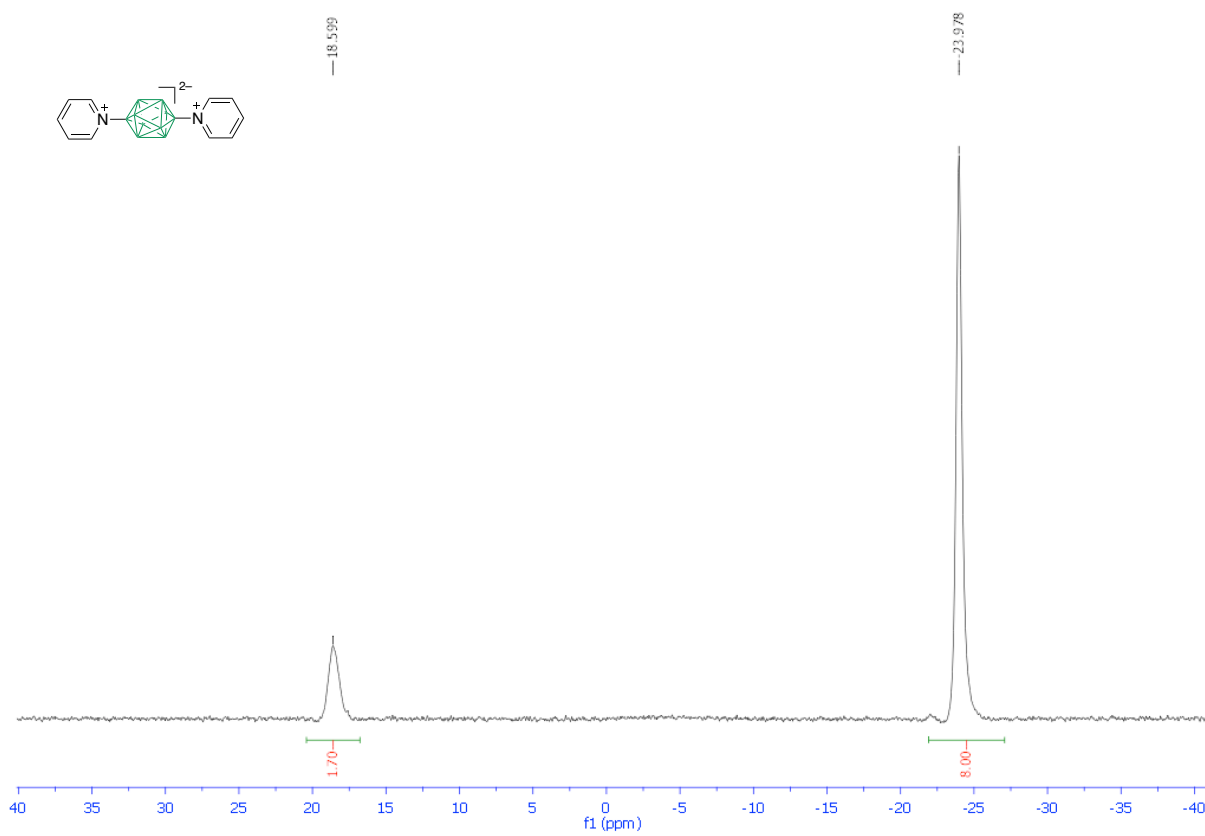


Figure S24. ^{11}B NMR decoupled spectrum for compound **1h**.

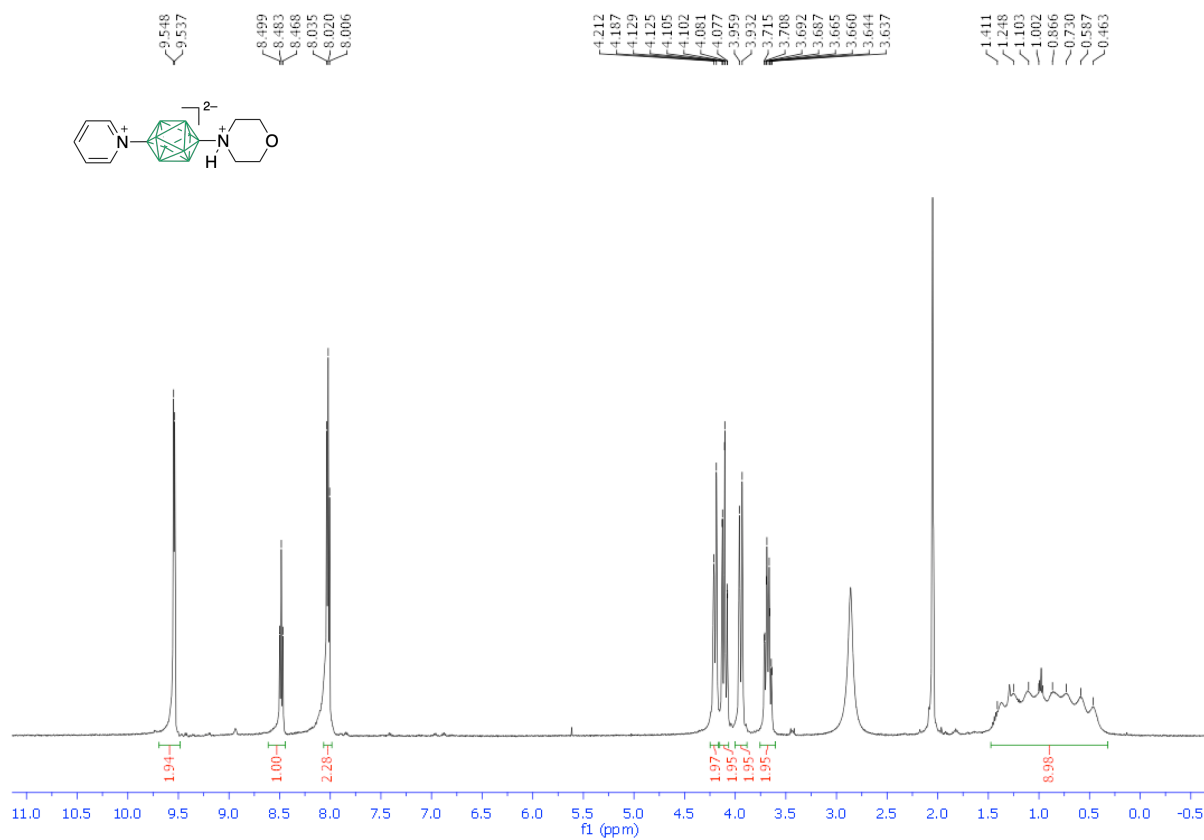


Figure S25. ¹H NMR spectrum for compound **1j**.

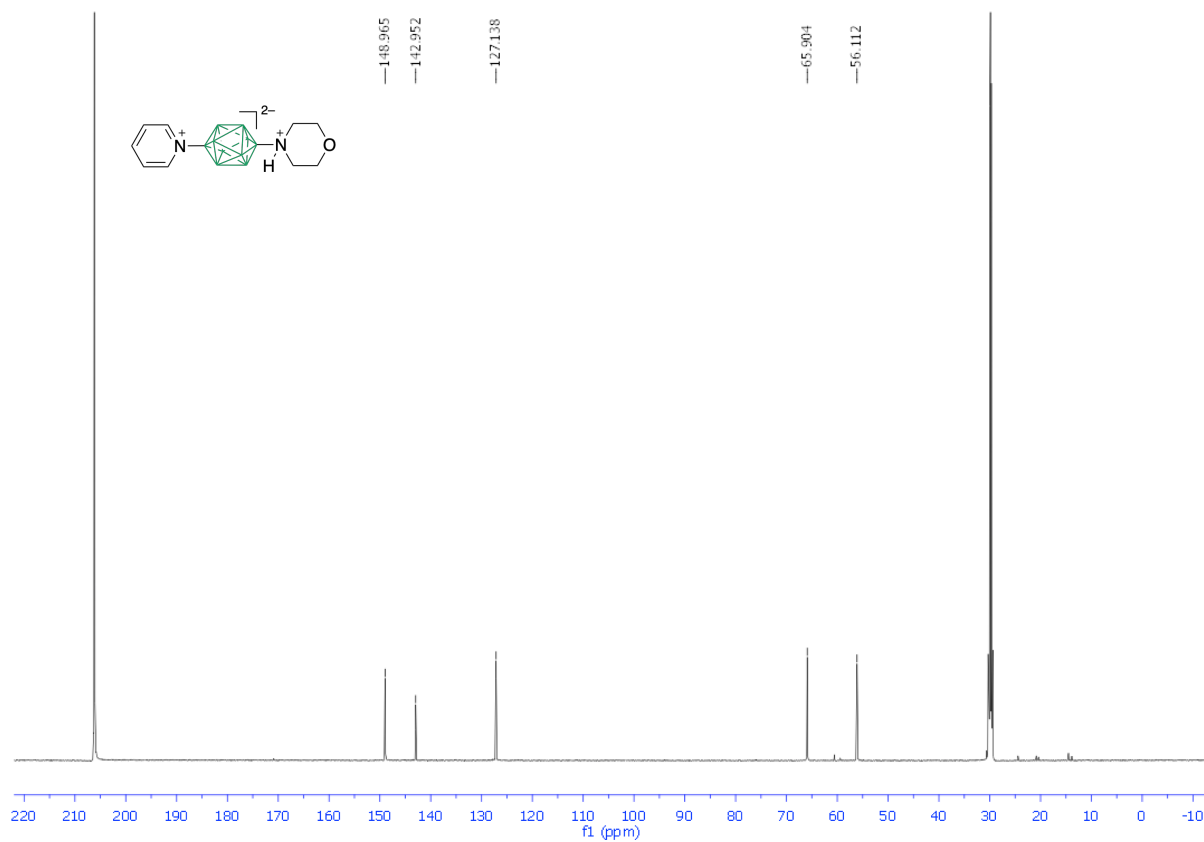


Figure S26. ^{13}C NMR spectrum for compound **1j**.

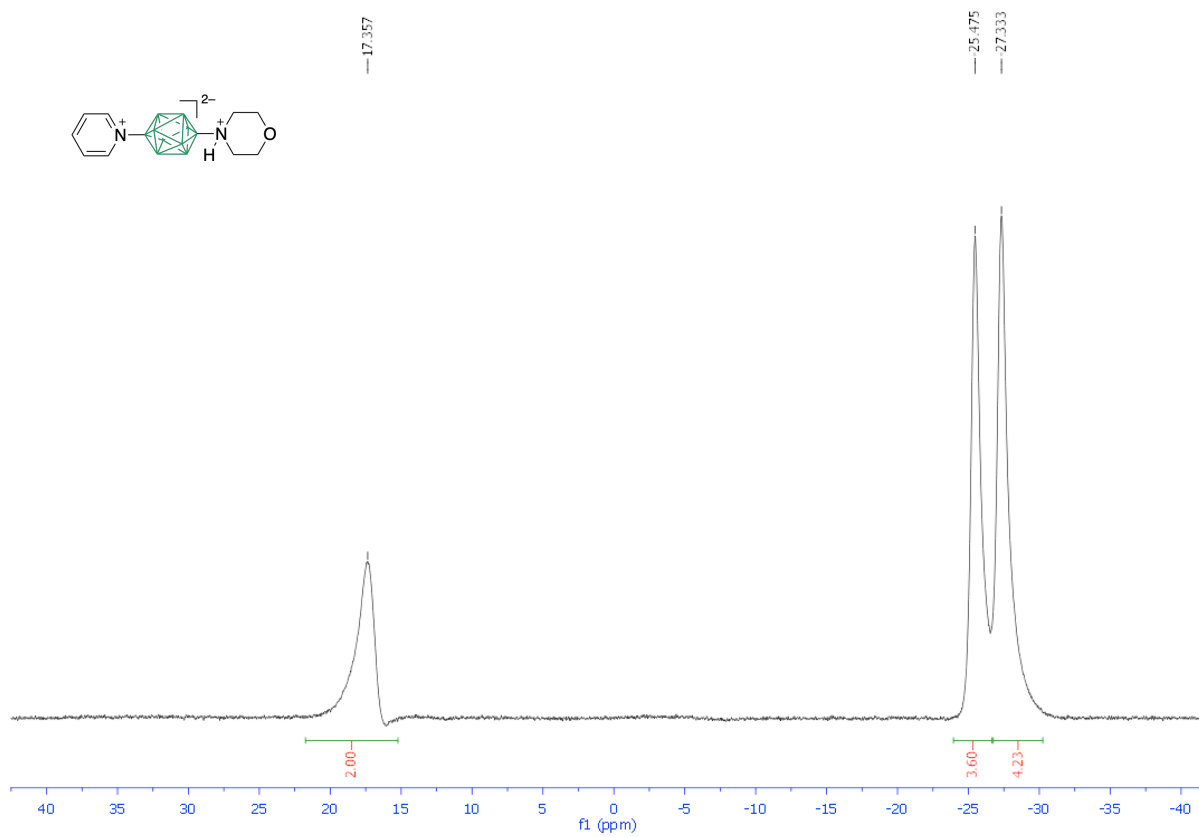
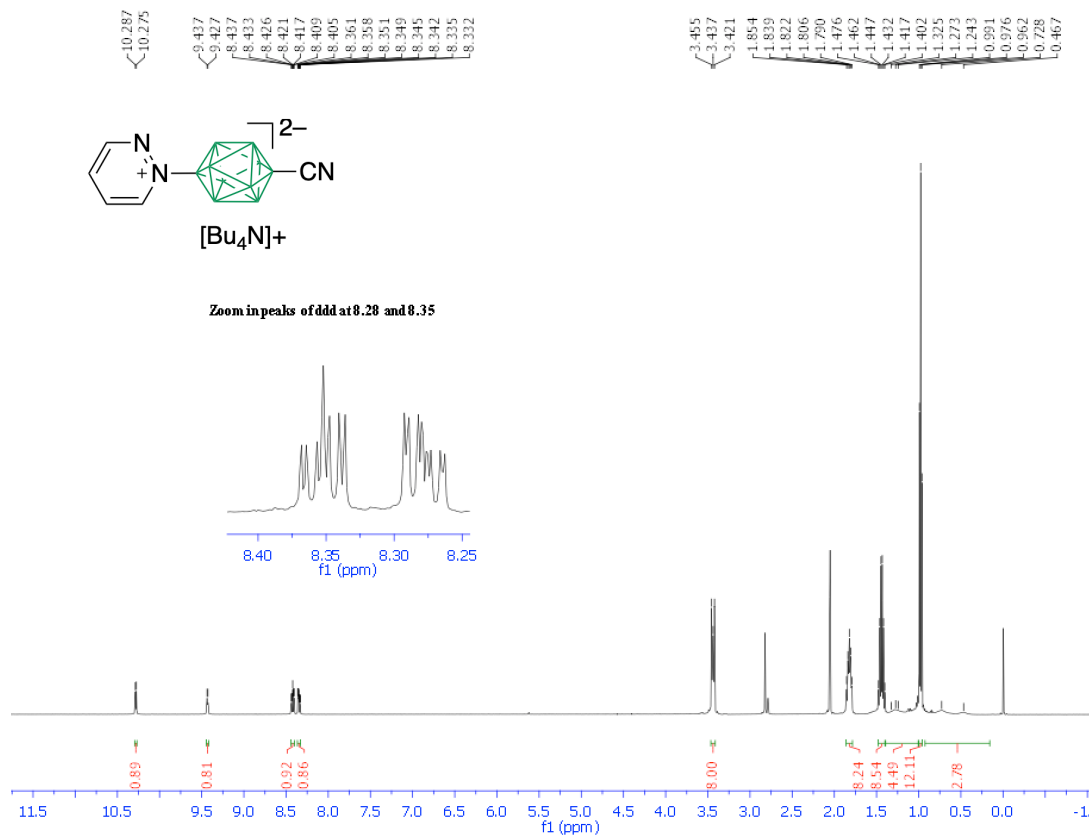


Figure S27. ^{11}B NMR spectrum for compound **1j**.

APPENDIX II: NMR Spectra of series 7, 8 and compound 10

**Figure S1:** ^1H NMR spectrum for compound 7a.

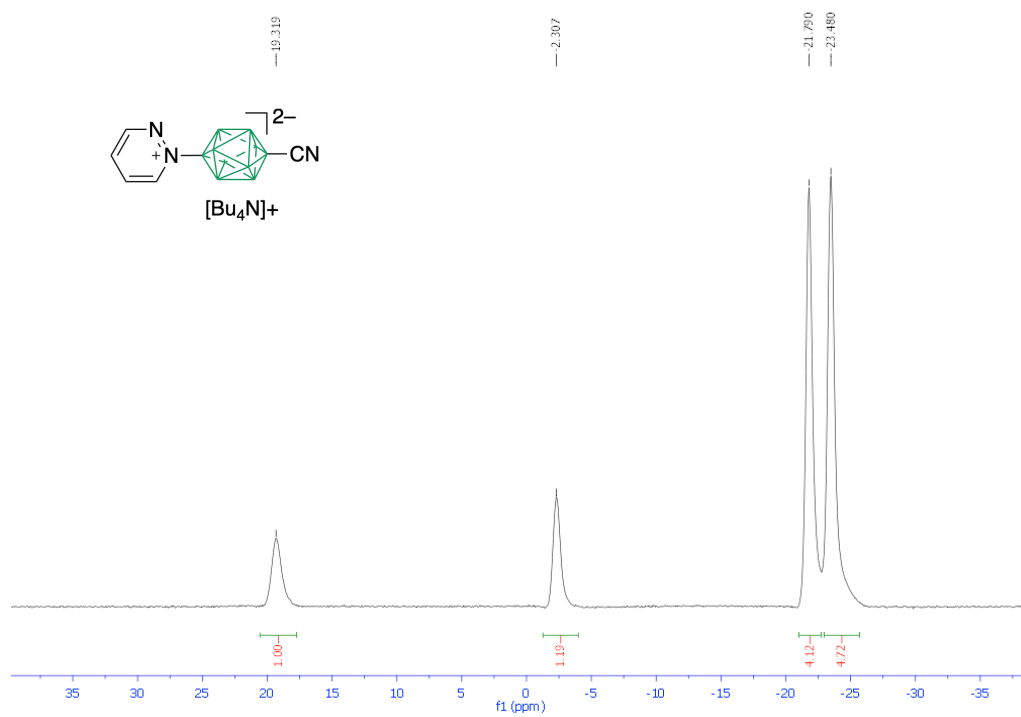


Figure S2: ^{11}B NMR spectrum for compound 7a.

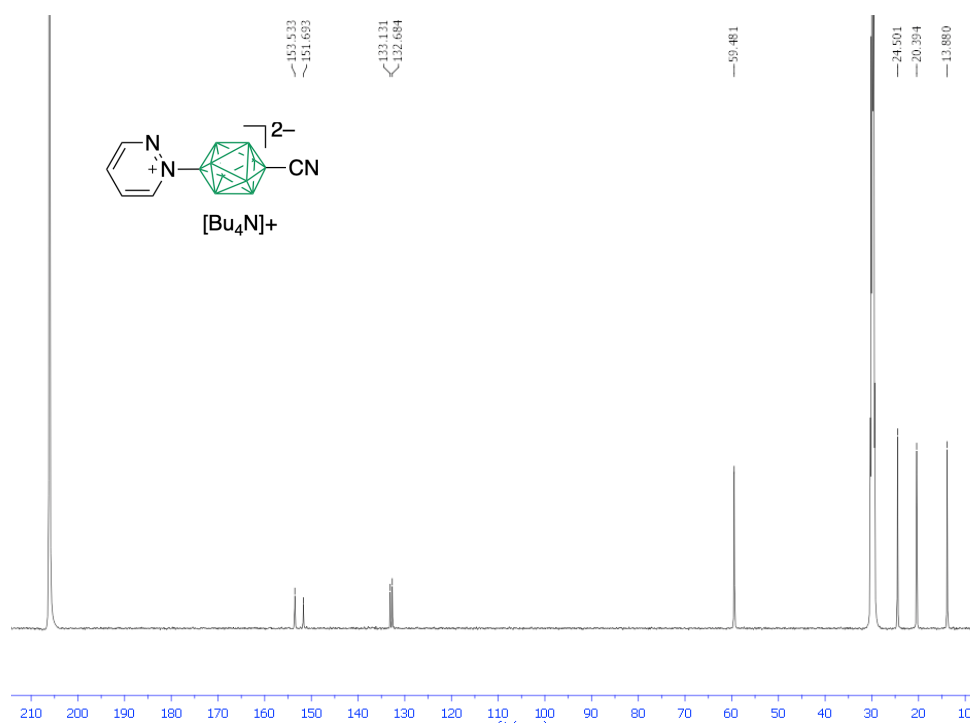
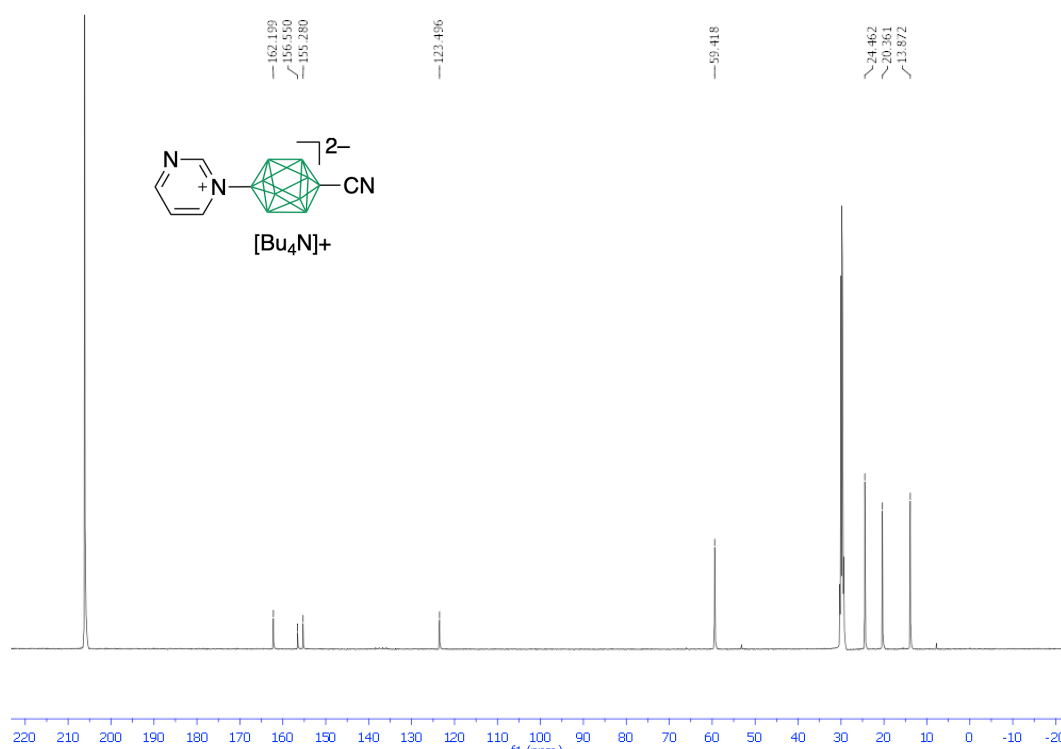


Figure S3: ^{13}C NMR spectrum for compound 7a.

Figure S5: ^{11}B NMR spectrum for compound **7b**.**Figure S6:** ^{13}C NMR spectrum for compound **7b**.

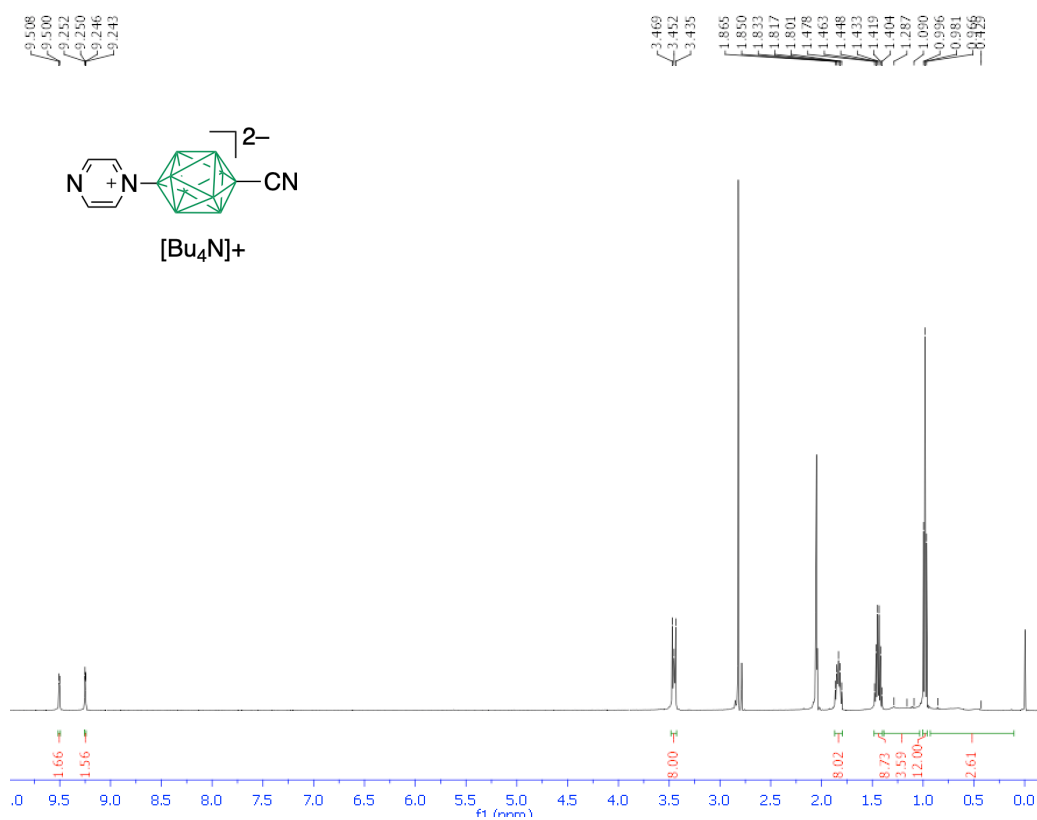


Figure S7: ¹H NMR spectrum for compound **7c**.

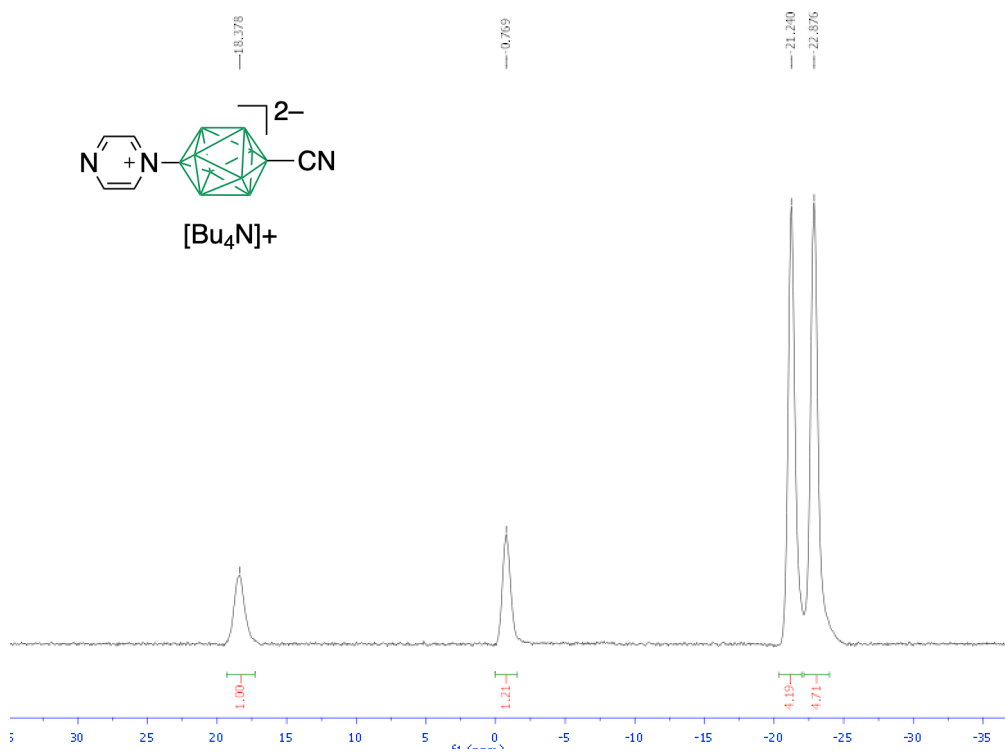


Figure S8: ¹¹B NMR spectrum for compound **7c**.

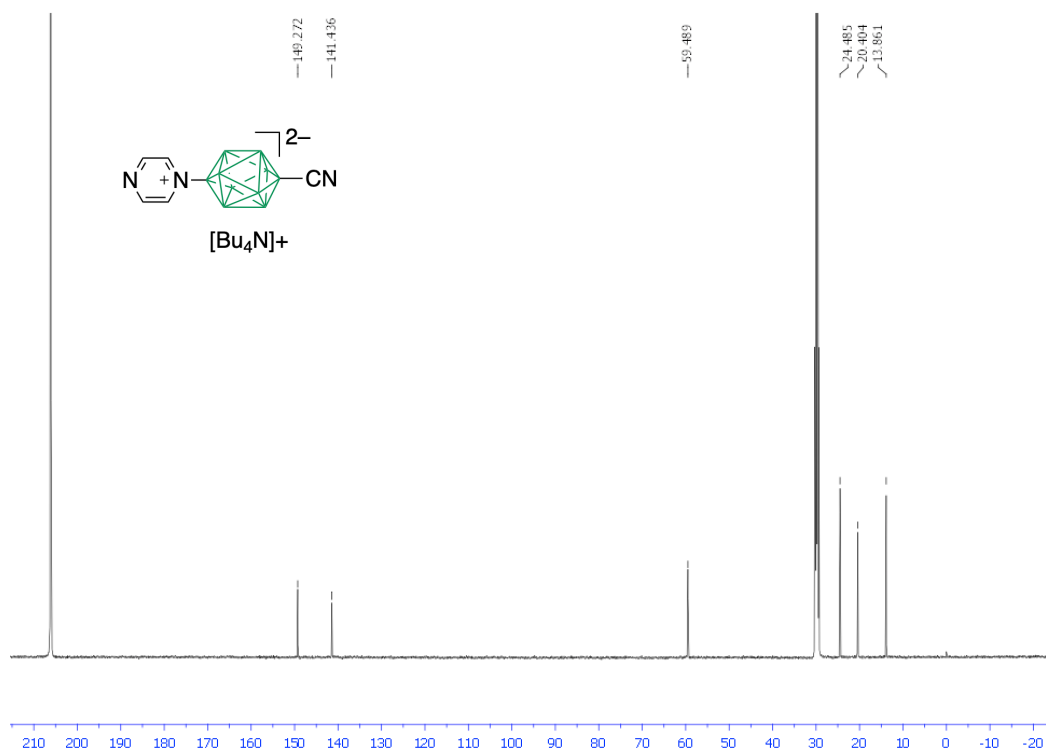


Figure S9: ^{13}C NMR spectrum for compound **7c**.

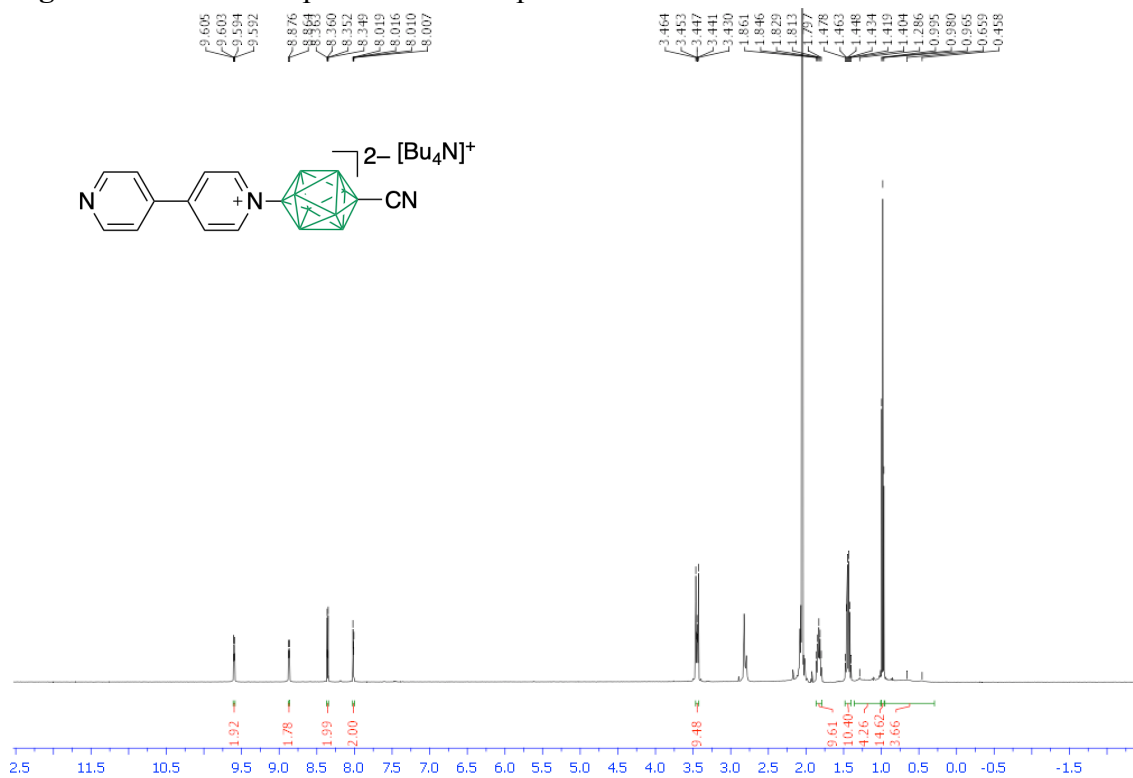
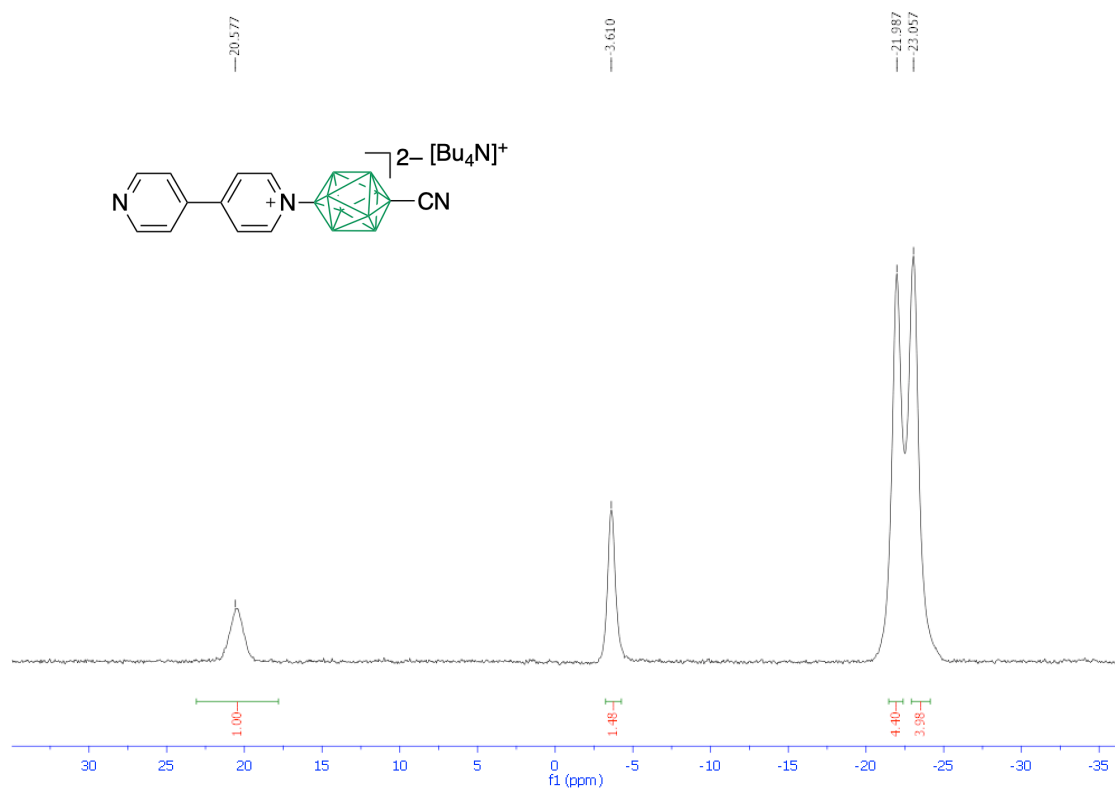


Figure S10: ^1H NMR spectrum for compound **7d**.**Figure S11:** ^{11}B NMR spectrum for compound **7d**.

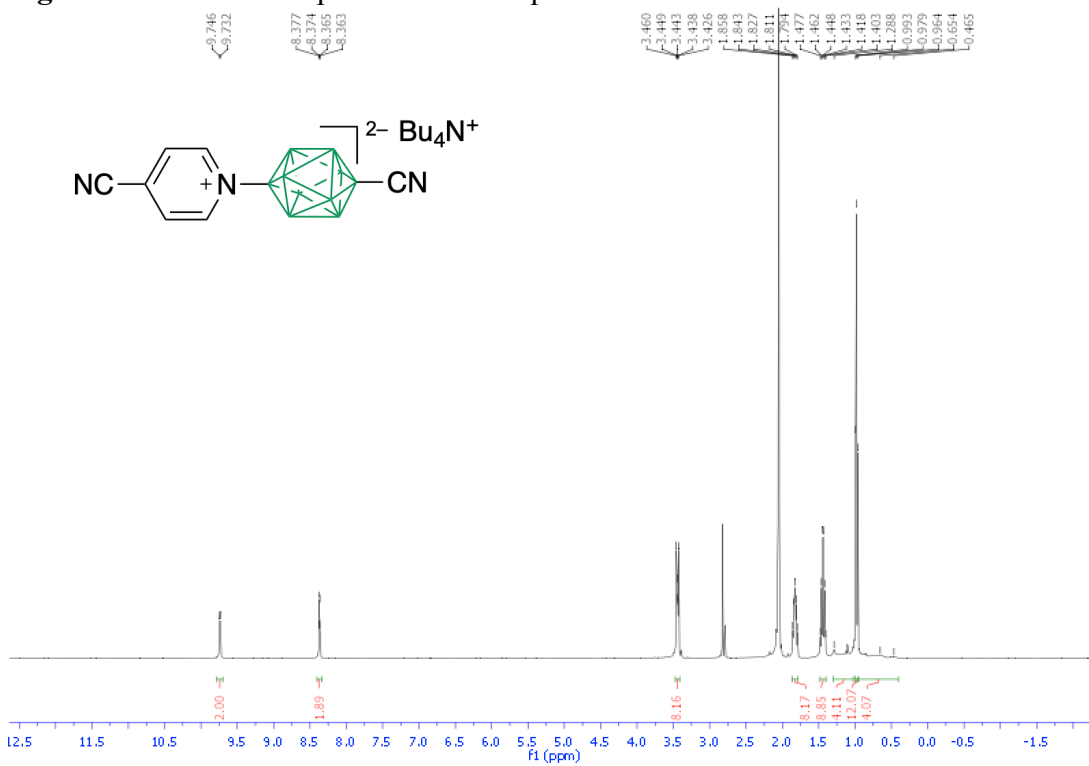
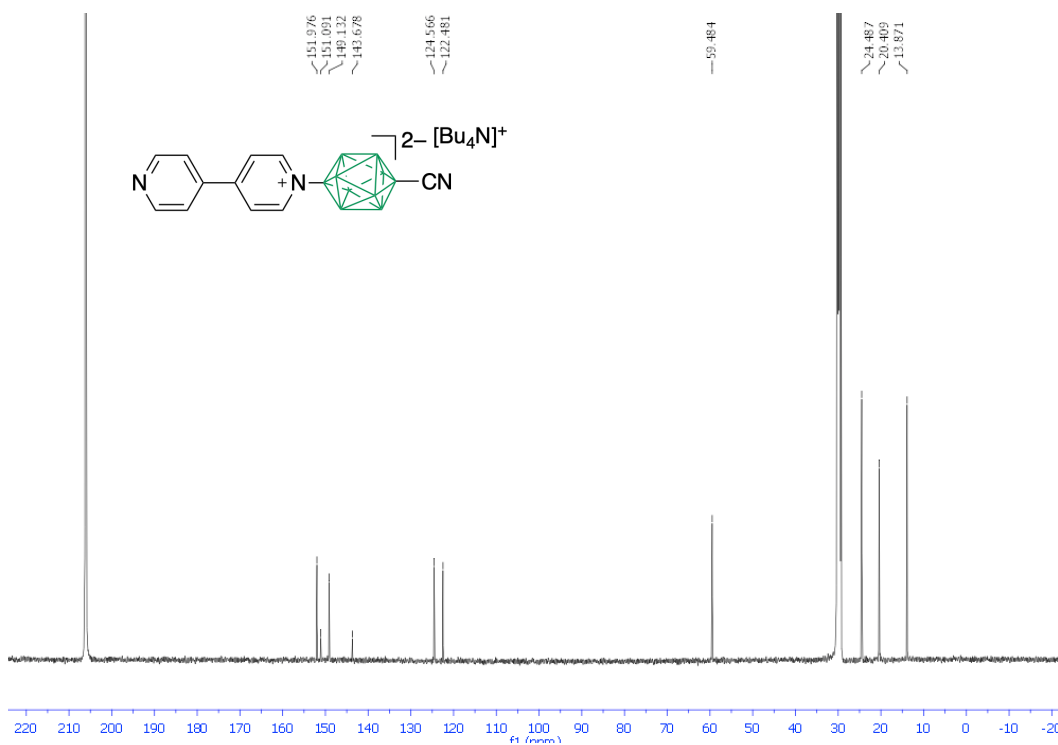


Figure S13: ^1H NMR spectrum for compound **7e**.

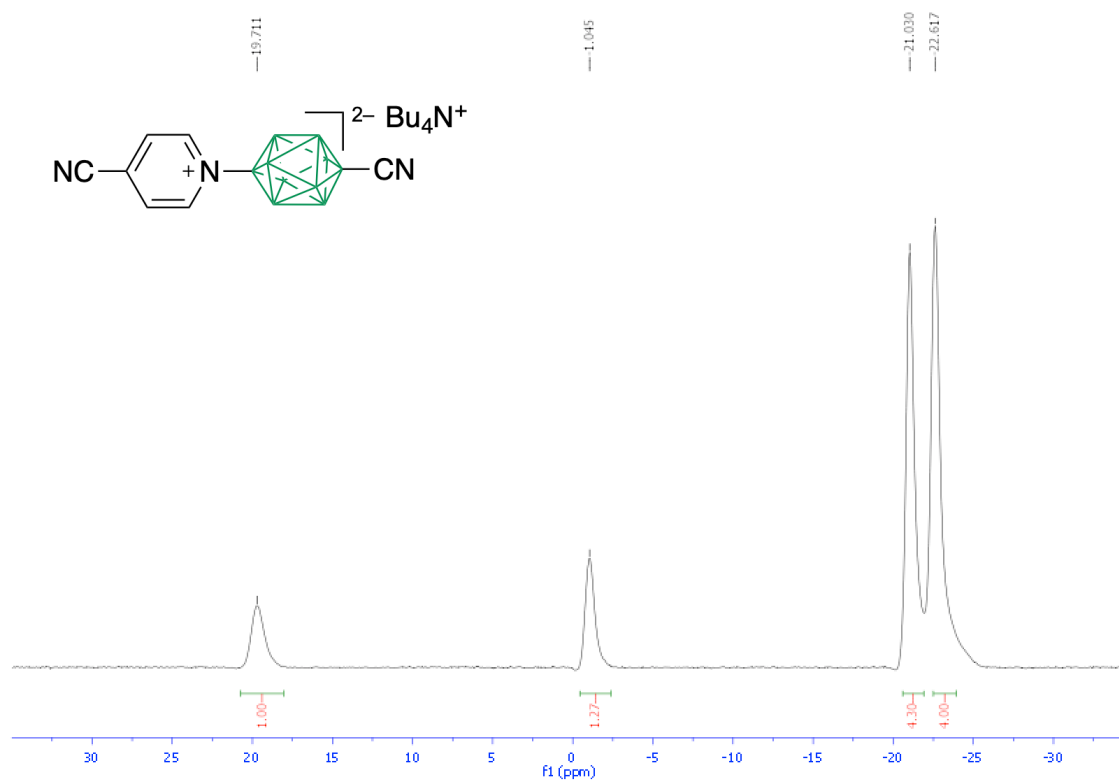


Figure S14: ¹¹B NMR spectrum for compound 7e.

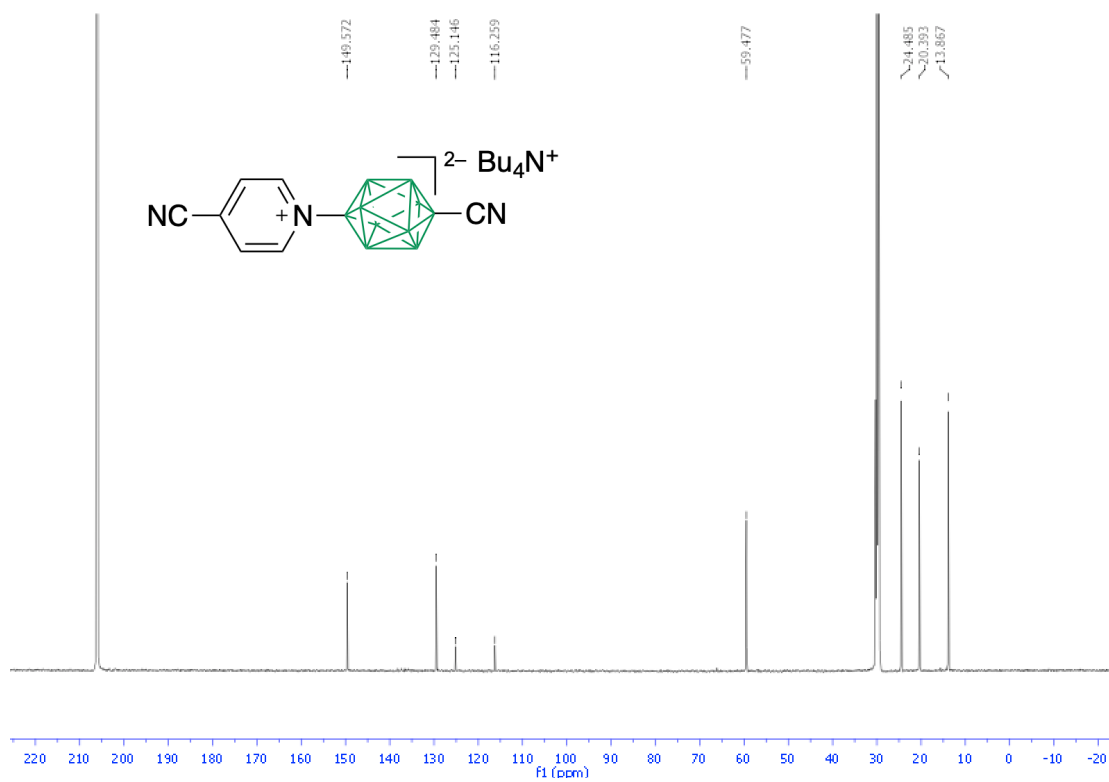
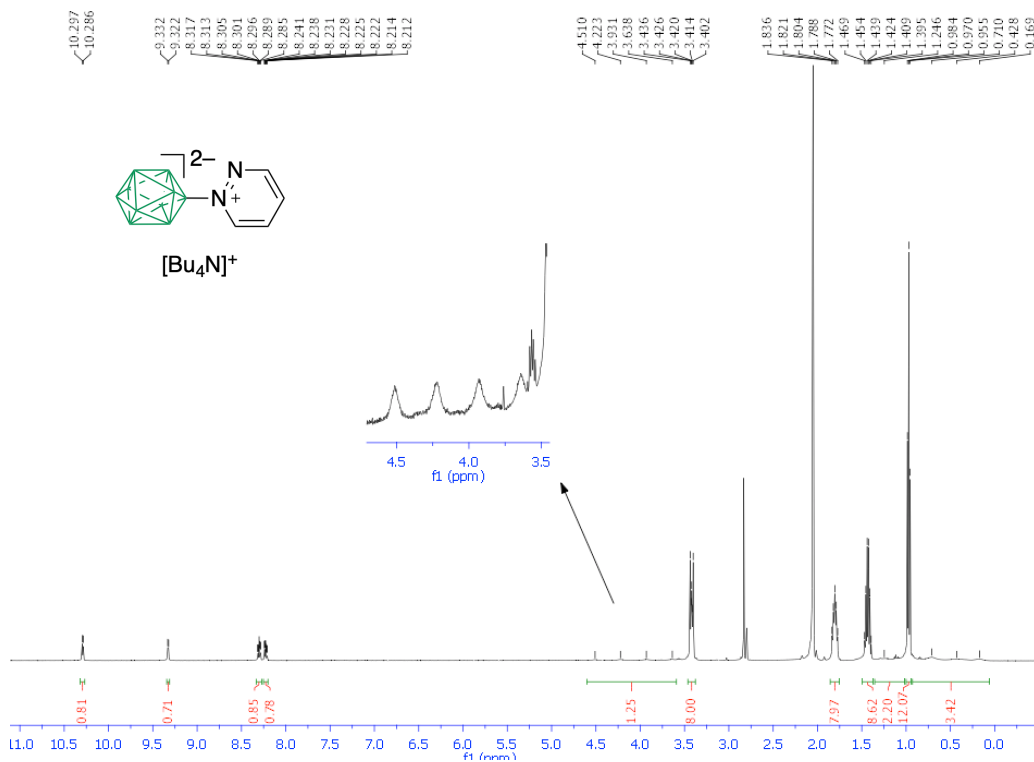


Figure S15: ^{13}C NMR spectrum for compound **7e**.**Figure S16:** ^1H NMR spectrum for compound **8a**.

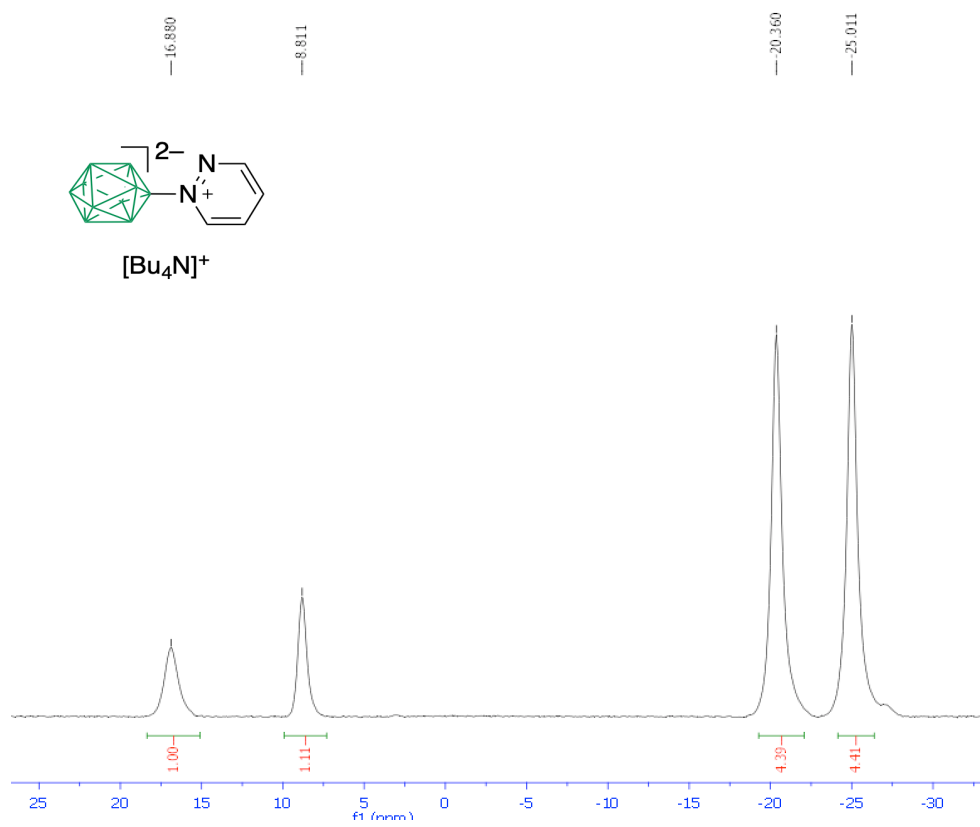


Figure S17: ^{11}B NMR spectrum for compound **8a**.

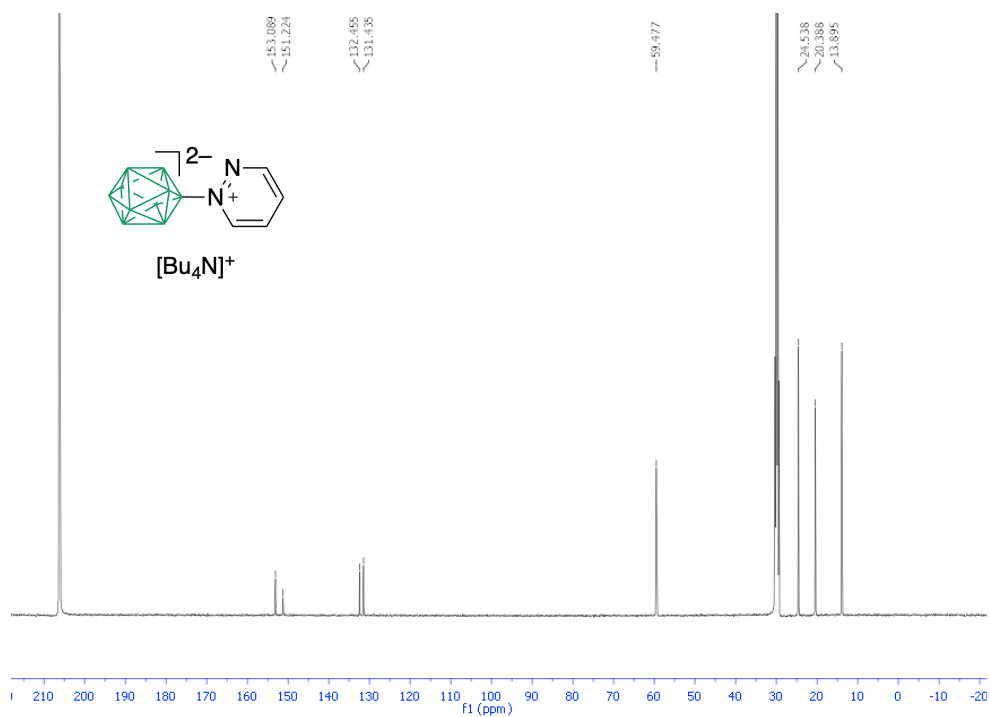


Figure S18: ^{13}C NMR spectrum for compound **8a**.

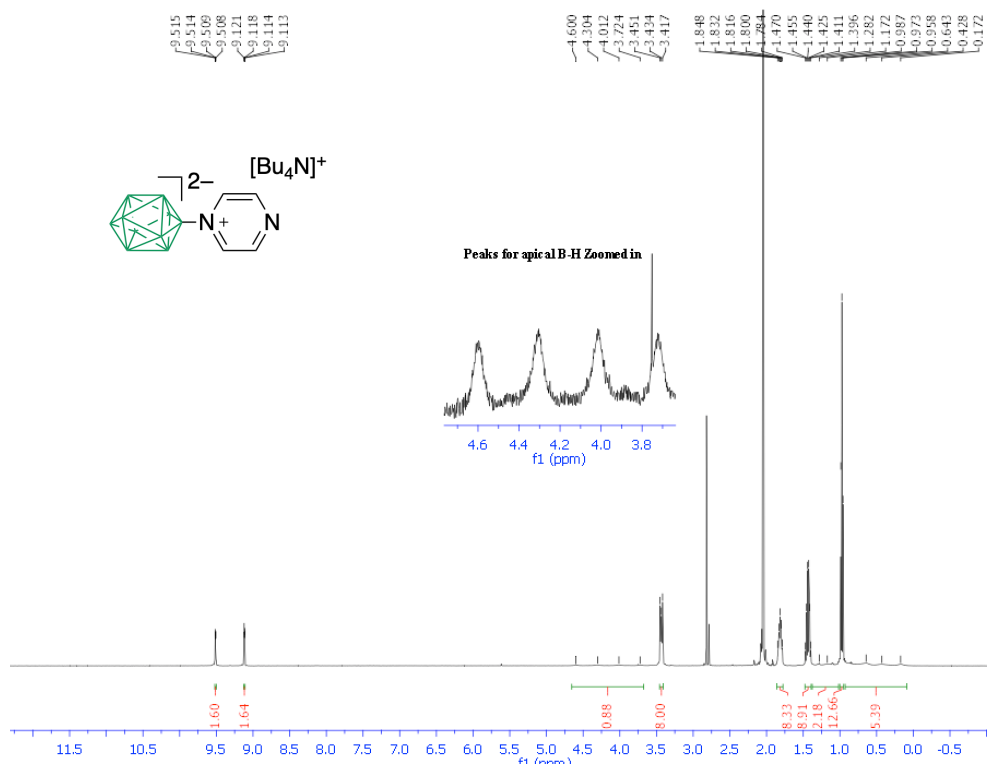


Figure S19: ¹H NMR spectrum for compound **8b**.

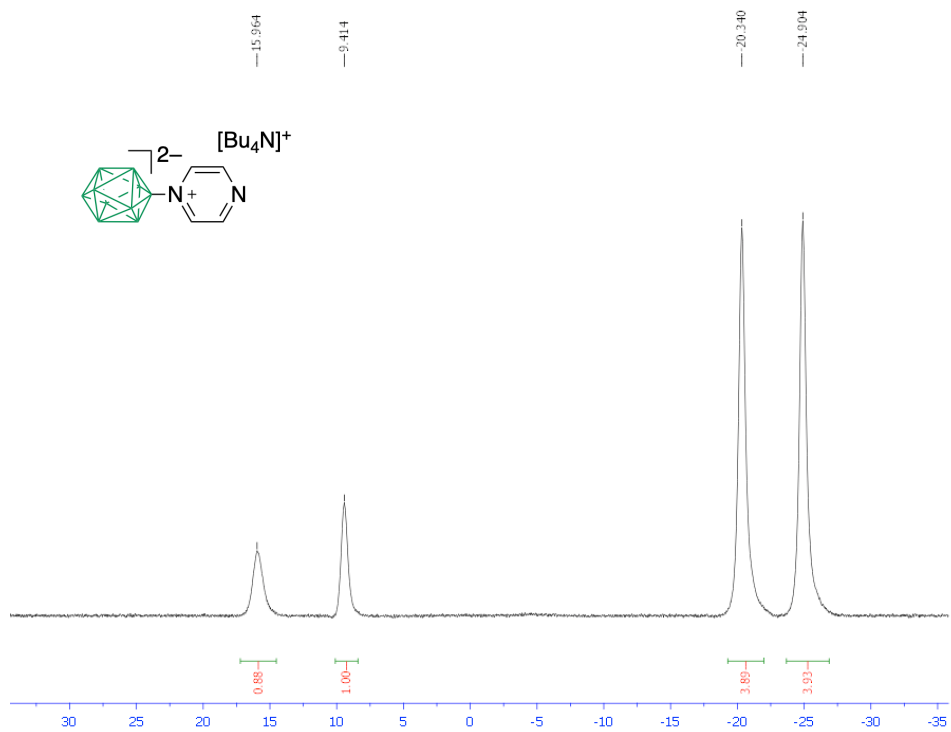
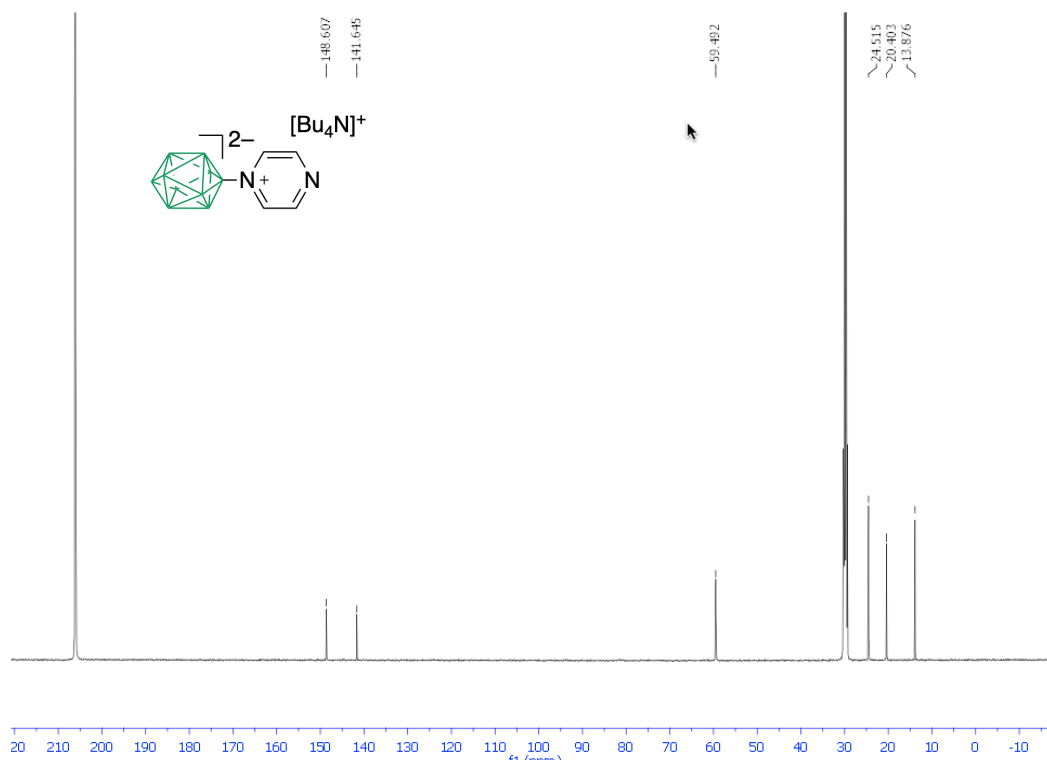


Figure S20: ^{11}B NMR spectrum for compound **8b**.**Figure S21:** ^{13}C NMR spectrum for compound **8b**.

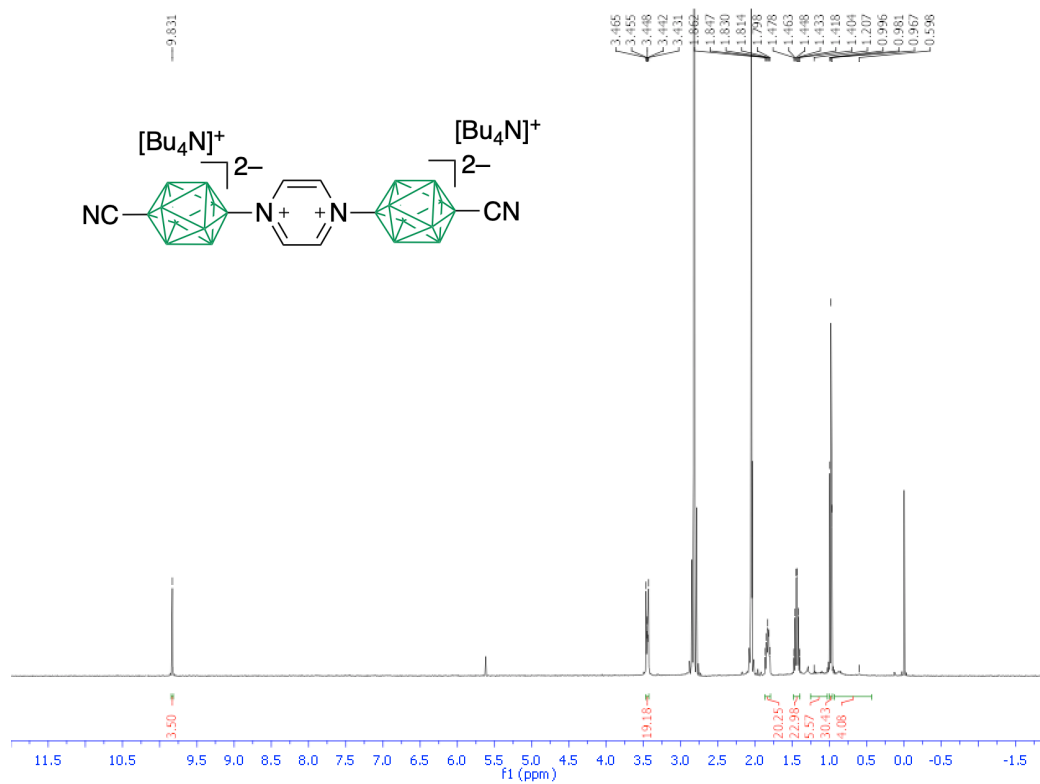


Figure S22: ^1H NMR spectrum for compound **10**.

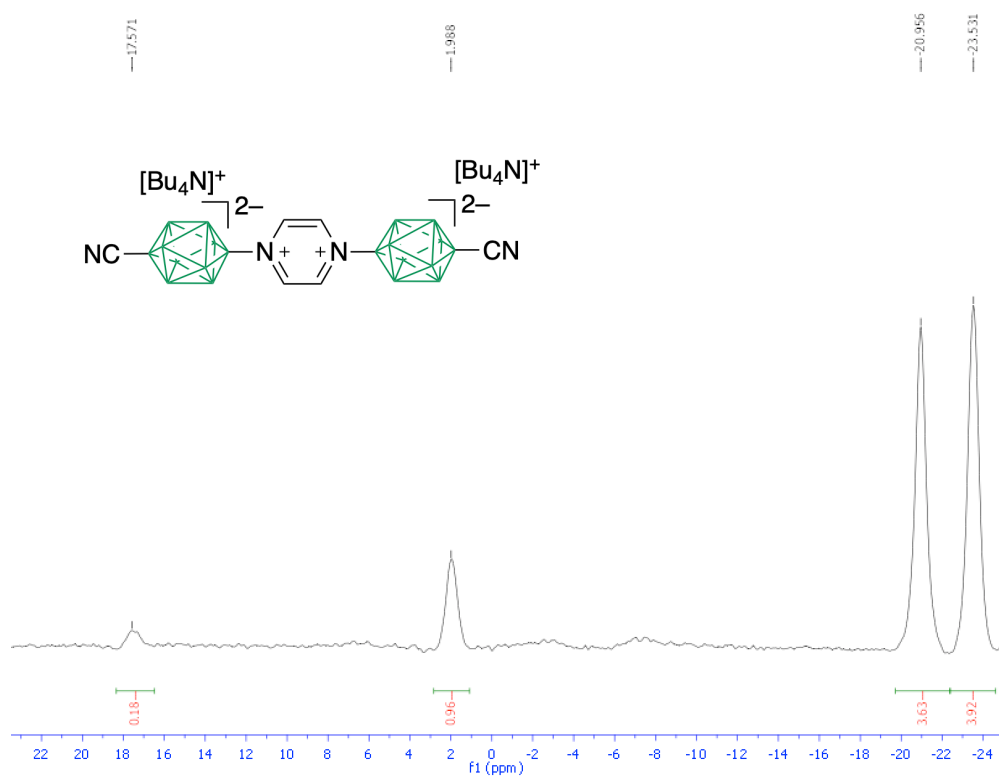


Figure S23: ^{11}B NMR spectrum for compound 10.

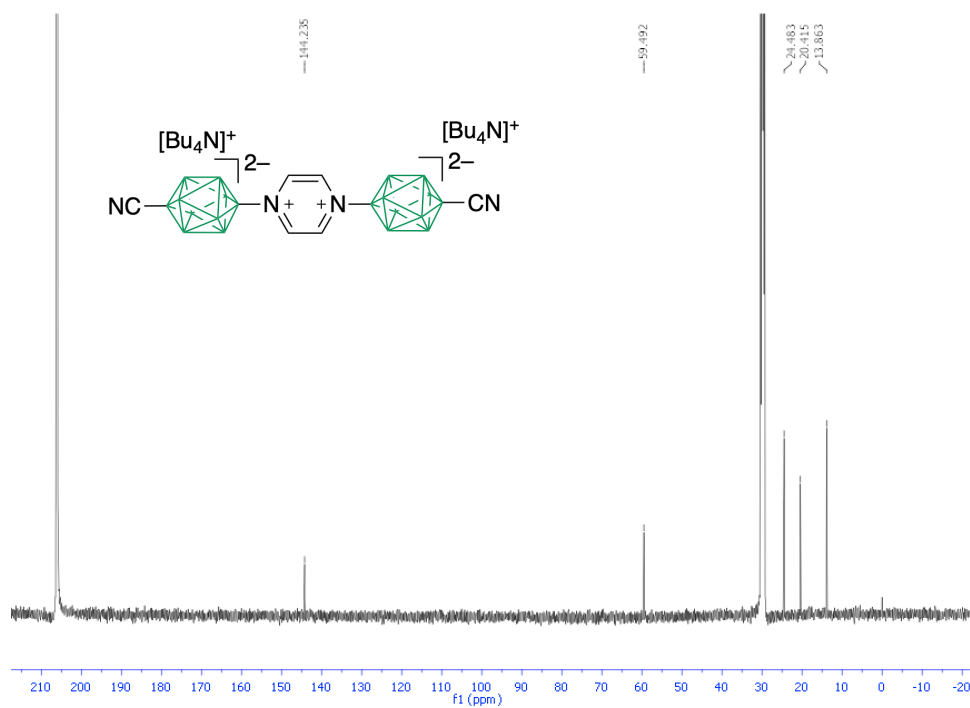


Figure S24: ^{13}C NMR spectrum for compound 10.



RightsLink®



Home



Help



Email Support



Sign in



Create Account

Enhanced π -Conjugation and Emission via Icosahedral Carboranes: Synthetic and Spectroscopic Investigation



Author: Barada Prasanna Dash, Rashmirekha Satapathy, Elizabeth R. Gaillard, et al

Publication: Inorganic Chemistry

Publisher: American Chemical Society

Date: Jun 1, 2011

Copyright © 2011, American Chemical Society

PERMISSION/LICENSE IS GRANTED FOR YOUR ORDER AT NO CHARGE

This type of permission/license, instead of the standard Terms & Conditions, is sent to you because no fee is being charged for your order. Please note the following:

- Permission is granted for your request in both print and electronic formats, and translations.
 - If figures and/or tables were requested, they may be adapted or used in part.
 - Please print this page for your records and send a copy of it to your publisher/graduate school.
 - Appropriate credit for the requested material should be given as follows: "Reprinted (adapted) with permission from (COMPLETE REFERENCE CITATION). Copyright (YEAR) American Chemical Society." Insert appropriate information in place of the capitalized words.
 - One-time permission is granted only for the use specified in your request. No additional uses are granted (such as derivative works or other editions). For any other uses, please submit a new request.
- If credit is given to another source for the material you requested, permission must be obtained from that source.

[BACK](#)

[CLOSE WINDOW](#)

Permission Request Form: mustapha abdulmojeed



CONTRACTS-COPYRIGHT (shared) <Contracts

-Copyright@rsc.org>

Mon 06/07/2020 10:27

To: Mustapha Abdulmojeed



Dear Mustapha

The Royal Society of Chemistry hereby grants permission for the use of the material specified below in the work described and in all subsequent editions of the work for distribution throughout the world, in all media including electronic and microfilm. You may use the material in conjunction with computer-based electronic and information retrieval systems, grant permissions for photocopying, reproductions and reprints, translate the material and to publish the translation, and authorize document delivery and abstracting and indexing services. The Royal Society of Chemistry is a signatory to the STM Guidelines on Permissions (available on request).

Please note that if the material specified below or any part of it appears with credit or acknowledgement to a third party then you must also secure permission from that third party before reproducing that material.

Please ensure that the published article carries a credit to The Royal Society of Chemistry (see <http://rsc.li/permissions> for details) and that any electronic version of the work includes a hyperlink to the article on the Royal Society of Chemistry website.

Regards

Gill Cockhead
Contracts & Copyright Executive

Gill Cockhead
Contracts & Copyright Executive
Royal Society of Chemistry,
Thomas Graham House,
Science Park, Milton Road,

Permission Request Form: mustapha abdulmojeed [



Mustapha Abdulmojeed

Sat 04/07/2020 21:07



To: CONTRACTS-COPYRIGHT (shared) <Contracts-Copyright@rsc.org>

Dear Chloe,

I kindly request permission to use the following images in my thesis, they are published in a review article titled: "Boron clusters in luminescent materials" written by Sanjoy Mukherjee and Pakkirisamy

Thilagar, DOI: [10.1039/C5CC08213G](https://doi.org/10.1039/C5CC08213G) *Chem. Commun.*, 2016, **52**, 1070-1093.

Image 1: Scheme 1, Molecular Formulae of the [3,3-(CO)₂-3-NO-*closo*-3,1,2-ReC₂B₉H₁₁] and [NEt₄][3,3,3-(CO)₃-8-*closo*-3,1,2-ReC₂B₉H₁₀]

Image 2: Scheme 4, Schematic formulae of [Au{(PR₂)₂C₂B₁₀H₁₀}L]⁺ and [Au-{(PR₂)₂C₂B₉H₁₀}L]. Thanks for responding to my request.

Mustapha Abdulmojeed
Graduate Teaching Assistant,
Graduate Student (MSc),
Chemistry Department,
Middle Tennessee State University.
6152434048



Permission Request Form: mustapha abdulmojeed [



Mustapha Abdulmojeed

Sat 04/07/2020 21:07



To: CONTRACTS-COPYRIGHT (shared) <Contracts-Copyright@rsc.org>

Dear Chloe,

I kindly request permission to use the following images in my thesis, they are published in a review article titled: "Boron clusters in luminescent materials" written by Sanjoy Mukherjee and Pakkirisamy

Thilagar, DOI: [10.1039/C5CC08213G](https://doi.org/10.1039/C5CC08213G) *Chem. Commun.*, 2016, **52**, 1070-1093.

Image 1: Scheme 1, Molecular Formulae of the [3,3-(CO)₂-3-NO-*closo*-3,1,2-ReC₂B₉H₁₁] and [NEt₄][3,3,3-(CO)₃-8-*closo*-3,1,2-ReC₂B₉H₁₀]

Image 2: Scheme 4, Schematic formulae of [Au{(PR₂)₂C₂B₁₀H₁₀}L]⁺ and [Au-{(PR₂)₂C₂B₉H₁₀}L]. Thanks for responding to my request.

Mustapha Abdulmojeed
Graduate Teaching Assistant,
Graduate Student (MSc),
Chemistry Department,
Middle Tennessee State University.
6152434048

